Inaugural-Dissertation

zur Erlangung der Doktorwürde
der
Naturwissenschaftlich-Mathematischen Gesamtfakultät
der
Ruprecht-Karls-Universität
Heidelberg

vorgelegt von
Diplom-Mathematiker Thomas Dunne
aus Heidelberg

Tag der mündlichen Prüfung: _____

Adaptive Finite Element Approximation of Fluid-Structure Interaction Based on Eulerian and Arbitrary Lagrangian-Eulerian Variational Formulations

20. Juni 2007

1. Gutachter: Prof. Dr. Rolf Rannacher

2. Gutachter: _____

Abstract

Aim of this work is the examination of numerical methods for fluid-structure interaction (FSI) problems. We use two approaches for the modelling of FSI problems. The well-known 'arbitrary Lagrangian-Eulerian' (ALE) approach as well as an unusual (to the authors knowledge novel) fully Eulerian approach. For both frameworks we derive a general variational framework for the adaptive finite element approximation of FSI problems.

The focal points of this thesis are the comparison of the ALE and the novel Eulerian approaches and the application of the 'dual weighted residual' (DWR) method to FSI problems. The DWR method is the basis of two techniques, a posteriori error estimation and goal-oriented mesh adaptivity.

Based on the developed models of FSI we apply the DWR method for a posteriori error estimation and goal-oriented mesh adaptation to FSI problems. Necessary aspects of DWR method and implementation for the ALE and Eulerian approach are discussed.

Several stationary as well as nonstationary examples are presented using both the ALE as well as the Eulerian framework. Results from both frameworks are in good agreement with each other. Also for both frameworks the DWR method is successfully applied.

Finally using benchmark results from the DFG joint research group FOR 493 (of which the author is a participating member) the discussed methods are verified for both frameworks.

Zusammenfassung

Ziel dieser Arbeit ist die Untersuchung von numerischen Verfahren für Probleme der Fluid-Strukur Wechselwirkung (FSW). Wir benutzen zwei Verfahren zur Modellierung solcher Probleme. Den bekannten 'arbitrary Lagrange-Eulerschen' (ALE) Ansatz als auch den ungewöhnlichen (und soweit dem Author bekannt, den neuen) ganz Eulerschen Ansatz. Für beide Ansätze leiten wir die allgemeine variationelle Formulierung her, welches wir für die adaptive finite-element Approximation von FSW-Probleme benutzen.

Die Schwerpunkte dieser Arbeit sind der Vergleich des ALE Ansatzes mit dem neuen Eulerschen Ansatz und die Anwendung der 'dual gewichteten residuen' (DWR) Methode für FSW-Probleme. Die DWR Methode dient als Grundlage zweier Verfahren, die der a posteriori Fehlerschätzung und ergebnisorientierte Gitteradaption.

Basierend auf den entwickelten FSW Modellen wenden wir die DWR Methode bei FSW Problemen an um einerseits eine a posteriori Fehlerschätzung zu erhalten als auch um einen ergebnisorientierte Gitteradaption zu betreiben. Notwendige Aspekte der DWR Methode und der Implementation für sowohl den ALE als auch den Eulerschen Ansatz werden besprochen.

Viele stationäre als auch instationäre Beispiele werden gezeigt für welches sowohl der ALE Ansatz als auch der Eulersche Ansatz benutzt werden. Ergebnisse von beiden Ansätzen

stimmen gut miteinander ein. Die DWR Methode wird auch bei beiden Ansätzen erfolgreich eingesetzt. Schließlich werden die vorgetragenen Methoden anhand von Benchmark-Ergebnisse der DFG Forschungsgruppe 493 (von der der Author ein teilnehmender Mitglied ist) für beide Ansätze bestätigt.

Contents

Chapter 1

Introduction

Computational fluid dynamics and computational structure mechanics are two major areas of numerical simulation of physical systems. With the introduction of high performance computing it has become possible to tackle systems with a coupling of fluid and structure dynamics. General examples of such fluid-structure interaction (FSI) problems are flow transporting elastic particles (particulate flow), flow around elastic structures (airplanes, submarines) and flow in elastic structures (haemodynamics, transport of fluids in closed containers). In all these settings the dilemma in modeling the coupled dynamics is that the fluid model is normally based on an Eulerian perspective in contrast to the usual Lagrangian approach for the solid model. This makes the setup of a common variational description difficult. However, such a variational formulation of FSI is needed as the basis of a consistent approach to residual-based a posteriori error estimation and mesh adaptation as well as to the solution of optimal control problems by the Euler-Lagrange method. This is the subject of this thesis.

Combining the Eulerian and the Lagrangian setting for describing FSI involves conceptional difficulties. On the one hand the fluid domain itself is time-dependent and depends on the deformation of the structure domain. On the other hand, for the structure the fluid boundary values (velocity and the normal stress) are needed. In both cases values from the one problem are used for the other, which is costly and can lead to a drastic loss of accuracy. A common approach to dealing with this problem is to separate the two models, solve each one after the other, and so converge iteratively to a solution, which satisfies both together with the interface conditions (Figure 1.1). Solving the separated problems serially multiple times is referred to as a 'partitioned approach'. For advanced examples of this approach see [Vi06, TeSa+06, LoCe+06, ScHeYi06, WaGe+06, BrBu+06, GeTo+06] in [BuSc+06].
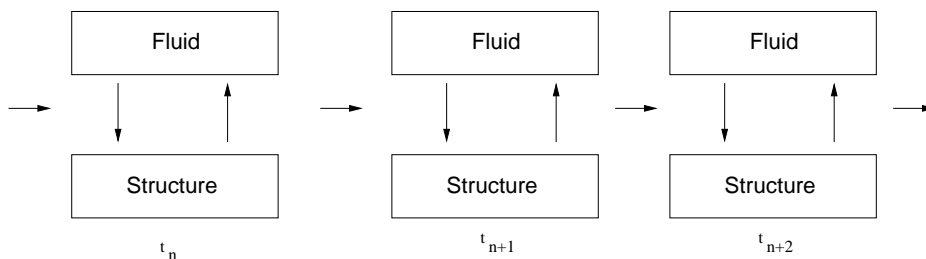
Figure 1.1: Partitioned approach, Lagrangian and Eulerian frameworks coupled.

A basic partitioned approach does not contain a variational equation for the fluid-structure interface. To achieve this, usually an auxiliary unknown coordinate transformation function ζ_f is introduced for the fluid domain. With its help the fluid problem is rewritten as one on the transformed domain, which is fixed in time. Then, all computations are done on the fixed reference domain and as part of the computation the auxiliary transformation function ζ_f has to be determined at each time step. Figure 1.2 illustrates this approach for the driven cavity problem considered in Chapter 9 below. Such, so-called 'arbitrary Lagrangian-Eulerian' (ALE) methods are used in this thesis as well as in [HronTurek206, HuertaLiu, Wa99], and corresponding transformed space-time finite element formulations in [TezBehLiouI, TezBehLiouII]. Multiple good examples and quantitative results can be found in [BuSc+06], e.g. [HronTurek206, TuHr06].
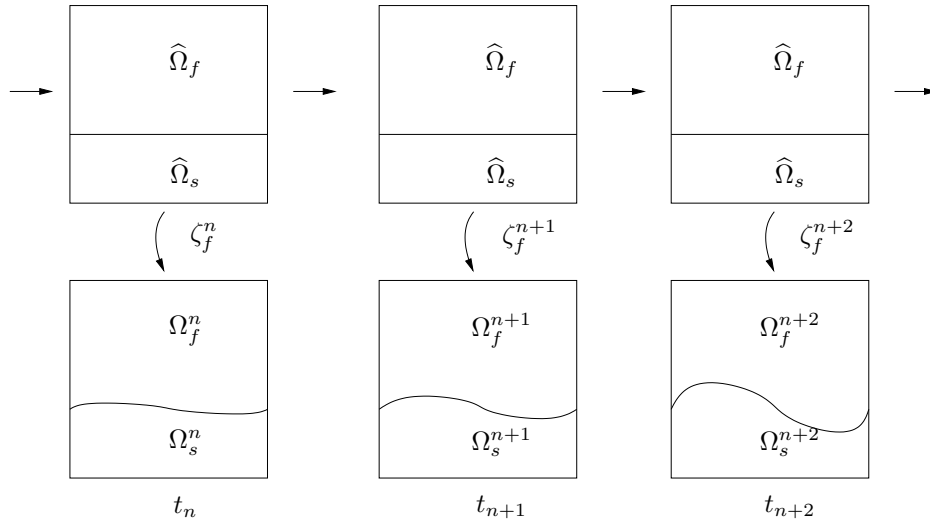
Figure 1.2: Transformation approach, both frameworks 'Lagrangian'

Both, the partitioned and the transformation approach overcome the Euler-Lagrange discrepancy by explicitly tracking the fluid-structure interface. This is done by mesh adjustment or aligning the mesh to match the interface and is generally referred to as 'interface tracking'. Both methods leave the structure problem in its natural Lagrangian setting.

In this thesis, we follow the alternative way of posing the fluid as well as the structure problem in a fully Eulerian framework. A similar approach has been used by Lui and Walkington [LuWa01] in the context of the transport of visco-elastic bodies in a fluid. In the Eulerian setting a phase variable is employed on the fixed mesh to distinguish between the different phases, liquid and solid. This approach to identifying the fluid-structure interface is generally referred to as 'interface capturing', a method commonly used in the simulation of multiphase flows, [JoRe93a, JoRe93b]. Examples for the use of such a phase variable are the Volume of Fluid (VoF) method [HiNi81] and the Level Set (LS) method [ChHoMeOs, OsherSethian, Sethian99]. In the classical LS approach the distance function has to continually be reinitialized, due to the smearing effect by the convection velocity in the fluid domain. This makes the use of the LS method delicate for modeling FSI problems particularly in the presence of cornered structures. To cope with this difficulty, we introduce a variant of the LS method that makes reinitialization unnecessary and which can easily

cope with cornered structures.

The method we describe does not depend on the specific structure model. The key variable in structure dynamics is the deformation, and since this depends on the deflection, it is understandable why structure dynamics is preferably described in the Lagrangian frame. To be able to describe the deformations in the Eulerian frame, we introduce the 'Initial Positions set' (IP set) of all structure points. This set is then transported with the structure velocity in each time step. Based on the IP set points and their Eulerian coordinates the displacement is now available in an Eulerian sense. Also its gradient has to be rewritten appropriately, which will be explained later in Section 4.7. Since the fluid-structure interface will be crossing through cells, we will have to also transport the IP set in the fluid domain.

If we were to use the fluid velocity for the convection of the IP set, this would lead to entanglement of the respective displacements, which would 'wreak havoc' on the interface cells. This is a known problem with LS approaches. A common way for fixing this problem has been to occasionally fix the LS field between the time steps. The problem with this approach is that the variational formulation is no longer consistent. As an alternative, we harmonically continue the structure velocity into the fluid domain. In the fluid domain we then use this velocity for the convection of the IP set. Since an IP set is available in both domains, we can always at each point determine if it belongs to the fluid or solid part of the model.

Again, this approach is similar to the LS approach. Actually, it is possible to also develop a model for FSI using the level set approach, [LeChBe04]. But when developing a complete variational formulation the two key characteristics of the LS approach also become the main cause of concern: reinitialization and the signed distance function. Although the problem of reinitialization here can also be avoided by using an harmonically extended velocity, the trouble concerning corner approximation persists. In contrast to this, by using an initial position set, we are deforming a virtual mesh of the structure, which is extended into the whole domain.

The equations we use are based on the momentum and mass conservation equations for the flow of an incompressible Newtonian fluid and the deformation of a compressible St. Venant-Kirchhoff or incompressible neo-Hookean solid. The spatial discretization is by a second-order finite element method with conforming equal-order (bilinear) trial functions using 'local projection stabilization' as introduced by Becker and Braack [BeBr01, BeBr03]. The time discretization uses the second-order 'fractional-step-θ' scheme originally proposed by Bristeau, Glowinski, and Periaux [BrGl+87]. This method has the same complexity as the Crank–Nicolson scheme but better stability properties [Rannacher00], see also [Rannacher04] and [Gl03].

Based on the Eulerian variational formulation of the FSI system, we use the 'dual weighted residual' (DWR) method, described in [BeRa95, BeRa01, BaRa03], to derive 'goal-oriented' a posteriori error estimates. The evaluation of these error estimates requires the approximate solution of a linear dual variational problem. The resulting a posteriori error indicators are then used for automatic local mesh adaption. The full application of the DWR method to FSI problems requires a Galerkin discretization in space as well as in time. Due to the use of a difference scheme in time, in this thesis we are limited to 'goal-oriented' mesh adaptation in

computing steady states or (somewhat heuristically) to quasi-steady states within the time stepping process.

As a validation of the Eulerian approach to structure mechanics we do a numerical study based on a basic structure with a piecewise constant material elasticity parameter. All calculations are done using both a conventional Lagrangian approach and the alternative Eulerian approach. In the first halve we show that for a given known solution the errors have an equal rate of convergence using both approaches. In the second halve we apply the DWR method to a similar problem. The material has a different elasticity parameter in the bottom and top halves of the domain. Here we demonstrate the efficiency of the DWR method for estimating the error of a given goal functional.

The method for computing FSI described in this thesis is validated at a stationary model problem that is a lid-driven cavity involving the interaction of an incompressible Stokes fluid with an incompressible neo-Hookean solid. Then, as a more challenging test the self-induced oscillation of a thin elastic bar immersed in an incompressible fluid is treated (FLUSTRUK-A benchmark described in [TuHr06] and [HronTurek206]). For this test problem, our method is also compared against a standard 'arbitrary Lagrangian-Eulerian' (ALE) approach. The possible potential of the fully Eulerian formulation of the FSI problem is indicated by its good behavior for large structure deformations. All computations and visualizations are done using the flow-solver package GASCOIGNE [Ga] and the graphics package VISUSIMPLE [BeDu06, Vi].

The outline of this thesis is as follows.

In the Chapters 2 and 3 we introduce the basic notation for all mathematical formulations that we later use. We explain the difference between the Eulerian and Lagrangian reference frames and why the natural frames of reference for fluids and solids are respectively Eulerian and Lagrangian.

In Chapter 4 we consequently introduce the governing equations for fluids and solids. We introduce the kinematic and dynamic interface conditions that have to be fulfilled at the common interface of the fluid and solid. For fluids we introduce the ALE framework and for structures we introduce the alternative Eulerian approach. This approach is based on the transport of the initial positions of the material points.

In Chapter 5 we write the complete variational fluid-structure interaction problem in a closed variational form. We do this for both approaches, first using the common ALE framework and then using the (to the authors knowledge, new) fully Eulerian framework.

In Chapter 6 we introduce the discretization of the complete variational problem. We explain the discretization of the mesh and the discretization of space and time. Based on this we explain the overall solution process. An important aspect is how we use the method of 'automatic differentiation' for calculation the directional derivatives of the monolithic problems.

In Chapter 7 we introduce the 'dual weighted residual' method, which is used to estimate the error of a given goal functional. This error estimator is used as an indicator for 'goal-oriented' mesh adaptation. We also discuss various numerical aspects that must be considered when implementing the Eulerian framework for FSI problems.

In Chapter 8 numeric tests are performed to compare and validate the Lagrangian and Eulerian approaches for elastic problems. In the first test we demonstrate for a basic configuration that the results of the Lagrangian and Eulerian approaches are in good agreement. In the second test we modify the structure to have a piecewise constant material parameter and so introduce a structure-structure interface problem. We do tests with two different interface orientations. In all tests we compare the Eulerian and Lagrangian frameworks in regards to the calculation of a specific goal functional. We apply the 'dual weighted residual' method for the approximation of the error of the goal functional. This is done initially for globally refined meshes as a validation of the error estimator for both the Lagrangian and the Eulerian frameworks. Finally we use the error estimator of the goal functional as a indicator for adaptively refining the meshes. We do this for both Eulerian and Lagrangian frameworks, and show that the results are in good agreement.

In Chapter 9 numeric tests are performed to compare and validate the Eulerian framework with the ALE framework for a basic fluid-structure interaction problem. As in the previous chapter the 'dual weighted residual' method is used to estimate the error of the given goal functional. This is first done on globally refined meshes. Later the estimator is used as an indicator for adaptive mesh refinement for both frameworks. Again, all results are in good agreement.

In Chapter 10 numeric tests are performed to compare and validate the fully Eulerian approach for an advanced fluid-structure interaction problem. The test is based on the FLUSTRUK-A benchmark [TuHr06]. The tests are broken down into four parts: transient tests of the structure in a resting fluid, drag and lift tests for the fluid with a very rigid structure, instationary tests displaying the periodic movement of the structure driven by the fluid flow, and finally transient tests for very large structure deformations in the resting fluid. These tests display two things. First, the capability of handling large deformations with the Eulerian approach. Second, three different refinement methods we demonstrate the advantage of using the DWR method.

Chapter 2

Mathematical notations and descriptions

In this chapter we introduce the basic notation for all mathematical formulations that we later use. We explain the difference between the Eulerian and Lagrangian reference frames and why the natural frames of reference for fluids and solids are respectively Eulerian and Lagrangian. Consequently we introduce the governing equations for fluids and solids. Finally we introduce the kinematic and dynamic interface conditions that have to be fulfilled at the common interface of the fluid and solid.

2.1 Notation

We begin with introducing some notation which will be used throughout the thesis. By $\Omega \subset \mathbb{R}^d$ ($d = 2$), we denote the domain of definition of the FSI problem. The domain Ω is supposed to be *time independent* but to consist of two time-dependent subdomains, the fluid domain $\Omega_f(t)$ and the structure domain $\Omega_s(t)$, with $t \in I_t := [0, T]$. Unless needed, the explicit time dependency will be skipped in this notation. The boundaries of Ω, Ω_f, and Ω_s are denoted by $\partial\Omega$, $\partial\Omega_f$, and $\partial\Omega_s$, respectively. The common interface between Ω_f and Ω_s is $\Gamma_i(t)$, or simply Γ_i.

The initial structure domain is denoted by $\widehat{\Omega}_s$. Spaces, domains, coordinates, values (such as pressure, displacement, velocity) and operators associated to $\widehat{\Omega}_s$ (or $\widehat{\Omega}_f$) will likewise be indicated by a 'hat'.

Given a subset $X \subset \Omega$ (e.g. $X = \Omega_f(t), X = \Omega_s(t)$ or any other subset), by $|X|$, we denote the volume of X. By $[f]_X$, we denote the jump $f_X^+ - f_X^-$ of a function f across the boundary ∂X. With f_X^+ and f_X^- we assume that f has a trace on ∂X, as seen from the 'inside' and 'outside' of X:

$$f_X^+(x) := \lim_{\epsilon \searrow 0} f(x + \epsilon n_X) \quad , \quad f_X^-(x) := \lim_{\epsilon \searrow 0} f(x - \epsilon n_X) \quad ,$$

where n_X is always the unit normal vector pointing out of X at points on the boundary ∂X.

2.2 Derivatives

Partial derivatives of a function f with respect to the $i-$th coordinate are denoted by $\partial_i f$, and the partial and total time-derivatives by $\partial_t f$ and $d_t f$. The divergences of vectors and tensors are written as $\mathrm{div} f = \sum_i \partial_i f_i$ and $(\mathrm{div} F)_i = \sum_j \partial_j F_{ij}$. The gradient of a vector valued function v is the tensor $(\nabla v)_{ij} = \partial_j v_i$.

Definition 2.1. Given a mapping $f : \Omega \to Y$ with $\Omega \subset X$ and X, Y are both normed vector spaces. The *'directional derivative'* of f at $x \in \Omega$ in the direction $\varphi \in X$ is defined as

$$f'(x)(\varphi) := \lim_{h \searrow 0} \frac{f(x + h\varphi) - f(x)}{h} \ ,$$

provided the limit exists. If the limit exists for any direction $\varphi \in X$ then f is simply called directionally differentiable at x.   ♮

Definition 2.2. In the context of Definition 2.1, if the mapping f is directionally differentiable at x and $f'(x)(\varphi)$ is continuous and linear for φ, then $f'(x) \in \mathrm{Hom}(X, Y)$ and $f'(x)$ is referred to as the *'Gâtaux derivative'* of f at x.   ♮

2.3 Function spaces

For a set X, we denote by $L^2(X)$ the Lebesque space of square-integrable functions on X equipped with the usual inner product and norm:

$$(f, g)_X := \int_X fg \ dx, \quad \|f\|_X^2 = (f, f)_X,$$

respectively, and correspondingly for scalar- and vector-valued functions. For matrix-valued functions, $(F, G)_X$ is to be understood as the tensor product $\int_X F : G \ dx$, with $F : G := \sum_{ij} F_{ij} G_{ij}$. Mostly the domain X will be Ω, in which case we will skip the domain index in products and norms. For Ω_f and Ω_s, we similarly indicate the associated spaces, products, and norms by a corresponding index 'f' or 's'.

Definition 2.3. A function $f \in L^2(X)$ has the *'(weak or distributional) derivative'* $v = \partial^\alpha f \in L^2(X)$ if
$$(\phi, v)_X = (-1)^{|\alpha|}(\partial^\alpha \phi, f)_X \quad \forall \phi \in C_0^\infty(X)$$
is satisfied, with the multi-index $\alpha = (\alpha_1, \ldots, \alpha_n), \alpha_i \in \mathbb{N}_0$. Here $|\alpha| := \alpha_1 + \cdots + \alpha_n$ and $\partial^\alpha := \partial^{|\alpha|}/(\partial^{\alpha_1} \ldots \partial^{\alpha_n})$. $C^\infty(X)$ denotes the space of infinitely differentiable functions and $C_0^\infty(X)$ denotes a subspace, whose elements are nonzero only on a subset of X. On this note we also define $x^\alpha := \Pi_{i=0}^n x_i^{\alpha_i}$, where $x = \{x_1, \cdots, x_n\}$.   ♮

Let $L_X := L^2(X)$ and $L_X^0 := L^2(X)/\mathbb{R}$. The functions in L_X (with $X = \Omega$, $X = \Omega_f(t)$, or $X = \Omega_s(t)$) with first-order distributional derivatives in L_X make up the Sobolev space

$H^1(X)$. Further, $H_0^1(X) = \{v \in H^1(X) : v_{|\partial X_D} = 0\}$, where ∂X_D is that part of the boundary ∂X at which Dirichlet boundary conditions are imposed. Further, we will use the function spaces $V_X := H^1(X)^d$, $V_X^0 := H_0^1(X)^d$, and for time-dependent functions

$$\mathcal{L}_X := L^2[0,T; L_X], \quad \mathcal{V}_X := L^2[0,T; V_X] \cap H^1[0,T; V_X^*],$$
$$\mathcal{L}_X^0 := L^2[0,T; L_X^0], \quad \mathcal{V}_X^0 := L^2[0,T; V_X^0] \cap H^1[0,T; V_X^*],$$

where V_X^* is the dual of V_X^0. Again, the X-index will be skipped in the case of $X = \Omega$, and for $X = \Omega_f$ and $X = \Omega_s$ a corresponding index 'f' or 's' will be used.

Chapter 3

Eulerian, Lagrangian and arbitrary Lagrangian-Eulerian reference frames

When modelling the movement of a spatial continuum two approaches are commonly used. The *Lagrangian* or *material* framework and the *Eulerian* or *spatial* framework. Both approaches have the simple goal of describing how a certain scalar value of interest $f : \mathbb{R}^2 \times I_t \to \mathbb{R}$ changes in space and with time.

Where the reference point of the value f is, is what distinguishes the two frameworks. We denote $x \in \mathbb{R}^2$ and $t \in I_t$ as the spatial and temporal coordinates. The function f is assumed to be sufficiently differentiable in space and time.

3.1 Lagrangian framework

In the Lagrangian framework one observes the value on a preselected point that is moving (and possibly accelerating) steadily through space. The initial position of the point at the initial time t_0 we define as $\hat{x}$. Thus the position (of the point) is a function of the initial position $\hat{x}$ and time t:

$$x = x(\hat{x}, t) .$$

We define the velocity v of this point as the total time derivative of its position x:

$$v(x, t) := d_t x(\hat{x}, t) = \partial_t x + \widehat{\nabla} x \, d_t \hat{x} .$$

Since $\hat{x}$ is the position of the point at an initial time it follows that it does not change in time, therefore $d_t \hat{x} = 0$ and $v = \partial_t x$.

To be more precise, in the Lagrangian framework we should refer to $f(x, t)$ as $\hat{f}(\hat{x}, t) := f(x(\hat{x}, t), t)$. Visually one can imagine that we are observing the value on a *material point* that was initially at the position $\hat{x}$ and is moving though space with the velocity v. The total time derivative of $\hat{f}$ in the Lagrangian framework can thus be written:

$$
\begin{aligned}
d_t \hat{f}(\hat{x}, t) &= \partial_t \hat{f}(\hat{x}, t) + \widehat{\nabla} \hat{f}(\hat{x}, t) \, d_t \hat{x} \\
&= \partial_t \hat{f}(\hat{x}, t) .
\end{aligned}
$$

Since the Lagrangian approach describes the movement and deformation of individual particles and volumes it follows that this framework is the natural approach for modelling structure dynamics.

3.2 Eulerian framework

In the Eulerian framework one observes the value at a fixed point x in space, hence this framework is also referred to as a spatial framework. Looking back at the Lagrangian framework one can imagine that at the point x at different times there will continuously be different material points moving through. Each such material point will have a respective initial position $\hat{x}$.

Thus the velocity v at this space-time position (x, t) is still to be understood as the velocity of the material point with the initial position $\hat{x}$:

$$v(x, t) := d_t x(\hat{x}, t) .$$

In an Eulerian framework the value of interest is written as $f(x, t)$, with t and x being anywhere within the permitted space-time continuum. Taking the total time derivative of the f leads to:
$$\begin{aligned} d_t f(x, t) &= \partial_t f(x, t) + \nabla f(x, t) \, d_t x \\ &= \partial_t f(x, t) + (v \cdot \nabla) f(x, t) . \end{aligned}$$

The second term is referred to as the *'transport'* or *'convection term'*. This term is a characteristic difference between the Eulerian and Lagrangian frameworks. In the Lagrangian framework when the total time-derivative is expanded into all its partial derivatives, there is no convective term due to the spatial parameter being constant in time. In contrast, in Eulerian frameworks convection can generally be expected in the expanded total time-derivative.

The Eulerian approach presents itself as the natural approach for modelling fluid flows. This follows as a consequence that one is less interested in the individual behavior of particles and more interested in flow properties at certain spatial points in the flow domain. In viscous fluids with behavior similar to soft materials, a Lagrangian approach would be plausible. Generally though particle movement in fluids is considerable and their initial positions in relation to each other have effectively nothing in common with their later relative positions. Hence the Eulerian framework presents itself as the natural approach to modelling fluid flows.

3.3 Arbitrary Lagrangian-Eulerian reference frame

The Lagrangian and Eulerian frameworks introduced in the previous sections are *natural* frameworks of reference. It is more common though that one will need a framework of reference that is *arbitrary* and independent of the initial particle positions or the spatial domain. A common example (one we will later also encounter in the numeric tests) is a fluid flow in a domain that changes with time: $\Omega(t)$. Instead of modelling and simulating the flow in $\Omega(t)$ one assumes the existence of an in space and time continuous and (for a fixed time t) C^2-diffeomorphic mapping $\hat{T}(\hat{x}, t) : \widehat{\Omega} \times I_t \to \Omega(t)$, with $\hat{\Omega}$ as the reference (and usually the initial) domain of $\Omega(t)$. The requirement of C^2-diffeomorphism means that the mapping is (in addition to being diffeomorphic) also two times continuously partially differentiable.

An approach that uses such an arbitrary framework of reference is called an *'arbitrary Lagrangian-Eulerian approach'* (ALE), see e.g. [HuLi+81]. We will also refer to an arbitrary framework as an *'ALE framework'*. For a good overview of the various methods of application using an ALE-framework see [BuSc+06] e.g. [HronTurek206].

With the help of the mapping $\hat{T}$ functions and operators in $\Omega(t)$ can be rewritten as such in the domain $\hat{\Omega}$. For this reason, as a preparatory measure, we introduce the most commonly needed transformation-identities in the following sections.

By $\hat{F}$ and $\hat{J}$, we denote the Jacobian matrix and determinant of $\hat{T}$ respectively:

$$\hat{F} := \widehat{\nabla}\hat{T} \quad , \quad \hat{J} := \det \hat{F} \ .$$

In the context of material deformations later the mapping $\hat{T}$ will also be referred to as the *'deformation'*, hence $\hat{F}$ will be referred to as the *'deformation gradient'*. Since $\hat{T}$ is a deformation, it must for each fixed time preserve orientation and *not annihilate* volume. This follows from the requirement, that it is continuous and diffeomorphic. Thus $0 < \hat{J}$.

Let $f(x,t)$ and $v(x,t)$ denote scalar- and vector-valued functions that are differentiable in time and space as in the previous sections (Section 3.1, 3.2).

With $\hat{T}$ we define $\hat{f}(\hat{x},t)$:

$$
\begin{aligned}
\hat{f}(\hat{x},t) &:= f(\hat{T}(\hat{x},t),t) \ , \\
\hat{v}(\hat{x},t) &:= v(\hat{T}(\hat{x},t),t) \ .
\end{aligned}
$$

3.3.1 Spacial derivatives

The respective reference based spatial derivatives of $\hat{f}$ can be attained by chain rule:

$$\widehat{\partial}_i \hat{f}(\hat{x},t) = \sum_j \partial_j f(\hat{T}(\hat{x}),t) \frac{\widehat{\partial}\hat{T}_j(\hat{x},t)}{\widehat{\partial}\hat{x}_i} \quad .$$

Thus we can write the gradient of $\hat{f}$:

$$\widehat{\nabla}\hat{f} = \hat{F}^T \, \nabla f \quad . \tag{3.1}$$

We apply equation (3.1) to $v(x,t)$, in this case the velocity-field, by applying it to its components:

$$\widehat{\nabla}\hat{v} = \nabla v \, \hat{F} \quad . \tag{3.2}$$

3.3.2 Temporal derivatives

Later we will need the partial time-derivative of a scaler function f in $\Omega(t)$. To this means we observe the partial time-derivative of $\hat{f}(\hat{x}, t) = f(\hat{T}(\hat{x}, t), t)$.

Proposition 3.1. (Fundamental ALE equation) Let $f(x, t) : \Omega \times I_t \to \mathbb{R}$ be continuously differentiable scalar function in space and time. The mapping $\hat{T}(\hat{x}, t) : \widehat{\Omega} \times I_t \to \Omega(t)$ is continuous in space and time and (for a fixed time t) a diffeomorphic mapping $\hat{\Omega} \to \Omega$. We express the values of f in the reference frame $\hat{\Omega}$ so that $\hat{f}(\hat{x}, t) = f(\hat{T}(\hat{x}, t), t)$. Then the partial and total time derivatives of f expressed in terms of $\hat{f}$ on the reference domain $\hat{\Omega}$ are,

$$
\begin{aligned}
\partial_t f &= \partial_t \hat{f} - (\hat{F}^{-1}\partial_t \hat{T} \cdot \widehat{\nabla})\hat{f} \,, & (3.3) \\
d_t f &= \partial_t \hat{f} + (\hat{F}^{-1}(\hat{v} - \partial_t \hat{T}) \cdot \widehat{\nabla})\hat{f} \,. & (3.4)
\end{aligned}
$$

Proof.

$$
\begin{aligned}
\partial_t \hat{f}(\hat{x}, t) &= \lim_{\Delta t \to 0} \frac{\hat{f}(\hat{x}, t + \Delta t) - \hat{f}(\hat{x}, t)}{\Delta t} \\
&= \lim_{\Delta t \to 0} \frac{f(\hat{T}(\hat{x}, t + \Delta t), t + \Delta t) - f(\hat{T}(\hat{x}, t), t)}{\Delta t} \\
&= \lim_{\Delta t \to 0} \frac{f(\hat{T}(\hat{x}, t + \Delta t), t + \Delta t) - f(\hat{T}(\hat{x}, t + \Delta t), t) + f(\hat{T}(\hat{x}, t + \Delta t), t) - f(\hat{T}(\hat{x}, t), t)}{\Delta t} \\
&= \partial_t f(\hat{T}(\hat{x}, t), t) + \nabla f(\hat{T}(\hat{x}, t), t) \cdot \partial_t \hat{T}(\hat{x}, t) \\
&= \partial_t f(x, t) + \nabla f(x, t) \cdot \partial_t \hat{T}(\hat{x}, t) \\
&= \partial_t f + (\partial_t \hat{T} \cdot \nabla) f & (3.5)
\end{aligned}
$$

Thus with equations (3.1) and (3.5) we can write the partial and total time-derivatives of f in the $\hat{\Omega}$ reference system:

$$
\begin{aligned}
\partial_t f &= \partial_t \hat{f} - (\hat{F}^{-1}\partial_t \hat{T} \cdot \widehat{\nabla})\hat{f} & (3.6) \\
d_t f &= \partial_t f + \nabla f \cdot v & (3.7) \\
&= \partial_t \hat{f} + ((v - \partial_t \hat{T}) \cdot \nabla) f & (3.8) \\
&= \partial_t \hat{f} + (\hat{F}^{-1}(\hat{v} - \partial_t \hat{T}) \cdot \widehat{\nabla})\hat{f} & (3.9)
\end{aligned}
$$

$\square$

Lemma 3.1. For a mapping $\hat{T}$ as in Proposition 3.1 and a vector-valued function $v : \Omega \times I_t \to \mathbb{R}^2$, whose components are as f in Proposition 3.1, the following holds,

$$
\begin{aligned}
\partial_t v &= \partial_t \hat{v} - (\hat{F}^{-1}\partial_t \hat{T} \cdot \widehat{\nabla})\hat{v} & (3.10) \\
d_t v &= \partial_t \hat{v} + (\hat{F}^{-1}(\hat{v} - \partial_t \hat{T}) \cdot \widehat{\nabla})\hat{v} & (3.11)
\end{aligned}
$$

Proof. Follows directly by applying (3.3) and (3.4) to the components of v. $\square$

3.3.3 Spacial integrals

Let $V \subset \Omega$ be an arbitrary volume in Ω, and $\hat{V} = \hat{T}^{-1}(V)$ the respective subset in $\hat{\Omega}$. With $\hat{f}(\hat{x}) = f(\hat{T}(\hat{x})) = f(x) \in L^2(\Omega)$ and $dx = \det\hat{T} \ d\hat{x} = \hat{J} \ d\hat{x}$, we transform the volume integral in V to an integral in $\hat{V}$:

$$\int_V f(x) \ dx = \int_{\hat{V}} \hat{f}(\hat{x}) \ \hat{J} \ d\hat{x} \ . \tag{3.12}$$

Theorem 3.1 (Divergence of the Piola transform). Let $\hat{T} : \hat{\Omega} \to \Omega$ be a C^2-diffeomorphism and the vector-valued function $v : \Omega \to \mathbb{R}^2$ be differentiable in Ω. The Piola transform of v is $\hat{J}\hat{F}^{-1}\hat{v}$. For the divergence of the Piola transform it holds,

$$\hat{J} \ \mathrm{div} v = \widehat{\mathrm{div}}(\hat{J}\hat{F}^{-1}\hat{v}) \qquad\qquad \forall x = \hat{T}(\hat{x}) \in \Omega \ . \tag{3.13}$$

Proof. For convenience we write $\hat{J}\hat{F}^{-1}$:

$$\hat{J}\hat{F}^{-1} = \begin{pmatrix} 1 + \widehat{\partial}_2\hat{u}_2 & -\widehat{\partial}_2\hat{u}_1 \\ -\widehat{\partial}_1\hat{u}_2 & 1 + \widehat{\partial}_1\hat{u}_1 \end{pmatrix} \ . \tag{3.14}$$

We expand $\widehat{\mathrm{div}}(\hat{J}\hat{F}^{-1}\hat{v})$:

$$\begin{aligned} \widehat{\mathrm{div}}(\hat{J}\hat{F}^{-1}\hat{v}) = & \ \widehat{\partial}_1(\ (1 + \widehat{\partial}_2\hat{u}_2)\hat{v}_1 + (\ -\widehat{\partial}_2\hat{u}_1)\hat{v}_2 \ ) \\ & + \widehat{\partial}_2(\ (\ -\widehat{\partial}_1\hat{u}_2)\hat{v}_1 + (1 + \widehat{\partial}_1\hat{u}_1)\hat{v}_2 \ ) \ . \end{aligned} \tag{3.15}$$

In (3.15) we apply the partial derivatives only to the left factors of all sums. Due to the regularity of $\hat{T}$, the partial derivatives may be switched,

$$\begin{aligned} (\ \widehat{\partial}_1(1 + \widehat{\partial}_2\hat{u}_2) \ \hat{v}_1 + \widehat{\partial}_1(\ -\widehat{\partial}_2\hat{u}_1) \ \hat{v}_2 \ ) & \\ + (\ \widehat{\partial}_2(\ -\widehat{\partial}_1\hat{u}_2) \ \hat{v}_1 + \widehat{\partial}_2(1 + \widehat{\partial}_1\hat{u}_1) \ \hat{v}_2 \ ) = & \ (\ \widehat{\partial}_1(1 + \widehat{\partial}_2\hat{u}_2) + \widehat{\partial}_2(\ -\widehat{\partial}_1\hat{u}_2) \ )v_1 \\ & + (\ \widehat{\partial}_1(\ -\widehat{\partial}_2\hat{u}_1) + \widehat{\partial}_2(1 + \widehat{\partial}_1\hat{u}_1) \ )v_2 \\ = & \ 0 \ . \end{aligned} \tag{3.16}$$

With (3.16) we write (3.15) as:

$$\begin{aligned} \widehat{\mathrm{div}}(\hat{J}\hat{F}^{-1}\hat{v}) = & \ (\ (1 + \widehat{\partial}_2\hat{u}_2)\widehat{\partial}_1\hat{v}_1 + (\ -\widehat{\partial}_2\hat{u}_1)\widehat{\partial}_1\hat{v}_2 \ ) \\ & + (\ (\ -\widehat{\partial}_1\hat{u}_2)\widehat{\partial}_2\hat{v}_1 + (1 + \widehat{\partial}_1\hat{u}_1)\widehat{\partial}_2\hat{v}_2 \ ) \\ = & \ \mathrm{tr}(\hat{J} \ \widehat{\nabla}\hat{v} \ \hat{F}^{-1}) = \hat{J} \ \mathrm{tr}(\nabla v) \\ = & \ \hat{J} \ \mathrm{div} v \ . \end{aligned} \tag{3.17}$$

$\square$

Remark 3.1. A byproduct of the first equality of (3.17) will later be useful for Reynold's transport theorem. We recall that $\hat{v}(\hat{x}) = d_t\hat{u}(\hat{x})$. For $\widehat{\mathrm{div}}(\hat{J}\hat{F}^{-1}\hat{v})$ we then obtain:

$$
\begin{aligned}
\widehat{\mathrm{div}}(\hat{J}\hat{F}^{-1}\hat{v}) =\ & (\ (1+\hat{\partial}_2\hat{u}_2)\hat{\partial}_1\hat{v}_1 + (\quad -\hat{\partial}_2\hat{u}_1)\hat{\partial}_1\hat{v}_2\ ) \\
& +(\ (\quad -\hat{\partial}_1\hat{u}_2)\hat{\partial}_2\hat{v}_1 + (1+\hat{\partial}_1\hat{u}_1)\hat{\partial}_2\hat{v}_2\ ) \\
=\ & \widehat{\mathrm{div}}\hat{v} + d_t(\hat{\partial}_2\hat{u}_2\hat{\partial}_1\hat{u}_1) - d_t(\hat{\partial}_2\hat{u}_1\hat{\partial}_1\hat{u}_2) \\
=\ & \widehat{\mathrm{div}}(d_t\hat{u}) + d_t(\hat{\partial}_2\hat{u}_2\hat{\partial}_1\hat{u}_1 - \hat{\partial}_2\hat{u}_1\hat{\partial}_1\hat{u}_2) \\
=\ & d_t(\widehat{\mathrm{div}}\hat{u} + \hat{\partial}_2\hat{u}_2\hat{\partial}_1\hat{u}_1 - \hat{\partial}_2\hat{u}_1\hat{\partial}_1\hat{u}_2) \\
=\ & d_t\hat{J}\ .
\end{aligned}
\tag{3.18}
$$

♮

Lemma 3.2. Let $v \in H^1(\Omega)$ and the mapping $\hat{T}$ is as previously defined. Let $V \subset \Omega$ be an arbitrary volume in Ω, and $\hat{V} = \hat{T}^{-1}(V)$ the respective subset in $\hat{\Omega}$. Then,

$$
\int_V \mathrm{div}v\ dx = \int_{\hat{V}} \widehat{\mathrm{div}}(\hat{J}\ \hat{F}^{-1}\ \hat{v})\ d\hat{x}\ .
\tag{3.19}
$$

Proof. Follows directly with (3.12) and Proposition 3.1. □

Lemma 3.3. Let $v \in H^1(\Omega)$ and the mapping $\hat{T}$ is as previously defined. Let $V \subset \Omega$ be an arbitrary volume in Ω, and $\hat{V} = \hat{T}^{-1}(V)$ the respective subset in $\hat{\Omega}$. Then,

$$
\int_{\partial V} v\cdot n\ dx = \int_{\partial\hat{V}} (\hat{J}\hat{F}^{-1}\hat{v})\cdot\hat{n}\ d\hat{x}\ .
\tag{3.20}
$$

Proof. We apply Gauss' theorem to the left and right boundary integrals in (3.20):

$$
\int_{\partial V} v\cdot n\ dx = \int_V \mathrm{div}v\ dx\ ,
\tag{3.21}
$$

$$
\int_{\partial\hat{V}} (\hat{J}\hat{F}^{-1}\hat{v})\cdot\hat{n}\ d\hat{x} = \int_{\hat{V}} \widehat{\mathrm{div}}(\hat{J}\hat{F}^{-1}\hat{v})\ d\hat{x}\ .
\tag{3.22}
$$

With Lemma 3.2 it follows that (3.21) and (3.22) are equal. □

Chapter 4

Equations

In the next two sections we introduce the equations that are used to model fluid flows and material deformations. Both are based on the assumption of conservation of certain properties. For fluid flows in the most general case one assumes in the model that mass, momentum, angular momentum and energy are conserved. In this thesis we will only be observing incompressible fluids, thus it is sufficient to use a model that only assumes the conservation of mass and momentum. For material deformations one only assumes the conservation of momentum and optionally also incompressibility.

An essential state variable in the momentum conservation equations is the Cauchy stress tensor. The tensor is used to model internal and surface forces of a body. The tensor has different constitutive laws depending on if it is in a fluid or solid, compressible or incompressible body. We briefly elucidate the Cauchy stress tensor.

4.1 Cauchy stress tensor

The tensor is a measure for the internal stress in a body. The basic principle, first proposed by Cauchy, is that within a body the forces an enclosed volume exerts outward towards the rest of the body are equal to the forces being exercised upon it from the outside inwards toward it.

The stress tensor field σ is a matrix-valued field. Provided a stress tensor field σ is known, the total force ΔF on a 'small' area ΔA can be calculated by applying σ to its normal n:

$$\Delta F = \sigma\, n\, |\Delta A|\ .$$

To be more precise $\sigma\, n$ at the point x is the force-density on an area ΔA with the normal n. To calculate the total force F on an enclosed volume V we apply this to the complete surface ∂V:

$$F = \int_{\partial V} \sigma\, n\, dx\ .$$

By applying Gauss' theorem the surface integral on ∂V can be replaced by a volume integral in V:

$$F = \int_{\partial V} \sigma\, n\, dx = \int_{V} \operatorname{div}\sigma\, dx\ . \tag{4.1}$$

The reference framework we have used so far is spatially based, hence Eulerian. We will though need the integrals in (4.1) in an arbitrary reference frame $\hat{V}$. We note that $(\mathrm{div}\sigma)_i = \sum_i \partial_j \sigma_{ij}$. We use the mapping $\hat{T}$ and notations described in Section 3.3 and apply the Lemmas 3.3 and 3.2 to (4.1):

$$F = \int_{\widehat{\partial V}} (\hat{J}\sigma\hat{F}^{-T})\,\hat{n}\;d\hat{x} = \int_{\hat{V}} \widehat{\mathrm{div}}(\hat{J}\sigma\hat{F}^{-T})\;d\hat{x}\;. \tag{4.2}$$

The 'transformed' stress tensor $\hat{J}\sigma\hat{F}^{-T}$ is also referred to as the *'first Piola-Kirchhoff stress tensor'*.

4.2 Reynold's transport theorem

For the conservation of mass and momentum we will need the following theorem.

Theorem 4.1 (Reynold's transport). Let $\hat{T} : \hat{\Omega} \times I_t \to \Omega$ be a C^2-diffeomorphism and the scalar function $f(x,t) : \Omega \times I_t \to \mathbb{R}$ be differentiable in $\Omega \times I_t$. Then for any subset $\hat{V} \subset \hat{\Omega}$ the following holds,

$$d_t \int_{V(t)} f\;dx = \int_{V(t)} \partial_t f + \mathrm{div}(fv)\;dx\;, \tag{4.3}$$

with $V(t) = \{x \in \Omega \mid \hat{T}^{-1}(x,t) \in \hat{V}\}$.

Proof. We transform the left integral of (4.3) into an integral on the reference domain. Since the integration domain is time invariant, integration and the total time derivative can then be switched:

$$d_t \int_{V(t)} f\;dx = d_t \int_{\hat{V}} \hat{f}\,\hat{J}\;d\hat{x} = \int_{\hat{V}} d_t\hat{f}\,\hat{J} + \hat{f}\,d_t\hat{J}\;d\hat{x}\;. \tag{4.4}$$

With Remark 3.1 we know $d_t\hat{J} = \widehat{\mathrm{div}}(\hat{J}\hat{F}^{-1}\hat{v})$:

$$d_t \int_{V(t)} f\;dx = \int_{\hat{V}} d_t\hat{f}\,\hat{J} + \hat{f}\,\widehat{\mathrm{div}}(\hat{J}\hat{F}^{-1}\hat{v})\;d\hat{x}\;. \tag{4.5}$$

With (3.12) and Lemma 3.2 we transform the reference integral back to V:

$$
\begin{aligned}
d_t \int_{V(t)} f\;dx &= \int_V d_t f + f\,\mathrm{div}v\;dx \\
&= \int_V \partial_t f + \nabla f\;v + f\,\mathrm{div}v\;dx \\
&= \int_V \partial_t f + \mathrm{div}(fv)\;dx\;.
\end{aligned}
$$

$\square$

Mass conservation follows immediately, by using for f the density ρ.

Theorem 4.2 (Mass conservation). Let $\hat{T} : \hat{\Omega} \times I_t \to \Omega$ be a C^2-diffeomorphism. Let the Lagrangian material density be $\hat{\rho}(\hat{x})$ be differentiable and the respective Eulerian density be defined by $\rho(x,t) := \hat{\rho}(\hat{T}^{-1}(x,t))$. Then for any subset $\hat{V} \subset \hat{\Omega}$ the following holds

$$\int_{V(t)} \partial_t \rho + \mathrm{div}(\rho v) \ dx \ = 0 \ , \tag{4.6}$$

with $V(t) = \{x \in \Omega \mid \hat{T}^{-1}(x,t) \in \hat{V}\}$.

Proof. We transform the integral of (4.6) into an integral on the reference domain. The total mass $M(\hat{V})$ on the reference domain is constant, thus $d_t M(\hat{V}) = 0$. With Theorem 4.1 it follows:

$$0 = d_t \int_{\hat{V}} \hat{\rho} \ \hat{J} \ d\hat{x} \ = d_t \int_{V(t)} \rho \ dx = \int_{V(t)} \partial_t \rho + \mathrm{div}(\rho v) \ dx \ . \tag{4.7}$$

$\square$

Lemma 4.1. (Continuity equation) Since ρ is continuous and (4.6) is valid for any $V \subset \Omega$. It follows for any $(x,t) \in \Omega \times I_t$:

$$\partial_t \rho + \mathrm{div}(\rho v) = 0 \ . \tag{4.8}$$

$\square$

4.3 Conservation of momentum

Both the fluid and structure models have the momentum conservation law in common. The model is based on Newton's second law, which states that the temporal change of momentum in a body with the volume $V \subset \Omega$ is equal to the surface and volume forces acting upon this body. The law is set in an Eulerian framework.

$$\underbrace{d_t \int_V \rho v \ dx}_{\text{change of momentum}} = \underbrace{\int_{\partial V} \sigma \, n \ dx}_{\text{surface force}} + \underbrace{\int_V \rho f \ dx}_{\text{volume force}} \tag{4.9}$$

We apply Reynold's Theorem 4.1 to the left integral and Gauss' theorem to the surface integral:

$$\int_V \partial_t(\rho v) + \mathrm{div}(\rho v \otimes v) - \mathrm{div}\sigma \ dx \ = \int_V \rho f \ dx \ , \tag{4.10}$$

with the outer product $\rho v \otimes v = \rho v v^T = \rho(v_i v_j)_{i,j=1}^2$. Of (4.10) we expand just $\partial(\rho v) +$ $\mathrm{div}(\rho v \otimes v)$ as:

$$
\begin{aligned}
\partial_t(\rho v) \;+\; \mathrm{div}(\rho v \otimes v) \;&=\; \partial_t \rho\, v + \rho\, \partial_t v \quad + v\, \mathrm{div}(\rho v) + \rho(v\cdot\nabla)v \\
&=\; \rho\, \partial_t v + \rho(v\cdot\nabla)v + v\, \underbrace{(\partial_t\rho + \mathrm{div}(\rho v))}_{=0\ \ (\text{Lemma 4.1})} \\
&=\; \rho\, \partial_t v + \rho(v\cdot\nabla)v \; .
\end{aligned}
\tag{4.11}
$$

We apply (4.11) to (4.10). With the additional assumption that the integrands are steady in V and since the equation (4.10) holds for arbitrary V, we conclude:

$$
\rho\partial_t v + \rho(v\cdot\nabla)v - \mathrm{div}\sigma \;=\; \rho f \; .
\tag{4.12}
$$

We will also need equation (4.12) in an ALE framework with the respective reference frame $\hat{V}$. We use the mapping $\hat{T}$ and notations described in Section 3.3 and apply the 'ALE equations' (3.11) and (4.2) to (4.10):

$$
\int_{\hat{V}} \hat\rho \hat{J} \partial_t \hat{v} + \hat\rho \hat{J}(\hat{F}^{-1}(\hat{v} - \partial_t\hat{T})\cdot\widehat{\nabla})\hat{v} - \widehat{\mathrm{div}}(\hat{J}\sigma\hat{F}^{-T})\, d\hat{x} \;=\; \int_{\hat{V}} \hat{J}\hat\rho\hat{f}\, d\hat{x} \; .
\tag{4.13}
$$

Steadiness of the integrands here follows from the mapping being continuously differentiable and the steadiness of the original integrands in the Eulerian framework. Based on this and since the equation (4.13) holds for arbitrary V (and respective $\hat{V}$), we conclude:

$$
\hat\rho \hat{J} \partial_t \hat{v} + \hat\rho \hat{J}(\hat{F}^{-1}(\hat{v} - \partial_t\hat{T})\cdot\widehat{\nabla})\hat{v} - \widehat{\mathrm{div}}(\hat{J}\sigma\hat{F}^{-T}) \;=\; \hat{J}\hat\rho\hat{f} \; .
\tag{4.14}
$$

4.4 Fluid flows

Fluid flows (liquid and gas) in the most general sense are modelled based on the assumption that mass, momentum, angular momentum and energy are conserved.

In this thesis we will only be observing 'incompressible Newtonian fluid flows'. From the incompressibility it follows that the density ρ is constant. The constitutive relation for the Cauchy stress tensor in the case of an incompressible Newtonian fluid is:

$$
\sigma := -pI + \rho\nu(\nabla v + \nabla v^T) \; ,
\tag{4.15}
$$

with the kinematic viscosity ν, the pressure p and the velocity v. Hence σ is symmetric. Angular momentum is automatically fulfilled for incompressible Newtonian fluid flows. Based on this the conservation equations for momentum and mass decouple from the energy conservation equation. We will not need the temperature or the specific internal energy-density state variables, hence we omit the energy conservation equation. Thus we only consider the conservation equations for momentum and mass (respectively):

$$
\begin{aligned}
\rho\partial_t v + \rho(v\cdot\nabla)v + \mathrm{div}\,\sigma \;&=\; \rho f \quad \text{in } \Omega_f \; , \\
\mathrm{div}\, v \;&=\; 0 \quad \text{in } \Omega_f \; .
\end{aligned}
\tag{4.16}
$$

The momentum equations (4.16) with the Cauchy stress tensor as defined in (4.15) are referred to as the 'Navier-Stokes equations'.

Remark 4.1. The Navier-Stokes equations for incompressible fluids are usually not written with the *full* stress tensor σ (4.15), but instead with a reduced version of the tensor $\tilde{\sigma} := -pI + \mu\nabla v$. This stems from the feature that $\mathrm{div}\nabla v^T = 0$ (provided v is two times continuously partially differentiable):

$$\mathrm{div}\nabla v^T = \mathrm{div}\left(\begin{array}{cc} \partial_1 v_1 & \partial_1 v_2 \\ \partial_2 v_1 & \partial_2 v_2 \end{array}\right) = \left(\begin{array}{c} \partial_1\partial_1 v_1 + \partial_2\partial_1 v_2 \\ \partial_1\partial_2 v_1 + \partial_2\partial_2 v_2 \end{array}\right) = \left(\begin{array}{c} \partial_1\mathrm{div}v \\ \partial_2\mathrm{div}v \end{array}\right) = 0 \ .$$

We refrain from using the reduced tensor $\tilde{\sigma}$, since this would lead to an incorrect representation of the boundary forces. The proper calculation of these forces is most important, since fluid-structure interaction is essentially driven by just these forces at the interface. ♮

Common notations for the stress tensor and various constituents are:

- *'deformation rate tensor'*, $\epsilon(v) := (\nabla v + \nabla v^T)/2$,
- *'dynamic viscosity'*, μ , the product of the density and kinematic viscosity: $\mu = \rho\nu$,
- *'isotropic or hydrostatic stress tensor'*, $-pI$,
- *'viscous or deviatoric stress tensor'*, $\tau := 2\mu(\epsilon - \frac{1}{d}\mathrm{tr}\epsilon\, I)$ (in d-dimensions),
- if finally the fluid is incompressible, we obtain the constitutive relation $\sigma = -pI + \tau$ (4.15), since $\mathrm{tr}\epsilon = \mathrm{div}v$.

Remark 4.2. The motivation for splitting the stress tensor into the two parts, hydrostatic and deviatoric stress, is to express it in a part that exerts the same force in all directions outwards and is independent of the velocity, hence hydrostatic, and a part that only depends on the velocity and does *not* exert the same force, hence deviatoric. ♮

Remark 4.3. We have omitted writing a superfluous 'f' index on all variables such as the density, velocity and pressure since in this context there is no mention of any structure variables. ♮

4.4.1 Boundary conditions

Generally when modelling flows using an Eulerian framework the boundaries are fixed and not moving. As a boundary condition in time an initial value v_0 for v at the initial time t_0 is prescribed. Spacially the boundary $\partial\Omega_f$ can be split in four non-overlapping parts

$$\partial\Omega_f = \Gamma_{fD} \cup \Gamma_{fN} \cup \Gamma_{fR} \cup \Gamma_i \ ,$$

with each part relating to a different boundary condition. The first three parts are the well-known conditions:

$$\begin{array}{rrccl} \text{Dirichlet} & : & v & = & v_{fD} \qquad \text{on } \Gamma_{fD} \ , \\ \text{Neumann} & : & \sigma n_f & = & g_f \qquad \text{on } \Gamma_{fN} \ , \\ \text{Robin} & : & \alpha v + \sigma n_f & = & 0 \qquad \text{on } \Gamma_{fR} \ , \alpha \in \mathbb{R} \ . \end{array}$$

In the fluid-structure interaction problems there is a moving interface boundary Γ_i, that is the common boundary to the structure. We assume that on this boundary momentum is conserved and that the velocity of the fluid and material particles just at the boundary are equal. This leads to the FSI boundary conditions on Γ_{fi} that must be fulfilled simultaneously: continuity of velocity and the continuity of the force-density acting onto the interface, hence:

$$v_f = v_s \qquad \text{on } \Gamma_i \,,$$
$$\sigma_f n_f = \sigma_s n_f \quad \text{on } \Gamma_i \,.$$

To differentiate the fluid and structure values we have added a respective 'f' or 's' suffix.

4.4.2 Variational formulation

The variational form of the Navier-Stokes equations (4.16) is now obtained by multiplying them with suitable test functions from the trail space V_f^0 for the momentum equations and L_f for the mass conservation equation. In the momentum equations we integrate by parts. The equations are written in an Eulerian framework in the time-dependent domain $\Omega_f(t)$. The physical unknowns are the scalar pressure field $p_f \in \mathcal{L}_f$ and the vector velocity field $v_f \in v_f^D + \mathcal{V}_f$.

Problem 4.1 (Variational fluid problem, Eulerian framework). *Find* $\{v_f, p_f\} \in \{v_f^D + \mathcal{V}_f^0\} \times \mathcal{L}_f$, *such that* $v_f(0) = v_f^0$, *and*

$$(\rho_f(\partial_t + v_f \cdot \nabla)v_f, \psi^v)_f + (\sigma_f, \nabla \psi^v)_f = (g_f, \psi^v)_{\Gamma_{Nf}} + (\sigma_f n_f, \psi^v)_{\Gamma_i} + (\rho_f f_f, \psi^v)_f,$$
$$(\text{div}\,v_f, \psi^p)_f = 0, \tag{4.17}$$

for all $\{\psi^v, \psi^p\} \in V_f^0 \times L_f$, *where*

$$\sigma_f := -p_f I + 2\rho_f \nu_f \epsilon(v_f), \quad \epsilon(v) := \tfrac{1}{2}(\nabla v + \nabla v^T).$$

Here, v_f^D is a suitable extension of the prescribed Dirichlet data on the boundaries (both moving or stationary) of Ω_f, and g_f is the Neumann boundary condition on Γ_{fN}. We have *hidden* the fluid-structure interface condition of steadiness of velocity in part of the boundary condition v_f^D. The fluid-structure interface condition of steadiness of $\sigma_f n_f$ we have let stand. The FSI boundary conditions will be treated in Section 5.2.

4.5 Fluid flows in an ALE framework

In fluid-structure interaction problems that we will later be observing the FSI domain Ω is time independent, but it is composed of the fluid domain Ω_f and the structure domain Ω_s, which will be changing with time. An approach to modelling a fluid flow in a dynamic domain is assuming that a reference domain $\hat{\Omega}_f$ and piecewise continuously differentiable invertible mapping $\hat{T}$ exist so that $\hat{T}(\hat{x}, t) : \hat{\Omega}_f \times I_t \to \Omega(t)$.

Based on this assumption we rewrite the Navier-Stokes equations in an ALE framework with the reference frame $\hat{\Omega}_f$. We use the mapping $\hat{T}$ and notations described in Section 3.3. We apply the equations (3.2), (3.13) and (4.14) to (4.16) and (4.15):

$$
\begin{aligned}
\hat{J}\rho\partial_t\hat{v} + \hat{J}\rho(\hat{F}^{-1}(\hat{v} - \partial_t\hat{T})\cdot\widehat{\nabla})\hat{v} - \widehat{\text{div}}(\hat{J}\hat{\sigma}\hat{F}^{-T}) &= \hat{J}\rho\hat{f} \quad \text{in } \hat{\Omega}_f \,, \\
\widehat{\text{div}}(\hat{J}\hat{F}^{-1}\hat{v}) &= 0 \quad\ \text{in } \hat{\Omega}_f \,,
\end{aligned}
$$

$$
\text{with} \quad \hat{\sigma} := -\hat{p}I + \rho\nu(\widehat{\nabla}\hat{v}\hat{F}^{-1} + \hat{F}^{-T}\widehat{\nabla}\hat{v}^T) \,, \hat{F} := \widehat{\nabla}\hat{T} \,, \hat{J} := \det\hat{F} \,.
$$

$$(4.18)$$

4.5.1 Boundary conditions

Similarly the boundary conditions must be set in the ALE framework. As a boundary condition in time the same initial value is prescribed $\hat{v}_0(\hat{x}, 0) = v_0(\hat{T}(\hat{x}, 0)) = v_0$ for $\hat{v}$, now set in the ALE framework, at the initial time t_0. The fluid boundary $\hat{\Omega}_f$ can be split into four non-overlapping parts:

$$
\partial\hat{\Omega}_f = \hat{\Gamma}_{fD} \cup \hat{\Gamma}_{fN} \cup \hat{\Gamma}_{fR} \cup \hat{\Gamma}_i \,,
$$

with each part relating to a different boundary condition. The first three parts are the well-known conditions:

$$
\begin{aligned}
\text{Dirichlet} \quad &: & \hat{v} &= \hat{v}_D & \text{on } \hat{\Gamma}_{fD} \,, \\
\text{Neumann} \quad &: & \hat{J}\hat{\sigma}\hat{F}^{-T}\hat{n} &= \hat{g} & \text{on } \hat{\Gamma}_{fN} \,, \\
\text{Robin} \quad &: & \alpha\hat{v} + \hat{J}\hat{\sigma}\hat{F}^{-T}\hat{n} &= 0 & \text{on } \hat{\Gamma}_{fR} \,.
\end{aligned}
$$

The moving boundary Γ_i is of course a fixed boundary $\hat{\Gamma}_i$ on the reference domain. In an Eulerian framework the boundary conditions on the moving boundary Γ_i are the same as in fluid flows case: continuity of velocity v and the normal-flux of the stress σn. In the reference configuration the velocity is not transformed. The stress though is transformed, since not the Cauchy stress tensor is used in the momentum conservation equations, but instead the first Piola-Kirchhoff stress tensor. This leads to the boundary conditions:

$$
\begin{aligned}
\hat{v}_f &= \hat{v}_s & \text{on } \hat{\Gamma}_i \,, \\
\hat{J}_f\hat{\sigma}_f\hat{F}_f^{-T}\hat{n}_f &= \hat{J}_s\hat{\sigma}_s\hat{F}_s^{-T}\hat{n}_f & \text{on } \hat{\Gamma}_i \,.
\end{aligned}
$$

To differentiate the fluid and material values we have added a respective 'f' or 's' suffix.

4.5.2 Variational formulation

The variational form of the Navier-Stokes equations in an ALE framework (4.18) is obtained by multiplying them with suitable test functions from the trail space $\hat{V}_f^0$ for the momentum equations and $\hat{L}_f$ for the mass conservation equation. In the momentum equations we integrate by parts. The equations are written in an ALE framework in the domain $\hat{\Omega}_f$. For

later purposes we take care to write all fluid specific variables with a respective 'f' suffix, this includes the domain mapping, now referred to as $\hat{T}_f$. The physical unknowns are the scalar pressure field $\hat{p}_f \in \hat{\mathcal{L}}_f$ and the vector velocity field $\hat{v}_f \in \hat{v}_f^D + \hat{\mathcal{V}}_f$.

Problem 4.2 (Variational fluid problem, ALE framework). *Find* $\{\hat{v}_f, \hat{p}_f\} \in \{\hat{v}_f^D + \hat{\mathcal{V}}_f^0\} \times \hat{\mathcal{L}}_f$, *such that* $\hat{v}_f(0) = \hat{v}_f^0$, *and*

$$(\hat{J}_f \rho_f \partial_t \hat{v}_f + \hat{J}_f \rho_f (\hat{F}_f^{-1}(\hat{v}_f - \partial_t \hat{T}_f) \cdot \widehat{\nabla}) \hat{v}_f, \hat{\psi}^v)_{\hat{f}} + (\hat{J}_f \hat{\sigma}_f \hat{F}_f^{-T}, \widehat{\nabla} \hat{\psi}^v)_{\hat{f}}$$
$$= (\hat{g}_f, \hat{\psi}^v)_{\hat{\Gamma}_{fN}} + (\hat{J}_f \hat{\sigma}_f \hat{F}_f^{-T} \hat{n}_f, \hat{\psi}^v)_{\hat{\Gamma}_i} + (\rho_f \hat{J}_f \hat{f}_f, \hat{\psi}^v)_{\hat{f}}, \qquad (4.19)$$
$$(\widehat{\text{div}}(\hat{J}_f \hat{F}_f^{-1} \hat{v}_f), \hat{\psi}^p)_{\hat{f}} = 0,$$

for all $\{\hat{\psi}^v, \hat{\psi}^p\} \in \hat{V}_f^0 \times \hat{L}_f$, *where*

$$\hat{\sigma}_f := -\hat{p}_f I + \rho_f \nu_f (\widehat{\nabla} \hat{v}_f \hat{F}_f^{-1} + \hat{F}_f^{-T} \widehat{\nabla} \hat{v}_f^T),$$
$$\hat{F}_f := \widehat{\nabla} \hat{T}_f, \hat{J}_f := \det \hat{F}_f.$$

Here, $\hat{v}_f^D$ is a suitable extension of the prescribed Dirichlet data on the boundaries of $\hat{\Omega}_f$, and $\hat{g}_f$ is the Neumann boundary condition on $\hat{\Gamma}_{fN}$. We have 'hidden' the fluid-structure interface condition of steadiness of velocity in part of the boundary condition $\hat{v}_f^D$. The fluid-structure interface condition of steadiness of $\hat{J}_f \hat{\sigma}_f \hat{F}_f^{-T} \hat{n}_f$ we have let stand for later purposes. The FSI boundary conditions will be treated in Section 5.1.

4.6 Material deformations

Materials deformations are modelled based on the assumption of conservation of momentum and optionally volume. The main value of interest is the vector field describing the displacement of the body from its initial state. Consequently the Lagrangian approach is the natural frame of reference.

In this thesis we will be observing *elastic* materials, that is to say the observed material returns to its initial state once all applied forces are removed. We refer to the domain of the initial state as $\hat{\Omega}_s$ and use the mapping $\hat{T}$ and notations described in Section 3.3. The reference domain is also referred to as the *'reference configuration'*.

The displacement $\hat{u}$ and mapping $\hat{T}$, also referred to as *'deformation'*, suffice the following equation:

$$\hat{T}(\hat{x}, t) = \hat{x} + \hat{u}(\hat{x}, t).$$

The gradient of $\hat{T}$ is the deformation gradient $\hat{F} = \widehat{\nabla} \hat{T}$. The used state variable fields are the density $\hat{\rho}$ in the initial state, the velocity $\hat{v}$, the displacement $\hat{u}$, the Cauchy stress tensor $\hat{\sigma}$, which is a function of $\hat{u}$ and optionally a pressure $\hat{p}$. The external force field we denote as $\hat{f}$, an example for $\hat{f}$ would be a gravitational force field.

The material elasticity is usually described by a set of two parameters, the Poisson ratio ν_s and the Young modulus E_s, or alternatively, the Lamé coefficients λ_s and μ_s. These parameters satisfy the following relations:

$$
\begin{aligned}
\nu_s &= \tfrac{\lambda_s}{2(\lambda_s+\mu_s)} \;, & E_s &= \mu_s \tfrac{3\lambda_s+2\mu_s}{\lambda_s+\mu_s} \;, \\
\mu_s &= \tfrac{E_s}{2(1+\nu_s)} \;, & \lambda_s &= \tfrac{\nu_s E_s}{(1+\nu_s)(1-2\nu_s)} \;,
\end{aligned}
\tag{4.20}
$$

where $\nu_s = \frac{1}{2}$ for incompressible and $\nu_s < \frac{1}{2}$ for compressible material. Common notations for the stress tensor and various constituents are:

$$
\begin{array}{ll}
1^{st} \text{and } 2^{nd} \text{ Piola-Kirchhoff stress tensors:} & P := \hat{J}\hat{\sigma}\hat{F}^{-T} \;,\; S := \hat{F}^{-1}P, \\
\text{Green-Lagrange strain tensor:} & \hat{E} := \tfrac{1}{2}(\hat{F}^T\hat{F} - I) \;, \\
\text{left and right Cauchy-Green deformation tensors:} & \hat{F}\hat{F}^T \;,\; \hat{F}^T\hat{F} \;.
\end{array}
\tag{4.21}
$$

We encountered the first Piola-Kirchhoff stress tensor as the 'transformed' stress tensor on the reference domain $\hat{\Omega}$ in Section 4.1.

Principally the momentum conservation equations here are the same as with fluid flows, the only differences are that they are commonly set in a Lagrangian framework and the constitutive equation for the Cauchy stress tensor is based on the displacement field and not the velocity field. The equations for the elastic materials below differ slightly due to the different constitutive laws for the stress tensor.

Remark 4.4. As with the fluid equations, to keep things terse, we will omitted writing a 's' index on many variables such as the density, velocity and pressure since in this context there is no mention of any fluid variables. ♮

4.6.1 Compressible St. Venant-Kirchhoff material

The St. Venant-Kirchhoff model is a classical nonlinear model for compressible elastic materials. It is well suited for large displacements with the limitation of small strains $\hat{E}$. The sought unknowns are the displacement $\hat{u}$ and velocity $\hat{v}$.

$$
\begin{aligned}
\hat{\rho}\,d_t\hat{v} - \widehat{\operatorname{div}}(\hat{J}\hat{\sigma}\hat{F}^{-T}) &= \hat{\rho}\hat{f} & \text{in } \hat{\Omega}_s \;, \\
d_t\hat{u} - \hat{v} &= 0 & \text{in } \hat{\Omega}_s \;,
\end{aligned}
\tag{4.22}
$$

with $\hat{\sigma} = \hat{J}^{-1}\hat{F}(\lambda_s(\operatorname{tr}\hat{E})I + 2\mu_s\hat{E})\hat{F}^T$.

4.6.2 Incompressible neo-Hookean material

Numerous materials can be subjected to strains without a noticeable change of volume. Typical examples of such materials are plastics and rubber-like substances. A common idealization in continuum and computational mechanics is to regard such materials as generally incompressible that only permit so-called *'isochoric'* deformations. The incompressibility

of the material is ensured by demanding that the deformation conserve volume, hence the additional constraint $\hat{J} = 1$. The sought unknowns are the displacement $\hat{u}$, the velocity $\hat{v}$ and $\hat{p}$, which is referred to as the (hydrostatic) pressure.

$$\begin{aligned} \hat{\rho}\, d_t \hat{v} - \widehat{\operatorname{div}}(\hat{\sigma} \hat{F}^{-T}) &= \hat{\rho} \hat{f} & \text{in } \hat{\Omega}_s\,, \\ d_t \hat{u} - \hat{v} &= 0 & \text{in } \hat{\Omega}_s\,, \\ \hat{J} &= 1 & \text{in } \hat{\Omega}_s\,, \end{aligned} \tag{4.23}$$

$$\text{with} \quad \hat{\sigma} = -\hat{p}I + \mu_s(\hat{F}\hat{F}^T - I)\,.$$

As a consequence of the incompressibility (the Poisson ratio is $\nu_s = 0.5$) it follows that only one material constant is needed to describe the material behavior. Usually this will either be the Young modulus E_s or the Lamé coefficient μ_s.

4.6.3 Boundary conditions

Generally when modelling materials the boundaries will be moving in time, in an Eulerian approach a moving boundary leads to complications when posing or enforcing boundary conditions. Thus a Lagrangian framework is the preferred approach, leading to 'no-hassle' boundary conditions in the reference configuration. As a boundary condition in time initial values $\hat{u}_0, \hat{v}_0$ for $\hat{u}, \hat{v}$ at the initial time t_0 are prescribed. Similar to the fluid boundary conditions, the material boundary Ω_s can be split into four non-overlapping parts:

$$\partial \hat{\Omega}_s = \hat{\Gamma}_{sD} \cup \hat{\Gamma}_{sN} \cup \hat{\Gamma}_{sR} \cup \hat{\Gamma}_i\,,$$

with each part relating to a different boundary condition. The first three parts are the well-known conditions:

$$\begin{aligned} \text{Dirichlet} \quad &: & \hat{u} = \hat{u}_D\,, \hat{v} &= \hat{v}_D & \text{on } \hat{\Gamma}_{sD}\,, \\ \text{Neumann} \quad &: & \hat{J}\hat{\sigma}\hat{F}^{-T}\hat{n} &= \hat{g} & \text{on } \hat{\Gamma}_{sN}\,, \\ \text{Robin} \quad &: & \alpha\hat{v} + \hat{J}\hat{\sigma}\hat{F}^{-T}\hat{n} &= 0 & \text{on } \hat{\Gamma}_{sR}\,. \end{aligned}$$

The moving boundary Γ_i is of course a fixed boundary $\hat{\Gamma}_i$ on the reference domain. We assume that an appropriate mapping of initial fluid domain $\hat{\Omega}_f$ on the present domain Ω_f is provided. With this in mind, we can rewrite the fluid values v and σ in an ALE framework. In an Eulerian framework the boundary conditions on the moving boundary Γ_i are the same as in fluid flows case (Section 4.7.1) : continuity of velocity v and the normal-flux of the stress σn. In the reference configuration the velocity is not transformed. The stress though is transformed, since not the Cauchy stress tensor is used in the momentum conservation equations, but instead the first Piola-Kirchhoff stress tensor. This leads to the boundary conditions:

$$\begin{aligned} \hat{v}_f &= \hat{v}_s & \text{on } \hat{\Gamma}_i\,, \\ \hat{J}_s \hat{\sigma}_s \hat{F}_s^{-T} \hat{n}_s &= \hat{J}_f \hat{\sigma}_f \hat{F}_f^{-T} \hat{n}_s & \text{on } \hat{\Gamma}_i\,. \end{aligned}$$

To differentiate the fluid and material values we have added a respective 'f' or 's' suffix. Similar to the structure variables the fluid variables are also denoted with a 'hat', this indicates that they are set in an ALE framework.

4.6.4 Variational formulation

For later purposes we take care to write all structure specific variables with a respective 's' suffix, this includes the domain mapping, now referred to as $\hat{T}_s$.

For the sake of simplicity, we assume that the only boundary displacements that take place are on $\hat{\Gamma}_i$, i.e.,

$$\hat{u}_s^D = \hat{v}_s^D = 0 \ \text{ on } \partial\hat{\Omega}_s \setminus \hat{\Gamma}_i.$$

St. Venant-Kirchhoff material

The variational form of the structure equations for compressible St. Venant-Kirchhoff materials in a Lagrangian framework (4.22) is obtained by multiplying them with suitable test functions from the trail space $\hat{V}_s^0$ for the momentum conservation and velocity equations. In the momentum equations we integrate by parts.

Problem 4.3 (Variational structure problem, St. Venant-Kirchhoff, Lagrangian framework).
Find $\{\hat{u}_s, \hat{v}_s\} \in \{\hat{u}_s^D + \hat{\mathcal{V}}_s^0\} \times \{\hat{v}_s^D + \hat{\mathcal{V}}_s^0\}$, *such that* $\hat{u}_s(0) = \hat{u}_s^0$, $\hat{v}_s(0) = \hat{v}_s^0$, *and*

$$(\hat{\rho}_s d_t \hat{v}_s, \hat{\psi}^v)_{\hat{s}} + (\hat{J}_s \ \hat{\sigma}_s \ \hat{F}_s^{-T}, \widehat{\nabla}\hat{\psi}^v)_{\hat{s}}$$
$$= (\hat{g}_s, \hat{\psi}^v)_{\hat{\Gamma}_{sN}} + (\hat{J}_s \hat{\sigma}_s \hat{F}_s^{-T} \ \hat{n}_s, \hat{\psi}^v)_{\hat{\Gamma}_i} + (\hat{\rho}_s \hat{f}_s, \psi^v)_{\hat{s}} \ , \qquad (4.24)$$
$$(d_t \hat{u}_s - \hat{v}_s, \hat{\psi}^u)_{\hat{s}} \ = 0 \ ,$$

for all $\{\hat{\psi}^u, \hat{\psi}^v\} \in \hat{V}_s^0 \times \hat{V}_s^0$, *where*

$$\hat{F}_s := I + \widehat{\nabla}\hat{u}_s, \quad \hat{J}_s := \det\hat{F}_s, \quad \hat{E}_s := \tfrac{1}{2}(\hat{F}_s^T \hat{F}_s - I),$$

$$\hat{\sigma}_s := \hat{J}_s^{-1}\hat{F}_s(\lambda_s(\mathrm{tr}\hat{E}_s)I + 2\mu_s \hat{E}_s)\hat{F}_s^T.$$

♮

Incompressible neo-Hookean material

Just as with the St. Venant-Kirchhoff material, the variational form of the structure equations for incompressible neo-Hookean materials in a Lagrangian framework (4.23) is obtained by multiplying them with suitable test functions from the trail spaces $\hat{V}_s^0, \hat{L}_s$ for the momentum conservation, velocity and incompressibility equations. In the momentum equations we integrate by parts.

Problem 4.4 (Variational structure problem, incompressible neo-Hookean, Lagrangian framework). *Find* $\{\hat{u}_s, \hat{v}_s, \hat{p}_s\} \in \{\hat{u}^D + \hat{\mathcal{V}}_s^0\} \times \{\hat{v}_s^D + \hat{\mathcal{V}}_s^0\} \times \hat{\mathcal{L}}_s$, *such that* $\hat{u}_s(0) = \hat{u}_s^0$, $\hat{v}_s(0) = \hat{v}_s^0$, *and*

$$(\hat{\rho}_s d_t \hat{v}_s, \hat{\psi}^v)_{\hat{s}} + (\hat{\sigma}_s \hat{F}_s^{-T}, \widehat{\nabla}\hat{\psi}^v)_{\hat{s}}$$
$$= (\hat{g}_s, \hat{\psi}^v)_{\hat{\Gamma}_{sN}} + (\hat{\sigma}_s \hat{F}_s^{-T} \ \hat{n}_s, \hat{\psi}^v)_{\hat{\Gamma}_i} + (\hat{\rho}_s \hat{f}_s, \psi^v)_{\hat{s}} \ , \qquad (4.25)$$
$$(d_t \hat{u}_s - \hat{v}_s, \hat{\psi}^u)_{\hat{s}} \ = 0 \ ,$$
$$(\det\hat{F}_s - 1, \hat{\psi}^p)_{\hat{s}} \ = 0 \ ,$$

for all $\{\hat{\psi}^u, \hat{\psi}^v, \hat{\psi}^p\} \in \hat{V}_s^0 \times \hat{V}_s^0 \times \hat{L}_s$, *where*

$$\hat{F}_s := I + \widehat{\nabla}\hat{u}_s , \quad \hat{\sigma}_s := -\hat{p}_s I + \mu_s(\hat{F}_s \hat{F}_s^T - I) .$$

♮

In both the St. Venant-Kirchhoff Problem 4.3 and the incompressible neo-Hookean Problem 4.4, $\hat{u}_s^D$ and $\hat{v}_s^D$ are suitable extensions of the prescribed Dirichlet data on the boundaries of $\hat{\Omega}_s$, and $\hat{g}_s$ is the Neumann boundary condition on $\hat{\Gamma}_{sN}$. Similarly as for the fluid problems (Problems 4.1, 4.2) we have 'hidden' the fluid-structure interface condition of steadiness of velocity in part of the boundary condition $\hat{v}_s^D$. The fluid-structure interface condition of steadiness of $\hat{J}_s \hat{\sigma}_s \hat{F}_s^{-T} \hat{n}_s$ we have let stand. The FSI boundary conditions will be treated in Section 5.1.

4.7 Material deformations in an Eulerian framework

In fluid-structure interaction problems that we will later be observing the FSI domain Ω is time independent, but it is composed of the fluid domain Ω_f and the structure domain Ω_s, which will be changing with time. We have already mentioned that one approach to treating this problem is to introduce a mapping $\hat{T}(\hat{x},t) : \hat{\Omega}_f \times I_t \to \Omega(t)$. With this mapping the fluid problem is rewritten in an ALE framework.

As an alternative we propose changing the reference frame of the structure equations.

All material stress values (4.21), (4.22), (4.23) are based on the *Lagrangian* deformation gradient $\hat{F} := (I + \widehat{\nabla}\hat{u})$. In an Eulerian framework we will still have the deformation since this is simply a value being specified in another reference frame: $u(x) = \hat{u}(\hat{x})$. What is not immediately available though is the 'hat gradient' of $\hat{u}$, since $\widehat{\nabla}\hat{u} \neq \nabla u$.

This though is easily fixed by introducing the *'inverse deformation'*

$$\begin{aligned} T(x,t) \quad &: \Omega_s(t) \times I_t \to \hat{\Omega}_s , \\ T(x,t) \quad &= \hat{x} = x - u(x,t) . \end{aligned}$$

Together with the deformation $\hat{T}(\hat{x},t)$ this leads to the identity

$$T(\hat{T}(\hat{x},t),t) = \hat{x}$$

Differentiating this spatially leads to

$$(I - \nabla u)(I + \widehat{\nabla}\hat{u}) = I$$

Thus

$$(I + \widehat{\nabla}\hat{u}) = (I - \nabla u)^{-1} \Leftrightarrow \widehat{\nabla}\hat{u} = (I - \nabla u)^{-1} - I . \tag{4.26}$$

Thus the gradients and Jakobi determinants of the deformation and inverse deformation relate to each other in the following manner

$$F := I - \nabla u = \hat{F}^{-1} \ , \ J := \det F = \det \hat{F}^{-1} = \hat{J}^{-1} \ .$$

The total time differentials of the velocity and displacement are expanded in the usual manner:

$$d_t v \quad = \partial_t v + (v \cdot \nabla) v \ , \tag{4.27}$$

$$d_t u \quad = \partial_t u + (v \cdot \nabla) u \ . \tag{4.28}$$

Based on the equations (4.26) - (4.28) we rewrite the structure equations for St. Venant-Kirchhoff materials (4.22) and incompressible neo-Hookean materials (4.23).

For terseness we combine both models for both the compressible St. Venant-Kirchhoff materials (STVK) and the incompressible neo-Hookean materials (INH).

The sought unknowns are the displacement u, the velocity v and in the INH case p, which is referred to as the (hydrostatic) pressure.

$$
\begin{aligned}
\hat{\rho} \, J \, \partial_t v + \hat{\rho} \, J \, (v \cdot \nabla) v - \mathrm{div} \sigma \ &= \hat{\rho} \, J \, f \quad &&\text{in } \Omega_s \ , \\
\partial_t u + (v \cdot \nabla) u - v \ &= 0 \quad &&\text{in } \Omega_s \ , \\
1 - J \ &= 0 \quad &&\text{in } \Omega_s \ , \text{(INH material)}
\end{aligned}
\tag{4.29}
$$

with

$$
\begin{aligned}
\sigma \quad &:= \begin{cases} J F^{-1} (\lambda_s (\mathrm{tr} E) I + 2\mu_s E) F^{-T} \quad &\text{(STVK material)} \ , \\ -pI + \mu_s (F^{-1} F^{-T} - I) \ , \quad &\text{(INH material)} \ , \end{cases} \\
E \quad &:= \tfrac{1}{2} (F^{-T} F^{-1} - I) \ , \ F := 1 - \nabla u \ , \ J := \det F \ .
\end{aligned}
\tag{4.30}
$$

4.7.1 Boundary conditions

Similarly the boundary conditions must be set in the Eulerian framework. As a boundary condition in time the same initial value is used, now in the Eulerian framework, v_0 for v at the initial time t_0 are prescribed. The fluid boundary Ω_s can be split into four non-overlapping parts:

$$\partial \Omega_s = \Gamma_{sD} \cup \Gamma_{sN} \cup \Gamma_{sR} \cup \Gamma_i \ ,$$

with each part relating to a different boundary condition. The first three parts are the well-known conditions:

$$
\begin{aligned}
\text{Dirichlet} \quad &: \quad v \ &&= \ v_D \quad &&\text{on } \Gamma_{sD} \ , \\
\text{Neumann} \quad &: \quad \sigma n \ &&= \ g \quad &&\text{on } \Gamma_{sN} \ , \\
\text{Robin} \quad &: \quad \alpha v + \sigma n \ &&= \ 0 \quad &&\text{on } \Gamma_{sR} \ .
\end{aligned}
$$

The fixed boundary $\hat{\Gamma}_i$ on the reference domain is now the moving boundary Γ_i, just as in fluid flow case. The boundary conditions on Γ_i are similar to the fluid flows case: continuity of velocity v and the normal-flux of the stress σn, hence

$$v_s = v_f \qquad \text{on } \Gamma_i \, ,$$
$$\sigma_s n_s = \sigma_f n_s \quad \text{on } \Gamma_i \, .$$

To differentiate the fluid and material values we have added a respective 'f' or 's' suffix.

4.7.2 Variational formulation

The variational form of the structure equations in an Eulerian framework (4.29) is obtained by multiplying them with suitable test functions from the trail space V_s^0 for the momentum equations and L_s for velocity/displacement and the optional incompressibility equations. In the momentum equations we integrate by parts. The equations are written in an Eulerian framework in the domain Ω_s. For later purposes we take care to write all structure specific variables with a respective 's' suffix. The physical unknowns are the vector displacement field $u_s \in u_s^D + \mathcal{V}_s$, vector velocity field $v_s \in v_s^D + \mathcal{V}_s$ and the optional scalar pressure field $p_s \in \mathcal{L}_s$.

Problem 4.5 (Variational structure problem, STVK, Eulerian framework). *Find $\{u_s, v_s\} \in \{u_s^D + \mathcal{V}_s^0\} \times \{v_s^D + \mathcal{V}_s^0\}$, such that $u_s(0) = u_s^0$, $v_s(0) = v_s^0$, and*

$$(\hat{\rho}_s \, J_s \, \partial_t v_s, \psi^v)_s + (\hat{\rho}_s \, J_s \, (v_s \cdot \nabla) v_s, \psi^v)_s + (\sigma_s, \nabla \psi^v)_s$$
$$= (g_s, \psi^v)_{\Gamma_{sN}} + (\sigma_s \, n_s, \psi^v)_{\Gamma_i} + (\hat{\rho}_s J_s f_s, \psi^v)_s \, , \qquad (4.31)$$
$$(\partial_t u_s + (v_s \cdot \nabla) u_s - v_s, \psi^u)_s = 0 \, ,$$

for all $\{\psi^u, \psi^v\} \in V_s^0 \times V_s^0$, where

$$\begin{aligned}
\sigma_s &:= J_s F_s^{-1}(\lambda_s (\mathrm{tr}E)I + 2\mu_s E)F_s^{-T} \, , \\
E &:= \tfrac{1}{2}(F_s^{-T} F_s^{-1} - I) \, , \\
F_s &:= 1 - \nabla u_s \, , \ J_s := \det F_s \, .
\end{aligned}$$

♮

Problem 4.6 (Variational structure problem, INH, Eulerian framework). *Find $\{u_s, v_s, p_s\} \in \{u_s^D + \mathcal{V}_s^0\} \times \{v_s^D + \mathcal{V}_s^0\} \times \mathcal{L}_s$, such that $u_s(0) = u_s^0$, $v_s(0) = v_s^0$, and*

$$(\hat{\rho}_s \partial_t v_s, \psi^v)_s + (\hat{\rho}_s (v_s \cdot \nabla) v_s, \psi^v)_s + (\sigma_s, \nabla \psi^v)_s$$
$$= (g_s, \psi^v)_{\Gamma_{sN}} + (\sigma_s \, n_s, \psi^v)_{\Gamma_i} + (\hat{\rho}_s f_s, \psi^v)_s \, ,$$
$$(\partial_t u_s + (v_s \cdot \nabla) u_s - v_s, \psi^u)_s = 0 \, , \qquad (4.32)$$
$$(1 - \det F_s, \psi^p)_s = 0 \, ,$$

for all $\{\psi^u, \psi^v, \psi^p\} \in V_s^0 \times V_s^0 \times L_s$, where

$$\begin{aligned}
\sigma_s &:= -p_s I + \mu_s (F_s^{-1} F_s^{-T} - I) \, , \\
E &:= \tfrac{1}{2}(F_s^{-T} F_s^{-1} - I) \, , \\
F_s &:= 1 - \nabla u_s \, , \ J_s := \det F_s \, .
\end{aligned}$$

♮

Just as in the Lagrangian framework, in both the St. Venant-Kirchhoff Problem 4.5 and the incompressible neo-Hookean Problem 4.6, u_s^D and v_s^D are suitable extensions of the prescribed Dirichlet data on the boundaries of Ω_s, and g_s is the Neumann boundary condition on Γ_{sN}. Similarly as for the fluid problems (Problems 4.1, 4.2) we have 'hidden' the fluid-structure interface condition of steadiness of velocity in part of the boundary condition v_s^D. The fluid-structure interface condition of steadiness of $\sigma_s \, n_s$ we have let stand. The FSI boundary conditions will be treated in Section 5.2.

Chapter 5

Fluid-Structure interaction formulation

In this chapter, we introduce the *'monolithic'* ALE and Eulerian variational formulations for fluid-structure interaction problems.

There are two general approaches to modelling fluid-structure interaction, the *'partitioned'* and *'monolithic'* approaches. In the partitioned approach each problem is solved separately. Since the boundary conditions and the domain deformations are not directly coupled, it becomes necessary that the results from the one problem are processed and provided to the other problem. Depending on how well one wants the fluid-structure interaction boundary conditions to be met, it may be necessary to solve the separate problems multiple times. Thus this approach is costly since it either implies multiple iterations or, when few iterations are desired, a loss of accuracy.

Hence the desire to solve both problems in a unified monolithic framework that implicitly demands that the natural fluid-structure interaction boundary conditions be fulfilled. Both the fluid and the structure problems, which are essentially momentum conservation problems, left in their *natural* framework, cannot be combined into one conservation equation due to the different reference frames.

The first well-known approach to this discrepancy is to rewrite the fluid problem in a structure-appropriate framework. This leads to the 'arbitrary Lagrangian-Eulerian' (ALE) framework, which essentially introduces a domain deformation function $\hat{T}(\hat{x}, t) : \hat{\Omega}_f \times I_t \to \Omega_f(t)$. Just as with the partitioned approach the structure problem is left in its natural framework, the interaction interface is tracked in the fluid domain by deforming the fluid mesh. Such approaches are generally referred to as *'interface tracking'* methods. With this function the fluid problem is rewritten as one on the reference domain $\hat{\Omega}_f$, which is fixed in time. We explain this approach in Section 5.1.

In this thesis, we also follow the alternative (to our knowledge new) way of posing the fluid as well as the structure problem in a fully Eulerian framework. Instead of changing the reference frame of the fluid problem to match the structure, we change the reference frame of the structure to match the Eulerian fluid frame. Since all structure state variables are now in an Eulerian framework it is necessary to introduce a variable that either contains the initial position or displacement of the material points.

We refer to this set of data as the *'Initial Position set'* (IP set). The set is convected with an appropriate velocity-field. It provides information for discerning not only material displacement but also for distinguishing between the different phases, fluid and structure.

Thus the IP set is also used for identifying the fluid-structure interface. Such an approach is generally referred to as *'interface capturing'*, a method commonly used in the simulation of multiphase flows, [JoRe93a, JoRe93b]. Examples for the use of such a phase variable are the Volume of Fluid (VoF) method [HiNi81] and the Level Set (LS) method [ChHoMeOs, OsherSethian, Sethian99].

We explain this approach in Section 5.2.

5.1 ALE variational form

The variational ALE formulation of the fluid problem 4.2 is handled on the domain $\hat{\Omega}_f$. The variational Lagrangian formulation of the structure problem 4.3 is handled on the domain $\hat{\Omega}_s$. By construction the fluid-structure interaction interface $\hat{\Gamma}_i$ of both problems match. We combine both problems into one complete problem on the combined domain $\Omega = \hat{\Omega} = \hat{\Omega}_f \cup \hat{\Gamma}_i \cup \hat{\Omega}_s$. Here, the steadiness of velocity across the fluid-structure interface $\hat{\Gamma}_i$ is strongly enforced by requiring one common continuous field for the velocity on Ω. This is akin to saying that $\hat{v}$ has at all times a trace on $\hat{\Gamma}_i$ which is akin to requiring that $\hat{v} \in \hat{v}^D + \hat{\mathcal{V}}^0$. The stress interface condition

$$\hat{J}_f \hat{\sigma}_f \hat{F}_f^{-T} \hat{n}_f = \hat{J}_s \hat{\sigma}_s \hat{F}_s^{-T} \hat{n}_f \quad \text{on } \hat{\Gamma}_i \,,$$

is still present in the form of a jump of the first Piola-Kirchhoff normal stresses of both systems

$$(\hat{J}_f \hat{\sigma}_f \hat{F}_f^{-T} \, \hat{n}_f, \hat{\psi}^v)_{\hat{\Gamma}_i} + (\hat{J}_s \hat{\sigma}_s \hat{F}_s^{-T} \, \hat{n}_s, \hat{\psi}^v)_{\hat{\Gamma}_i} \tag{5.1}$$

on the right hand side. By omitting the boundary integral jump (5.1) the (weak) continuity of the normal stress becomes an implicit condition of the combined variational formulation.

The combined formulation though implies that a domain mapping functiong $\hat{T}_f$ for the fluid domain be known. Such a mapping is obtained by adding an auxiliary problem to the fluid and structure problems. The boundary conditions to the mapping are clear. There is no deformation on all "outer" boundaries $\hat{\Omega}_f \setminus \hat{\Gamma}_i$, and the deformation on $\hat{\Gamma}_i$ should be equal to $\hat{u}_s$. Thus the global deformation $\hat{u}$ with $\hat{u}_{|\Omega_s} = \hat{u}_s$ must have a trace on $\hat{\Gamma}_i$, which implies that $\hat{u} \in \hat{u}^D + \hat{\mathcal{V}}^0$.

The deformation itself can be sought as the solution to various deformation problems, the simplest being the harmonic deformation. If it is necessary that the deformation preserve volume an incompressibility condition can be added in the form of $\hat{J}_f = \det(1 + \widehat{\nabla}\hat{u}_s) = 1$ or in a simplified form $\widehat{\text{div}}\hat{u}_s = 0$. If the deformation should be as "smooth" as possible, then as an alternative the biharmonic equations can be solved.

The remaining parts of the Neumann data $\hat{g}_f$ and $\hat{g}_s$ now form the Neumann boundary data on $\hat{\Gamma}_N = \hat{\Gamma}_{fN} \cup \hat{\Gamma}_{sN}$ and are combined to $\hat{g}$. The right hand side functions $\hat{f}_f$ and $\hat{f}_s$ are combined to $\hat{f}$. We write the Cauchy stress tensor for the whole domain as follows:

$$\hat{\sigma} := \hat{\chi}_f \hat{\sigma}_f + \hat{\chi}_s \hat{\sigma}_s \,.$$

Here, $\hat{\chi}_f$ and $\hat{\chi}_s$ are the characteristic functions of $\hat{\Omega}_f$ and $\hat{\Omega}_s$, respectively, which are determined by the domain:

$$\hat{\chi}_f(\hat{x}) := \begin{cases} 1, & \hat{x} \in \hat{\Omega}_f, \\ 0, & \hat{x} \in \hat{\Omega}_s \cup \hat{\Gamma}_i, \end{cases} \qquad \hat{\chi}_s := 1 - \chi_f . \tag{5.2}$$

In Problem 5.1 we first state the complete variational form for fluid-structure interaction in an arbitrary Lagrangian-Eulerian framework. For terseness we combine both models for both the compressible St. Venant-Kirchhoff materials (STVK) and the incompressible neo-Hookean materials (INH). The structure displacement $\hat{u}_s$ is continued harmonically into the fluid domain. In the thereafter following Problem 5.2 we state the complete variational form with a biharmonically continued structure displacement.

Problem 5.1 (Variational fluid-structure problem, ALE framework, harmonic continuation).
Find $\{\hat{u}, \hat{v}, \hat{p}\} \in \{\hat{u}^D + \hat{\mathcal{V}}^0\} \times \{\hat{v}^D + \hat{\mathcal{V}}^0\} \times \hat{\mathcal{L}}^*$, *such that* $\hat{u}|_{t=0} = \hat{u}^0, \hat{v}|_{t=0} = \hat{v}^0$, *and*

$$(\hat{\chi}_s \hat{\rho}_s d_t \hat{v}, \hat{\psi}^v) + (\hat{\chi}_f \hat{J} \rho_f (\partial_t \hat{v} + (\hat{F}^{-1}(\hat{v} - \partial_t \hat{T}) \cdot \widehat{\nabla})\hat{v}), \hat{\psi}^v)$$
$$+ (\hat{J}\hat{\sigma}\hat{F}^{-T}, \widehat{\nabla}\psi^v) \quad = (\hat{g}, \hat{\psi}^v)_{\hat{\Gamma}_N} + ((\hat{\chi}_s \hat{\rho}_s + \hat{\chi}_f \rho_f \hat{J})\hat{f}, \psi^v) ,$$

$$(\hat{\chi}_f \widehat{\mathrm{div}}(\hat{J}\hat{F}^{-1}\hat{v}), \hat{\psi}^p) + (\hat{\chi}_s \hat{\alpha}_p \widehat{\nabla}\hat{p}, \widehat{\nabla}\hat{\psi}^p) \quad = 0 , \quad \text{(STVK material)} ,$$
$$(\hat{\chi}_f \widehat{\mathrm{div}}(\hat{J}\hat{F}^{-1}\hat{v}), \hat{\psi}^p) + (\hat{\chi}_s(\hat{J} - 1), \hat{\psi}^p) \quad = 0 , \quad \text{(INH material)} ,$$

$$(\hat{\chi}_s(d_t \hat{u} - \hat{v}), \hat{\psi}^u) + (\hat{\chi}_f \hat{\alpha}_u \widehat{\nabla}\hat{u}, \widehat{\nabla}\hat{\psi}^u) \quad = 0 ,$$

$$\tag{5.3}$$

for all $\{\hat{\psi}^u, \hat{\psi}^v, \hat{\psi}^p\} \in \hat{V}^0 \times \hat{V}^0 \times \hat{L}^*$, *where* $\hat{\alpha}_p, \hat{\alpha}_u$ *are small positive constants and* $\hat{\sigma} := \hat{\chi}_f \hat{\sigma}_f + \hat{\chi}_s \hat{\sigma}_s$, *with*

$$\hat{\chi}_f := \begin{cases} 1, & \hat{x} \in \hat{\Omega}_f, \\ 0, & \hat{x} \in \hat{\Omega}_s \cup \hat{\Gamma}_i, \end{cases} \qquad \hat{\chi}_s := 1 - \hat{\chi}_f , \tag{5.4}$$

and

$$\begin{aligned} \hat{\sigma}_f &:= -\hat{p}I + \rho_f \nu_f (\widehat{\nabla}\hat{v}\hat{F}^{-1} + \hat{F}^{-T}\widehat{\nabla}\hat{v}^T), \\ \hat{\sigma}_s &:= \begin{cases} \hat{J}^{-1}\hat{F}(\lambda_s(\mathrm{tr}\hat{E})I + 2\mu_s\hat{E})\hat{F}^T , & \text{(STVK material)} , \\ -\hat{p}I + \mu_s(\hat{F}\hat{F}^T - I) , & \text{(INH material)} , \end{cases} \\ \hat{F} &:= \widehat{\nabla}\hat{T} , \hat{J} := \det\hat{F} , \hat{T} := I + \widehat{\nabla}\hat{u} , \\ \{\hat{\mathcal{L}}^*, \hat{L}^*\} &:= \begin{cases} \{\hat{\mathcal{L}}, \hat{L}\} , & \text{(INH material)} , \\ \{\hat{\mathcal{L}} \cap \hat{\mathcal{V}}_s^0, \hat{L} \cap \hat{V}_s^0\} , & \text{(STVK material)} . \end{cases} \end{aligned} \tag{5.5}$$

$\natural$

As a modification the next Problem 5.2 continues the structure displacement biharmonically into the fluid domain. Instead of requiring the biharmonic equation $-\widehat{\Delta}^2 \hat{u} = 0$ be satisfied in the fluid domain, we introduced an auxiliary equation $\hat{w} = \widehat{\Delta}\hat{u}$ on the whole domain and then require the harmonic equation $-\widehat{\Delta}\hat{w} = 0$ be satisfied in the fluid domain. Details can be found in [Ci78, BaOsPi80]

Problem 5.2 (Variational fluid-structure problem, ALE framework, biharmonic continuation).
Find $\{\hat{u}, \hat{v}, \hat{w}, \hat{p}\} \in \{\hat{u}^D + \hat{\mathcal{V}}^0\} \times \{\hat{v}^D + \hat{\mathcal{V}}^0\} \times \hat{\mathcal{V}} \times \hat{\mathcal{L}}^*$, *such that* $\hat{u}|_{t=0} = \hat{u}^0, \hat{v}|_{t=0} = \hat{v}^0$, *and*

$$(\hat{\chi}_s \hat{\rho}_s d_t \hat{v}, \hat{\psi}^v) + (\hat{\chi}_f \hat{J} \rho_f (\partial_t \hat{v} + (\hat{F}^{-1}(\hat{v} - \partial_t \hat{T}) \cdot \widehat{\nabla})\hat{v}), \hat{\psi}^v)$$
$$+ (\hat{J}\hat{\sigma}\hat{F}^{-T}, \widehat{\nabla}\hat{\psi}^v) \;\; = (\hat{g}, \hat{\psi}^v)_{\hat{\Gamma}_N} + (((\hat{\chi}_s \hat{\rho}_s + \hat{\chi}_f \rho_f \hat{J})\hat{f}, \hat{\psi}^v) \,,$$

$$(\hat{\chi}_f \widehat{\operatorname{div}}(\hat{J}\hat{F}^{-1}\hat{v}), \hat{\psi}^p) + (\hat{\chi}_s \hat{\alpha}_p \widehat{\nabla}\hat{p}, \widehat{\nabla}\hat{\psi}^p) \;\; = 0 \,, \quad \textit{(STVK material)} \,,$$
$$(\hat{\chi}_f \widehat{\operatorname{div}}(\hat{J}\hat{F}^{-1}\hat{v}), \hat{\psi}^p) + (\hat{\chi}_s (\hat{J} - 1), \hat{\psi}^p) \;\; = 0 \,, \quad \textit{(INH material)} \,,$$

$$(\hat{w}, \hat{\psi}^w) + (\widehat{\nabla}\hat{u}, \widehat{\nabla}\hat{\psi}^w) \;\; = 0 \,,$$
$$(\hat{\chi}_s (d_t \hat{u} - \hat{v}), \hat{\psi}^u) + (\hat{\chi}_f \hat{\alpha}_w \widehat{\nabla}\hat{w}, \widehat{\nabla}\hat{\psi}^u) \;\; = 0 \,,$$

$$(5.6)$$

for all $\{\hat{\psi}^u, \hat{\psi}^v, \hat{\psi}^w, \hat{\psi}^p\} \in \hat{V}^0 \times \hat{V}^0 \times \hat{V} \times \hat{L}^*$, *where* $\hat{\alpha}_p, \hat{\alpha}_w$ *are small positive constants and*
$\hat{\sigma} := \hat{\chi}_f \hat{\sigma}_f + \hat{\chi}_s \hat{\sigma}_s$, *with all other definitions as in the equations in (5.4)-(5.5).*　♮

For later purposes we also pose the stationary version of Problem 5.1.

Problem 5.3 (Variational stationary fluid-structure problem, ALE framework, harmonic continuation). *Find* $\{\hat{u}, \hat{v}, \hat{p}\} \in \{\hat{u}^D + \hat{V}^0\} \times \{\hat{v}^D + \hat{V}^0\} \times \hat{L}^*$, *such that*

$$(\hat{\chi}_f \hat{J} \rho_f (\hat{F}^{-1}\hat{v} \cdot \widehat{\nabla})\hat{v}, \hat{\psi}^v) + (\hat{J}\hat{\sigma}\hat{F}^{-T}, \widehat{\nabla}\hat{\psi}^v) \;\; = (\hat{g}, \hat{\psi}^v)_{\hat{\Gamma}_N} + (((\hat{\chi}_s \hat{\rho}_s + \hat{\chi}_f \rho_f \hat{J})\hat{f}, \hat{\psi}^v) \,,$$

$$(\hat{\chi}_f \widehat{\operatorname{div}}(\hat{J}\hat{F}^{-1}\hat{v}), \hat{\psi}^p) + (\hat{\chi}_s \hat{\alpha}_p \widehat{\nabla}\hat{p}, \widehat{\nabla}\hat{\psi}^p) \;\; = 0 \,, \quad \textit{(STVK material)} \,,$$
$$(\hat{\chi}_f \widehat{\operatorname{div}}(\hat{J}\hat{F}^{-1}\hat{v}), \hat{\psi}^p) + (\hat{\chi}_s (\hat{J} - 1), \hat{\psi}^p) \;\; = 0 \,, \quad \textit{(INH material)} \,,$$

$$(5.7)$$

$$(\hat{\chi}_s \hat{v}, \hat{\psi}^u) + (\hat{\chi}_f \hat{\alpha}_u \widehat{\nabla}\hat{u}, \widehat{\nabla}\hat{\psi}^u) \;\; = 0 \,,$$

for all $\{\hat{\psi}^u, \hat{\psi}^v, \hat{\psi}^p\} \in \hat{V}^0 \times \hat{V}^0 \times \hat{L}^*$, *where* $\hat{\alpha}_p, \hat{\alpha}_u$ *are small positive constants and* $\hat{\sigma} :=$
$\hat{\chi}_f \hat{\sigma}_f + \hat{\chi}_s \hat{\sigma}_s$, *with all other definitions as in the equations in (5.4)-(5.5).*　♮

5.2 Eulerian variational form

The variational Eulerian formulation of the fluid problem 4.1 is handled on the domain Ω_f.
The Eulerian framework for treating elastic material deformations was presented in Section
4.5.2. The variational Eulerian formulation of the structure problem (4.5 in the St. Venant-
Kirchhoff case or 4.6 in the incompressible neo-Hookean case) is handled on the domain
$\Omega_s(t)$.

By construction the fluid-structure interaction interface Γ_i of both problems match. We
combine both problems into one complete problem on the combined domain $\Omega = \Omega_f \cup \Gamma_i \cup \Omega_s$.

Again, exactly as in the ALE situation in the previous section, steadiness of velocity across
the fluid-structure interface Γ_i is strongly enforced by requiring one common continuous field
for the velocity on Ω. This is akin to the velocity having at all times a trace on Γ_i, which
is akin to requiring $v \in v^D + \mathcal{V}^0$. The stress interface condition

$$\sigma_f n_f = \sigma_s n_f \quad \text{on } \Gamma_i \,,$$

is still present in the form of a jump of the Cauchy normal stresses of both systems

$$(\sigma_f \, n_f, \psi^v)_{\Gamma_i} + (\sigma_s \, n_s, \psi^v)_{\Gamma_i} \tag{5.8}$$

on the right hand side. By omitting the boundary integral jump (5.8) the (weak) continuity of the normal stress becomes an implicit condition of the combined variational formulation.

The remaining parts of the Neumann data g_f and g_s now form the Neumann boundary data on $\Gamma_N = \Gamma_{fN} \cup \Gamma_{sN}$ and are combined to g. The right hand side functions f_f and f_s are combined to f. We write the Cauchy stress tensor for the whole domain as follows:

$$\sigma := \chi_f \sigma_f + \chi_s \sigma_s \ .$$

Here, χ_f and χ_s are the characteristic functions of Ω_f and Ω_s, respectively, which are now determined by x and u:

$$\chi_f(x) := \begin{cases} 1, & x - u \in \Omega_f \\ 0, & x - u \in \Omega_s \cup \Gamma_i, \end{cases} \qquad \chi_s := 1 - \chi_f \ . \tag{5.9}$$

The requirement and definition of the characteristic functions χ_f, χ_s implies that the deformation no longer be restricted to the structure domain, and that 'some kind' of deformation u be provided on the fluid domain.

We will want the Eulerian characteristic functions to have the same behavior as their Lagrangian counterparts in regards to theirs limits on Γ_i depending on the 'incoming' direction. Thus for any sequence of (permissible) points with the Lagrangian positions $\hat{x}_i$ with the limit $\hat{x}_\infty$ the Eulerian sequence of the spatial positions (of the same points) $\hat{x}_i = x_i + u(x_i)$ must have the same limit $\hat{x}_\infty = x_\infty + u(x_\infty)$. This requires that u be smooth not only its restriction to Ω_s or its (yet to be determined) restriction to Ω_f, but that it have a trace on Γ_i. Thus $u \in u^D + \mathcal{V}^0$.

5.2.1 Initial position set

We introduce the *'Initial Position set'* (IP set) $\phi(\Omega, t) : \Omega \times I_t \to \Omega$. If we look at a given 'material' point at the position $x \in \Omega$ and the time $t \in I_t$, then the value $\phi(x, t)$ will tell us what the initial position of this point was at time $t = 0$. This set of values is transported in the full domain with a certain velocity w. The convection velocity in the structure will be the structure velocity itself, $w_{|\Omega_s} = v_s$. If the fluid velocity were to be used for convection in the fluid domain, then the displacements there would eventually become very entangled. For this reason we use an alternative velocity. We explain this in more detail below. With this notation, the mapping ϕ is determined by the following variational problem:

Problem 5.4 (Initial position set). *Find $\phi \in \phi_0 + \mathcal{V}^0$, such that*

$$(\partial_t \phi + (w \cdot \nabla)\phi, \psi) = 0 \quad \forall \psi \in V^0 \ , \tag{5.10}$$

where ϕ_0 is a suitable extension of the Dirichlet data along the boundaries,

$$\begin{aligned} \phi(x, 0) &= x, & x \in \Omega, \\ \phi(x, t) &= x, & \{x, t\} \in \partial\Omega \times I_t. \end{aligned}$$

♮

Since $\hat{x} = \phi(\hat{x}, 0) = \phi(x, t)$, $\hat{u}(\hat{x}, t) = u(x, t)$ and $\hat{x} + \hat{u}(\hat{x}, t) = x$ it follows that

$$x = \phi + u . \tag{5.11}$$

Using this in the IP set equation (5.10) yields

Problem 5.5 (Reduced initial position set). *Find* $u \in u_0 + \mathcal{V}^0$, *such that*

$$(\partial_t u - w + (w \cdot \nabla) u, \psi) = 0 \quad \forall \psi \in V^0 , \tag{5.12}$$

where u_0 *is a suitable extension of the Dirichlet data along the boundaries,*

$$
\begin{aligned}
u(x, 0) &= 0, \quad x \in \Omega, \\
u(x, t) &= 0, \quad \{x, t\} \in \partial\Omega \times (0, T].
\end{aligned}
$$

♮

The value of u in the fluid domain will be determined by the choice of the convection velocity w in Ω_f. If we were to use the fluid velocity this would eventually lead to increasing entanglement, which would necessitate a continual reinitialization of the IP set. The method of reinitialization is often used when using the Level Set method for example when modelling multi-phase flows [JoRe93a, JoRe93b].

As an alternative, we use the harmonic continuation of the structure velocity into the fluid domain Ω_f, which is denoted by w and satisfies

$$(\chi_s(w - v), \psi) + (\chi_f \alpha_w \nabla w, \nabla \psi) = 0, \quad \forall \psi \in V^0, \tag{5.13}$$

where α_w is a small positive parameter. By this construction, the displacement u_f in the fluid domain becomes an artificial quantity without any real physical meaning, i.e., $d_t u_s = v_s$, but generally $d_t u_f \neq v_f$.

Complete formulation

We combine the fluid Problem (4.1), the structure Problem (4.5 in the St. Venant-Kirchhoff case or 4.6 in the incompressible neo-Hookean case) and the reduced Initial Position set Problem (5.5), to obtain a complete variational formulation of the FSI problem in an Eulerian framework. In the case of STVK material the (non-physical) pressure p_s in the structure subdomain is determined as harmonic continuation of the flow pressure p_f.

Problem 5.6 (Variational fluid-structure problem, Eulerian framework). *Find fields* $\{u, v, w, p\} \in \{u^D + \mathcal{V}^0\} \times \{v^D + \mathcal{V}^0\} \times \mathcal{V}^0 \times \mathcal{L}^*$, *such that* $v|_{t=0} = v^0$, $u|_{t=0} = u^0$, *and*

$$
\begin{aligned}
((\chi_f \rho_f + \chi_s J\hat{\rho}_s)(\partial_t v + (v \cdot \nabla) v), \psi^v) + (\sigma, \nabla \psi^v) &= (g, \psi^v)_{\Gamma_N} + ((\chi_f \rho_f + \chi_s J\hat{\rho}_s)f, \psi^v) , \\
(\chi_f \mathrm{div} v, \psi^p) + (\chi_s \alpha_p \nabla p, \nabla \psi^p) &= 0 , \quad \textit{(STVK material)} , \\
(\chi_f \mathrm{div} v, \psi^p) + (\chi_s (1 - J), \psi^p) &= 0 , \quad \textit{(INH material)} , \\
(\partial_t u - w + w \cdot \nabla u, \psi^u) &= 0 , \\
(\chi_s(w - v), \psi^w) + (\chi_f \alpha_w \nabla w, \nabla \psi^w) &= 0 ,
\end{aligned}
$$

$$\tag{5.14}$$

for all $\{\psi^u, \psi^v, \psi^w, \psi^p\} \in V^0 \times V^0 \times V^0 \times L^*$, *where* α_p, α_w *are small positive constants and* $\sigma := \chi_f \sigma_f + \chi_s \sigma_s$, *with*

$$\chi_f := \begin{cases} 1, & x - u \in \hat{\Omega}_f \\ 0, & x - u \in \hat{\Omega}_s \cup \hat{\Gamma}_i, \end{cases} \qquad \chi_s := 1 - \chi_f, \tag{5.15}$$

and

$$\begin{aligned}
\sigma_f &:= -pI + 2\rho_f \nu_f \epsilon(v), \\
\sigma_s &:= \begin{cases} -pI + \mu_s(F^{-1}F^{-T} - I) & \text{(INH material)}, \\ JF^{-1}(\lambda_s(\text{tr}E)I + 2\mu_s E)F^{-T} & \text{(STVK material)}, \end{cases} \\
E &:= \tfrac{1}{2}(F^{-T}F^{-1} - I), \ \epsilon(\psi) := \tfrac{1}{2}(\nabla\psi + \nabla\psi^T), \\
F &:= I - \nabla u, \ J := \det F, \\
\{\mathcal{L}^*, L^*\} &:= \begin{cases} \{\mathcal{L}, L\}, & \text{(INH material)}, \\ \{\mathcal{L} \cap \mathcal{V}_s^0, L \cap V_s^0\}, & \text{(STVK material)}. \end{cases}
\end{aligned} \tag{5.16}$$

In this variational formulation the position of the fluid structure interface Γ_i is implicitly given by the displacement u:

$$\Gamma_i(t) = \{x \in \Omega \mid x - u(x,t) \in \hat{\Gamma}_i\}. \tag{5.17}$$

Notice that the system (5.14) is *nonlinear* even if in a simplified form the two subproblems are linear, e.g., for a Stokes fluid interacting with a linear elastic structure.

5.2.2 Formulation of the 'stationary' FSI problem

In some situations the solution of an FSI problem may tend to a 'steady state' as $t \to \infty$. For later purposes, we derive the set of equations determining such a steady state solution $\{u^*, v^*, w^*, p^*\} \in \{u^D + V^0\} \times \{v^D + V^0\} \times V^0 \times L^*$. The corresponding limits of the characteristic functions and subdomains are denoted by χ_f^*, χ_s^* and Ω_f^*, Ω_s^*, respectively. Further, the fluid velocity becomes constant in time, $v_f^* := \lim_{t\to\infty} v_{|\Omega_f}$, and the structure velocity vanishes, $v_s^* \equiv 0$, which in turn implies $w^* \equiv 0$.

The steady state structure displacement u_s^* is likewise well defined, but the corresponding ('non-physical') fluid displacement is merely defined by $u_f^* = u_f^{\text{lim}} := \lim_{t\to\infty} u_{|\Omega_f}$ and therefore depends on the chosen construction of $w_{|\Omega_f}$ as harmonic extension of $w_{|\Omega_s}$. Alternatively, it could be defined by any suitable continuation of u_s^* to all of Ω, e.g., by harmonic continuation.

The steady state pressure p^* is determined from the limiting equations. Then, with suitable extensions u^D and v^D of the prescribed Dirichlet data on $\partial\Omega$, the equations (5.14) of the Eulerian FSI Problem 5.6 reduce to the following 'stationary' form (dropping for simplicity the stars):

Problem 5.7 (Variational 'stationary' fluid-structure problem, Eulerian framework). *Find* $\{u, v, p\} \in \{u^D + V^0\} \times \{v^D + V^0\} \times L^*$, *such that*

$$
\begin{aligned}
(\chi_f \rho_f v \cdot \nabla v, \psi^v) + (\sigma, \nabla \psi^v) &= (g, \psi^v)_{\Gamma_N} + ((\chi_f \rho_f + \chi_s J \hat{\rho}_s) f, \psi^v) , \\
(\chi_f \mathrm{div} v, \psi^p) + (\chi_s \alpha_p \nabla p, \nabla \psi^p) &= 0 , \quad (STVK\ material) , \\
(\chi_f \mathrm{div} v, \psi^p) + (\chi_s (1 - J), \psi^p) &= 0 , \quad (INH\ material) , \\
(\chi_f (u - u_f^{\mathrm{lim}}), \psi^u) + (\chi_s v, \psi^u) &= 0 , \quad (static\ continuation\ of\ u_s), \\
(\chi_f \alpha_u \nabla u, \nabla \psi^u) + (\chi_s v, \psi^u) &= 0 , \quad (or\ harmonic\ continuation\ of\ u_s),
\end{aligned}
\tag{5.18}
$$

for all $\{\psi^u, \psi^v, \psi^p\} \in V^0 \times V^0 \times L^*$, *where* α_p *and optionally* α_u *are small positive constants and* $\sigma := \chi_f \sigma_f + \chi_s \sigma_s$, *with all other definitions as in the equations in (5.15) and (5.16).*
♮

5.2.3 Theoretical results

Theoretical results for fluid-structure interaction can be found for certain reduced systems. Many results can be found in literature based on interaction of fluid with fixed rigid structures. In [DeEs99, DeEs00] the authors show that solutions exist for a a finite number of rigid non-colliding structures embedded in the fluid. The considered fluids are incompressible as well as compressible isentropic fluids modelled by the Navier-Stokes equations. Previous work in this direction can be found in [De99].

Using an approach similar to that in [DeEs99, DeEs00] the authors of [DeEs+01] prove the existence of weak solutions for an instationary fluid-elastic interaction model. This is achieved with 'Leray's method', i.e. by finding weak solutions that satisfy bounds of the energy estimate of the complete system. The authors model the elastic structure as a compressible linearized neo-Hookean material with a finite number of elastic modes.

In [LeMa00] the authors investigate an instationary linearized fluid-structure interaction problem for a viscous fluid and a thin elastic shell with small displacements. The authors simplify the problem by neglecting changes to the geometry. Based on these premises by using energy estimates they show that the problem is well posed, that a weak solution exists and that the discrete approximation, based on their discretization, converges to the continuous solution.

Chapter 6

Discretization

In this chapter, we detail methods used for discretizing and solving the FSI Problems in the ALE and Eulerian frameworks presented in the previous chapters. The method we use is based on conforming finite elements (FE), for a general introduction to the FE method we refer to [Br97, BrSc94, Ci78]. First we provide the framework for the finite element method. Then we describe the complete variational forms, which are the basis for the Galerkin discretizations. We then describe the Galerkin discretization. Since we are using an 'equal-order' approach, the solutions to the discrete formulations do not fulfill the 'inf-sup' condition (see [Br97, GiRa86]). To manage this instability we use the 'local projection stabilization' method introduced by Becker and Braack [BeBr01, BeBr03]. We briefly mention the overall solution process. The time discretization is based on using a fractional-step-θ or implicit Euler scheme [Rannacher00, Rannacher04, Gl03, BrGl+87, MU94].

At each time-step a nonlinear problem is solved using a Newton iteration. This relies on solving the linear defect-correction problem, which in turn requires that the Jakobi matrix of the complete FSI problem be known. Due to the nonlinear and large nature of the complete FSI problems in the ALE or Eulerian frameworks, calculating the Jakobi matrix can be cumbersome. We explain how this can be done using using an approach that is also used in the method of 'automatic differentiation'.

6.1 Finite element triangulation and mesh notation

We will be using the known finite element method for discretizing and solving the problems. This approach demands that the domain Ω be fully partitioned into convex non-overlapping quadrilateral cells K, with the partitioning referred to as the triangulation $\mathbb{T}_h := \{K\}$.

$$\bar{\Omega} = \bigcup_{i=1...N} \bar{K}_i \, .$$

Such a triangulation is referred to as *'regular'*, if any cell edge is either a subset of the domain boundary $\partial\Omega$ or a compete edge of another cell.

The mesh parameter h is a scalar cell-wise constant function. On each cell K, its value is the cells diameter $h_{|K} = \text{diam}(K)$.

To ensure approximation properties of the finite element spaces which are constructed based on the mesh $\mathbb{T}_h$, we require that the uniform-shape and uniform-size conditions be fulfilled.

Definition 6.1. A mesh $\mathbb{T}_h$ fulfills the *'uniform-shape condition'*, if there is a constant $C_{ush} = C_{ush}(\mathbb{T}_h)$, so that

$$\frac{h_K}{\rho_K} \leq C_{ush} \quad \forall K \in \mathbb{T}_h \ ,$$

with ρ_K being the inner diameter of K. ♮

Definition 6.2. A mesh $\mathbb{T}_h$ fulfills the *'uniform-size condition'*, if there is a constant $C_{usi} = C_{usi}(\mathbb{T}_h)$, so that

$$\frac{h_{max}}{h_K} \leq C_{usi} \quad \forall K \in \mathbb{T}_h \ ,$$

with h_{max} being the maximal cell diameter $h := \max_{K \in \mathbb{T}_h} h_{|K}$. ♮

To increase the number of cells in a triangulation, we employ *'refinement'*, which consists of subdividing a cell into four subcells. Cell subdivision is done by connecting the midpoints of opposing edges on each cell. A refinement is global if this is done for each cell. An example of a regular mesh and two global refinements is shown in Figure 6.1. Each of the resulting meshes after refinement is also regular. *'Coarsening'* of four cells is possible if they were generated by prior refinement of some *'parent cell'*. A group of four such cells is referred to as a *'patch'*.
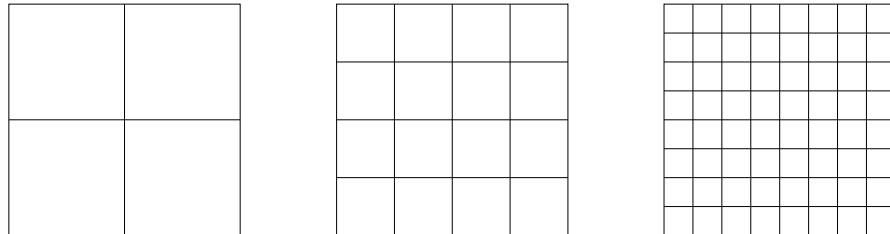

Figure 6.1: A regular mesh after two global refinement cycles.

In addition to global refinement, we will also use local refinement. This consists of only subdividing some cells in a given triangulation. Such refinement leads to cells nodes that are placed on the middle of the neighboring cells' edges. Such nodes are referred to as *hanging nodes*. No 'hanging node refinement' will be done that leads to more than one hanging node per edge. In Figure 6.2 local refinement is applied twice leading to hanging nodes shown as dots.
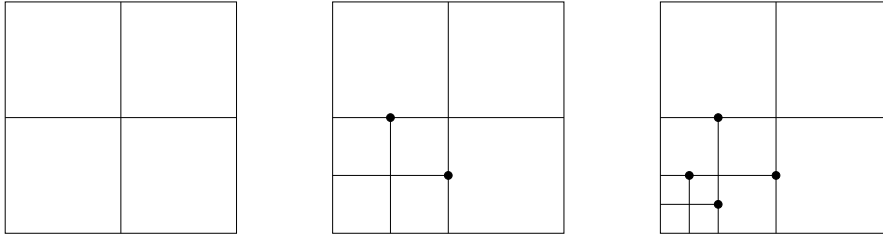
Figure 6.2: A regular mesh and two local refinement cycles with hanging nodes.

These 'hanging nodes' do not carry degrees of freedom and the corresponding function values are determined by (linear) interpolation of neighboring 'regular' nodal points. For more details on this approach see [CaOd84] or [BaRa03].

The *'finest level'* of cells of a triangulation $\mathbb{T}_h$ consists of all cells that can be removed by coarsening in one sweep. The resulting coarsened triangulation is referred to as $\mathbb{T}_{2h}$.

Sometimes we will require that a triangulation $\mathbb{T}_h$ is organized in a patchwise manner. This means that $\mathbb{T}_h$ is the result of global refinement of the coarser triangulation $\mathbb{T}_{2h}$, as shown in Figure 6.3.
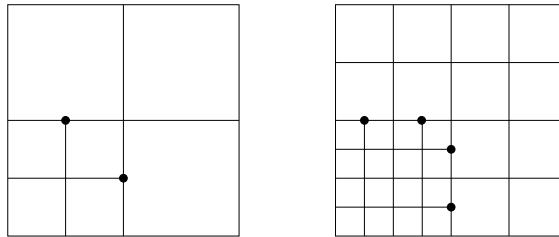

Figure 6.3: A triangulation $\mathbb{T}_{2h}$ with hanging nodes (left) is refined globally once to obtain a triangulation $\mathbb{T}_h$ with patch structure (right).

6.2 Finite element spaces

We discretize function spaces using the usual conforming finite element method as explained in literature, e.g. [Br97, BrSc94, Ci78].

Given a function space V, the triangulation $\mathbb{T}_h$ and the cell-wise space of polynomial functions $Q(K)$, we construct the finite element function space $V_h \subset V$ by

$$V_h := \left\{ \varphi \in V \ \big| \ \varphi_{|K} \in Q(K) \ \ \forall K \in \mathbb{T}_h \right\}.$$

Each polynomial function space $Q(K)$ is actually defined on a reference cell $\hat{K} := (0,1)^2$ as the reference function space $\hat{Q}(\hat{K})$. The function space of polynomials of degree $p \geq 0$ on $\hat{K}$

we denote as

$$\hat{Q}^p(\hat{K}) := \text{span}\left\{ \hat{x}^\alpha \mid \hat{x} = \{\hat{x}_1, \ldots, \hat{x}_n\} , \ \alpha \in \{0, \ldots, p\}^2 \right\} ,$$

where the multi-index α and its use are as in Definition 2.3. In this thesis we will only be using bilinear elements, thus $p = 1$ and we will omit the degree p (if not otherwise noted) and simply refer to $\hat{Q}(\hat{K})$. The reference function space $\hat{Q}(\hat{K})$ is mapped to the respective cell K with help of the mapping $T_K : \hat{K} \to K$,

$$Q(K) = \left\{ \varphi(x) = \hat{\varphi}(T_K(\hat{x})) \ \middle| \ \hat{\varphi} \in \hat{Q}(\hat{K}) \right\} .$$

The mapping T_K of $\hat{K}$ to K (Figure 6.4) is uniquely described by the eight coordinate values of the corners of K. Since a normal one dimensional bilinear quadrilateral finite element function on $\hat{K}$ can be uniquely determined by prescribing values on all four corners, it follows that $T_K \in \hat{Q}(\hat{K})^2$. Thus the reference function space and the mapping function space are the same. Such finite elements are referred to as *'isoparametric'*.
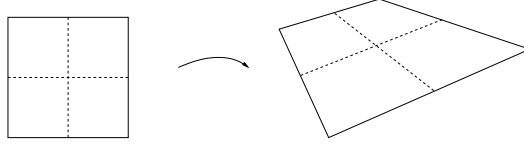

Figure 6.4: Mapping of $\hat{K}$ to K.

It is clear that the numbering of the nodes on the reference cell $\hat{K}$ and actual cell K should be in the same order and orientation. If this were not so, it would make a 'flipping' of the reference cell possible, which is equivalent to the mapping's Jakobi determinant being negative and thus its area being counted as negative.

6.3 Complete variational formulations

6.3.1 ALE

We introduce the spaces

$$
\begin{aligned}
\hat{W}^{ah,0} &:= \hat{V}^0 \times \hat{V}^0 \times \hat{L}^* , \\
\hat{\mathcal{W}}^{ah} &:= \hat{\mathcal{V}}^0 \times \hat{\mathcal{V}}^0 \times \hat{\mathcal{L}}^* , \\
\hat{\mathcal{W}}^{ah,0} &:= \left\{ \hat{\Psi} \in \hat{\mathcal{W}}^{ah} \mid \hat{\Psi} = \{\hat{\psi}^v, \hat{\psi}^u, \hat{\psi}^p\} , \ \hat{\psi}^u_{|t=0} = \hat{\psi}^v_{|t=0} = 0 \right\} .
\end{aligned}
$$

We introduce the semilinear forms $\hat{F}^{ah}(\hat{U})(\hat{\Psi})$, $\hat{A}^{ah}(\hat{U})(\hat{\Psi})$ as the sums of the right- and left-hand side equations (5.3) of Problem 5.1 (in the harmonic continuation case):

$$
\begin{aligned}
\hat{F}^{ah}(\hat{U})(\hat{\Psi}) :=\ & (\hat{g}, \hat{\psi}^v)_{\hat{\Gamma}_N} + ((\hat{\chi}_s\hat{\rho}_s + \hat{\chi}_f\rho_f\hat{J})\hat{f}, \psi^v)\,, \\
\hat{A}^{ah}(\hat{U})(\hat{\Psi}) :=\ & (\hat{\chi}_s\hat{\rho}_s d_t\hat{v}, \hat{\psi}^v) + (\hat{\chi}_f\hat{J}\rho_f(\partial_t\hat{v} + (\hat{F}^{-1}(\hat{v} - \partial_t\hat{T})\cdot\widehat{\nabla})\hat{v}), \hat{\psi}^v) \\
& +(\hat{J}\hat{\sigma}\hat{F}^{-T}, \widehat{\nabla}\hat{\psi}^v) \\
& + \left\{ \begin{array}{ll}
(\hat{\chi}_f\widehat{\text{div}}(\hat{J}\hat{F}^{-1}\hat{v}), \hat{\psi}^p) + (\hat{\chi}_s\hat{\alpha}_p\widehat{\nabla}\hat{p}, \widehat{\nabla}\hat{\psi}^p) & \text{(STVK material)}\,, \\
(\hat{\chi}_f\widehat{\text{div}}(\hat{J}\hat{F}^{-1}\hat{v}), \hat{\psi}^p) + (\hat{\chi}_s(\hat{J} - 1), \hat{\psi}^p) & \text{(INH material)}\,,
\end{array}\right. \\
& +(\hat{\chi}_s(d_t\hat{u} - \hat{v}), \hat{\psi}^u) + (\hat{\chi}_f\hat{\alpha}_u\widehat{\nabla}\hat{u}, \widehat{\nabla}\hat{\psi}^u)\,,
\end{aligned}
\tag{6.1}
$$

with $\hat{U} = \{\hat{v}, \hat{u}, \hat{p}\}$.

With this notation, we can write the variational Problem 5.1 in compact form:

Problem 6.1 (FSI, ALE, harmonic continuation, Galerkin form). *Find* $\hat{U} \in \hat{U}^D + \hat{\mathcal{W}}^{ah,0}$, *such that* $\hat{U}|_{t=0} = \hat{U}^0$, *and,*

$$
\hat{A}^{ah}(\hat{U})(\hat{\Psi}) - F^{ah}(\hat{U})(\hat{\Psi}) = 0 \quad \forall\,\hat{\Psi} \in \hat{W}^{ah,0},
\tag{6.2}
$$

where $\hat{U}^D = \{\hat{v}^D, \hat{u}^D, 0\}$ *is an appropriate extension of the Dirichlet boundary conditions. The semilinear forms and all further notation are as defined in the Equations (6.1) and the Problem 5.1.* ♮

For later purposes we summarize in this notation the stationary FSI ALE Problem 5.3 and define the semilinear form $\hat{A}^{ahs}(\hat{U})(\hat{\Psi})$ as the sum of the left-hand side equations (5.7).

Problem 6.2 (Stationary FSI, ALE, harmonic continuation, Galerkin form). *Find* $\hat{U} \in \hat{U}^D + \hat{W}^{ah,0}$, *such that*

$$
\hat{A}^{ahs}(\hat{U})(\hat{\Psi}) - F^{ah}(\hat{U})(\hat{\Psi}) = 0 \quad \forall\,\hat{\Psi} \in \hat{W}^{ah,0},
\tag{6.3}
$$

where $\hat{U}^D = \{\hat{v}^D, \hat{u}^D, 0\}$ *is an appropriate extension of the Dirichlet boundary conditions.* ♮

6.3.2 Eulerian

We introduce the spaces

$$
\begin{aligned}
W^{e,0} \ & := V^0 \times V^0 \times V^0 \times L^*\,, \\
\mathcal{W}^e \ & := \mathcal{V}^0 \times \mathcal{V}^0 \times \mathcal{V}^0 \times \mathcal{L}^*\,, \\
\mathcal{W}^{e,0} \ & := \{\Psi \in \mathcal{W}^e \mid \Psi = \{\psi^v, \psi^u, \phi^w, \psi^p\}\,,\ \psi^u_{|t=0} = \psi^v_{|t=0} = 0\}\,.
\end{aligned}
$$

We introduce the semilinear form $A^e(U)(\Psi)$ as the sum of the equations (5.14) of Problem 5.6:

$$
\begin{aligned}
A^e(U)(\Psi) := \ & ((\chi_f \rho_f + \chi_s \hat{\rho}_s J)(\partial_t v + (v \cdot \nabla)v), \psi^v) + (\sigma, \nabla \psi^v) - (g, \psi^v)_{\Gamma_N} - ((\chi_f \rho_f + \chi_s \hat{\rho}_s J)f, \psi^v) \\
& + \begin{cases} (\chi_f \mathrm{div} v, \psi^p) + (\chi_s \hat{\alpha}_p \nabla p, \nabla \psi^p) & \text{(STVK material)} \\ (\chi_f \mathrm{div} v, \psi^p) + (\chi_s(1-J), \psi^p) & \text{(INH material)} \end{cases} \\
& + (\partial_t u - w + w \cdot \nabla u, \psi^u) \\
& + (\chi_s(w-v), \psi^w) + (\chi_f \hat{\alpha}_w \nabla w, \nabla \psi^w) \,,
\end{aligned}
$$

$$(6.4)$$

with $U = \{v, u, w, p\}$.

With this notation, we write the variational Problem 5.6 in compact form:

Problem 6.3 (FSI, Eulerian, Galerkin form). *Find $U \in U^D + \mathcal{W}^{e,0}$, such that $U|_{t=0} = U^0$, and,*

$$A^e(U)(\Psi) = 0 \quad \forall \, \Psi \in W^{e,0}, \tag{6.5}$$

where $U^D = \{v^D, u^D, 0, 0\}$ is an appropriate extension of the Dirichlet boundary conditions. The semilinear form and all further notations are as defined in the Equation (6.4) and the Problem 5.6. ♮

For later purposes we summarize in this notation the stationary FSI Eulerian Problem 5.7 and define the semilinear form $A^{es}(U)(\Psi)$ as the sum of the equations (5.18). The semilinear form A^{es} is essentially the definition of A^e without the time differentials.

Problem 6.4 (Stationary FSI, Eulerian, harmonic continuation, Galerkin form). *Find $U \in U^D + W^{es,0}$, such that*

$$A^{es}(U)(\Psi) = 0 \quad \forall \, \Psi \in W^{es,0}, \tag{6.6}$$

where $U = \{v, u, p\} \in W^{es,0} := V^0 \times V^0 \times L^*$, $\Psi = \{\psi^v, \psi^u, \psi^p\} \in W^{es,0}$ and $U^D = \{v^D, u^D, 0\}$ is an appropriate extension of the Dirichlet boundary conditions. ♮

6.4 Spacial discretization

For discretizing the Problems 6.1 (ALE framework) or 6.3 (Eulerian framework) in space, we use equal-order Q_1 finite elements (as described above) for all unknowns, where the corresponding finite element spaces are denoted by $L_h \subset L$, $V_h \subset V$, $W_h \subset W$, etc.. Within the present abstract setting the discretization in time is likewise thought as by a Galerkin method, such as the dG(r) ('discontinuous' Galerkin) or the cG(r) ('continuous' Galerkin) method. Here, the dG(0) method is closely related to the backward Euler scheme and the dG(1) method to the Crank–Nicolson scheme. However, in the test computations described below, we have used a Galerkin method only in space but finite difference schemes in time. The full space-time Galerkin framework is mainly introduced as basis for a systematic approach to residual-based a posteriori error estimation as described below.

The spatial discretization by 'equal-order' finite elements for velocity and pressure needs stabilization in order to compensate for the missing 'inf-sup stability'. We use the so-called 'local projection stabilization' (LPS) introduced by Becker and Braack [BeBr01, BeBr03]. We use an analogous approach for the ALE and Eulerian frameworks in all variations (instationary, stationary, compressible St. Venant-Kirchhoff, incompressible neo-Hookean).

We detail the stabilization terms for the instationary FSI problem in the Eulerian incompressible neo-Hookean case. We also use the approach for stabilizing the convection as well as in the transport equation for the displacement u. We define the mesh-dependent bilinear form

$$(\varphi, \psi)_\delta := \sum_{K \in \mathbb{T}_h} \delta_K \, (\varphi, \psi)_K,$$

$$\delta_K := \frac{1}{\alpha\big(\chi_f \rho_f \nu_f \frac{1}{h_K^2} + \chi_s \mu_s \frac{1}{h_K^2} + \beta\rho|v_h|_{\infty;K}\frac{1}{h_K} + \gamma|w_h|_{\infty;K}\frac{1}{h_K}\big)} \ .$$

Further, we introduce the 'fluctuation operator' $\pi_h : V_h \to V_{2h}$ on the finest mesh level $\mathbb{T}_h$ by $\pi_h = I - P_{2h}$, where $P_{2h} : V_h \to V_{2h}$ is the L^2-projection. The operator π_h measures the fluctuation of a function in V_h with respect to its projection into the next coarser space V_{2h}. With this notation, we define the stabilization form

$$\begin{aligned} S^{e,\delta}(U_h)(\Phi_h, \Psi_h) \ := & (\nabla\pi_h\phi_h^p, \nabla\pi_h\psi_h^p)_\delta + (\rho v_h \cdot \nabla\pi_h\phi_h^v, v_h \cdot \nabla\pi_h\psi_h^v)_\delta \\ & + (w_h \cdot \nabla\pi_h\phi_h^u, w_h \cdot \nabla\pi_h\psi_h^u)_\delta \end{aligned}$$

where the first term stabilizes the pressure, the second one the transport in the flow model, and the third one the transport of the displacement u_h. Then, the stabilized Galerkin approximation of problem (6.6) reads: *Find $U_h \in U_h^D + \mathcal{W}_h^{e,0}$, such that*

$$\int_0^T A^{e,\delta}(U_h)(\Psi_h)dt = 0 \,, \quad \forall\Psi_h \in \mathcal{W}_h^{e,0} \,, \tag{6.7}$$

$$\text{with } A^{e,\delta}(U_h)(\Psi_h) := A^e(U_h)(\Psi_h) + S^{e,\delta}(U_h)(U_h, \Psi_h) \,. \tag{6.8}$$

The LPS has the important property that it acts only on the diagonal terms of the coupled system and that it does not contain any second-order derivatives. However, it is only 'weakly' consistent, as it does not vanish for the continuous solution, but it tends to zero with the right order as $h \to 0$. The choice of the numbers α, β, γ in the stabilization parameter δ_K is, based on practical experience, in our computations $\alpha = 1/2$, and $\beta = \gamma = 1/6$.

6.5 Time discretization

The discretization in time is by the so-called 'fractional-step-θ scheme' in which each time step $t_{n-1} \to t_n$ is split into three substeps $t_{n-1} \to t_{n-1+\theta} \to t_{n-\theta} \to t_n$. For brevity, we formulate this time stepping method for an abstract differential-algebraic equation (DAE)

$$\begin{bmatrix} M & 0 \\ 0 & 0 \end{bmatrix} \begin{bmatrix} \dot{v}(t) \\ \dot{p}(t) \end{bmatrix} + \begin{bmatrix} A(v(t)) & B \\ -B^T & C \end{bmatrix} \begin{bmatrix} v(t) \\ p(t) \end{bmatrix} = \begin{bmatrix} b(t) \\ c(t) \end{bmatrix}, \tag{6.9}$$

which resembles the operator form of the spatially discretized incompressible Navier-Stokes equations with pressure stabilization. With the parameters $\theta = 1 - \sqrt{2}/2 = 0.292893...$, $\theta' = 1 - 2\theta$, $\alpha \in (1/2, 1]$, and $\beta = 1 - \alpha$, the fractional-step-θ scheme reads:

$$\begin{bmatrix} M + \alpha\theta k A^{n-1+\theta} & \theta k B \\ -B^T & C \end{bmatrix} \begin{bmatrix} v^{n-1+\theta} \\ p^{n-1+\theta} \end{bmatrix} = \begin{bmatrix} [M - \beta\theta k A^{n-1}]v^{n-1} + \theta k b^{n-1} \\ c^{n-1+\theta} \end{bmatrix}$$

$$\begin{bmatrix} M + \beta\theta' k A^{n-\theta} & \theta' k B \\ -B^T & C \end{bmatrix} \begin{bmatrix} v^{n-\theta} \\ p^{n-\theta} \end{bmatrix} = \begin{bmatrix} [M - \alpha\theta' k A^{n-1+\theta}]v^{n-1+\theta} + \theta' k b^{n-\theta} \\ c^{n-\theta} \end{bmatrix}$$

$$\begin{bmatrix} M + \alpha\theta k A^{n} & \theta k B \\ -B^T & C \end{bmatrix} \begin{bmatrix} v^{n} \\ p^{n} \end{bmatrix} = \begin{bmatrix} [M - \beta\theta k A^{n-\theta}]v^{n-\theta} + \theta k b_h^{n-\theta} \\ c^{n} \end{bmatrix},$$

where $A^{n-1+\theta} := A(x^{n-1+\theta})$, $b^{n-1} := b(t_{n-1})$, etc.. This scheme is of second order and has a similar work complexity as the well-known Crank–Nicholson scheme (case $\alpha = 1/2$). The fractional-step-θ scheme was originally proposed in form of an operator splitting scheme separating the two complications 'nonlinearity' and 'incompressibility' within each cycle $t_{n-1} \rightarrow t_{n-1+\theta} \rightarrow t_{n-\theta} \rightarrow t_n$. However, it has also very attractive features as a pure time-stepping method. Being *strongly* A-stable, for any choice of $\alpha \in (1/2, 1]$, it possesses the full smoothing property in the case of rough initial data, in contrast to the Crank–Nicholson scheme which is only conditionally smoothing (for $k \sim h^2$). Furthermore, it is less dissipative than most of the other second-order implicit schemes and therefore suitable for computing oscillatory solutions; for more details, we refer to [Rannacher00], [Rannacher04], [Gl03], [BrGl+87] and [MU94].

For computing steady state solutions, we use a pseudo-time stepping techniques based on the simple (first-order) backward Euler scheme, which in the notation from before reads

$$\begin{bmatrix} M + k A^{n} & k B \\ -B^T & C \end{bmatrix} \begin{bmatrix} v^{n} \\ p^{n} \end{bmatrix} = \begin{bmatrix} M v^{n-1} + k b_h^{n-1} \\ c^{n} \end{bmatrix},$$

6.6 Solution of the algebraic systems

After time and space discretization, in each substep of the fractional-step-θ scheme (or any other fully implicit time-stepping scheme) a quasi-stationary nonlinear algebraic system has to be solved. This is done by a standard Newton-type method with adaptive step-length selection, in which all nonlinear terms (i.e. the transport terms, the structure stress terms, the ALE mapping terms) are correctly linearized. The linearization of theses terms is detailed in the next sections. Only the stabilization terms and the terms involving the characteristic function χ_f, determining the position of the interface, are treated by a simple functional iteration. In all cases the iteration starts from the values at the preceding time level. The resulting linear subproblems are then solved by the Generalized Minimal Residual Method (GMRES) method [Saad] with preconditioning by a geometric multigrid method with block-ILU smoothing. In general solving the linear subproblems with such an approach is rather standard nowadays, we omit its details and refer to the relevant literature, e.g., [Turek99], [Rannacher00], or [HronTurek206]. For the implementational details of using the multigrid on locally refined meshes we refer to Becker and Braack [BeBr00].

6.7 Directional derivatives

The first step for solving the Problems 5.1 (in the ALE framework) and 5.6 (the Eulerian framework) is using discrete spatial subspaces and using a time-stepping scheme to approximate the time-differentials.

At each time-step the discrete problems are nonetheless *nonlinear*. To solve the nonlinear problems we use a Newton iteration, the basis of which is solving a linear defect correction problem. The linear operator of the problem is essentially (if time-stepping parts and factors stemming from the approximating of the temporal derivatives are neglected) the directional derivative of $\hat{A}^{ah}(\hat{U}, \hat{\Psi})$ (in the ALE framework) or $A^e(U, \Psi)$ (the Eulerian framework):

$$\hat{A}^{ah'}(\hat{U}_0)(\hat{\Phi}, \hat{\Psi}) := \tfrac{d}{d\epsilon}\hat{A}^{ah}(\hat{U}_0 + \epsilon\hat{\Phi})(\hat{\Psi})|_{\epsilon=0} \ ,$$

$$A^{e'}(U_0)(\Phi, \Psi) := \tfrac{d}{d\epsilon}A^e(U_0 + \epsilon\Phi)(\Psi)|_{\epsilon=0} \ .$$

For linear or almost-linear systems such as the Navier-Stokes equations obtaining the directional derivative is a straight forward task without much difficulty. For structure mechanical systems (for example based on the St. Venant-Kirchhoff material law) though, writing down the explicit directional derivative can become a tenuous task. For example in the Lagrangian case the tensor product $(\hat{J}\hat{\sigma}\hat{F}^{-T}, \widehat{\nabla}\hat{\varphi}^v)$ is notably nonlinear regarding $\hat{u}$ since:

$$\hat{J}\hat{\sigma}\hat{F}^{-T} = \hat{F}(\lambda_s(\mathrm{tr}\hat{E})I + 2\mu_s\hat{E}),$$

$$\text{with} \quad \hat{F} = I + \widehat{\nabla}\hat{u} \ , \ \hat{E} = \tfrac{1}{2}(\hat{F}^T\hat{F} - I) \ .$$

Using the alternative Eulerian framework the observed tensor product is $(\sigma, \nabla\varphi)$. It does not become any easier, since the Cauchy stress tensor σ is based on the inverse of the 'reverse deformation gradient' $(I - \nabla u)$ since

$$\sigma \ = JF^{-1}(\lambda_s(\mathrm{tr}E)I + 2\mu_s E)F^{-T},$$

$$\text{with} \quad F = (I - \nabla u) \ , \ E = \tfrac{1}{2}(F^{-T}F^{-1} - I) \ .$$

6.7.1 Automatic differentiation

To alleviate this problem we use a method that is the basis of *'automatic differentiation'* [Gr89, Rall81]. The method is used to determine the derivative of a function at a given position. It is based on the technique of mechanically applying the basic rules of differentiation to the 'serialized evaluation' of a function. This is achieved by breaking down the evaluation of the function for a given value into a sequence or chain of basic elementary evaluations. Consequently, since evaluation is done in sequence, the resulting values from one evaluation are used in a later evaluation. To these elementary parts the rules of differentiation (i.e. the chain rule, the sum rule and the product rule) are applied.

The method of automatic differentiation lies between those of symbolic differentiation and the approximation of derivatives by divided differences. It is similar to symbolic differentiation

in so far that the results are calculated by evaluating the same sequence of functions. It is thus just as accurate as symbolic differentiation. The difference is that, in contrast to symbolic differentiation, all 'parsing' is done before compilation of the program, when the function evaluation is serialized and differentiation is applied to all levels of the serialization. This parsing before compilation is what gives the method a slight similarity to the method of divided differences. Due to the method of evaluation though, it is by nature faster than divided differences.

The full theory of automatic differentiation usually also includes implementing the method in the form of a precompiler that completely relieves the user of applying the method and literally generates the derivatives in an automatic and efficient fashion, e.g. ADIFOR [BiCa+92], JAKEF [Hi85], GRESS [HoWo+88], PADRE2 [IrKu87].

In this work we only use the method, differentiation is done 'manually'. We implement the method of 'reverse differentiation'. In a first step, the 'forward sweep', the function is broken down into a sequence or chain of basic elementary evaluations. Each of these evaluations is stored in a variable. In the second step, the 'reverse sweep', the rules of differentiation are applied. As a basic example we calculate the derivative of a given function $f(x) = \sin(x\tanh(x))\log(x - 1/x)$ at the position x_0.

$$
\begin{array}{llll}
& \overbrace{\text{forward sweep}} & & \overbrace{\text{reverse sweep}} \\[2mm]
f_1 & := & 1/x_0 & \\
f_2 & := & \log(x_0 - f_1) & \\
f_3 & := & \tanh(x_0) & \\
f_4 & := & x_0 f_3 & \\
f_5 & := & \sin(f_4) & \\
f_6 & := & f_5 f_2 & \\
f(x_0) & = & f_6 &
\end{array}
$$

$$
\begin{array}{lll}
f_1' & := & -1/x_0^2 \\
f_2' & := & (1 - f_1')/(x_0 - f_1) \\
f_3' & := & 1 - \tanh^2(x_0) \\
f_4' & := & f_3 + x_0 f_3' \\
f_5' & := & f_4' \cos(f_4) \\
f_6' & := & f_5' f_2 + f_5 f_2' \\
f'(x_0) & = & f_6'
\end{array}
$$

For reasons of brevity we will only demonstrate how the method of automatic differentiation can be used to obtain the directional derivatives of the stationary incompressible neo-Hookean FSI Problems in the ALE (Problem 5.3) and Eulerian (Problem 5.7) frameworks.

6.7.2 ALE framework

As a first step towards 'serialized evaluation' of the semilinear form $\hat{A}^{ahs}(\hat{U})(\hat{\Phi})$ (Problem 5.3) we define the following values.

Definition 6.3.

$$
\begin{aligned}
B_1 \quad &:= \hat{v} \,, B_2 := \widehat{\nabla}\hat{v} \,, B_3 := \widehat{\nabla}\hat{u} \,, \\
B_4 \quad &:= I + B_3 \,, & (\quad &= \hat{F} &) \,, \\
B_5 \quad &:= B_4^{-1} \,, & (\quad &= \hat{F}^{-1} &) \,, \\
B_6 \quad &:= B_4 B_5 - I \,, & (\quad &= 0 &) \,, \\
B_7 \quad &:= \det B_4 \,, & (\quad &= \hat{J} &) \,, \\
B_8 \quad &:= B_7 B_5 B_1 \,, & (\quad &= \hat{J}\hat{F}^{-1}\hat{v} &) \,, \\
B_9 \quad &:= B_2 B_5 \,, & (\quad &= \widehat{\nabla}\hat{v}\hat{F}^{-1} &) \,, \\
B_{10} \quad &:= B_4 B_4^T \,, & (\quad &= \hat{F}\hat{F}^T &) \,, \\
B_{11} \quad &:= -\hat{p}I + \rho_f \nu_f (B_9 + B_9^T) \,, & (\quad &= \hat{\sigma}_f &) \,, \\
B_{12} \quad &:= -\hat{p}I + \mu_s(B_{10} - I) \,, & (\quad &= \hat{\sigma}_s &) \,, \\
B_{13} \quad &:= \hat{\chi}_f B_{11} + \hat{\chi}_s B_{12} \,, & (\quad &= \hat{\sigma} &) \,, \\
B_{14} \quad &:= B_7 B_{13} B_5^T \,, & (\quad &= \hat{J}\hat{\sigma}\hat{F}^{-T} &) \,, \\
B_{15} \quad &:= B_7 B_9 B_1 \,, & (\quad &= \hat{J}(\hat{F}^{-1}\hat{v}\cdot\widehat{\nabla})\hat{v} &) \,, \\
B_{16} \quad &:= \widehat{\mathrm{div}}B_8 \,, & (\quad &= \widehat{\mathrm{div}}(\hat{J}\hat{F}^{-1}\hat{v}) &) \,.
\end{aligned}
$$

(6.10)

♮

We express the evaluation of the semilinear form $\hat{A}^{ahs}$ in terms of the presented definitions:

$$
\begin{aligned}
\hat{A}^{ahs}(\hat{U})(\hat{\Psi}) = \ & (\rho_f \hat{\chi}_f \hat{B}_{15}, \quad \hat{\psi}^v) + (\quad B_{14}, \widehat{\nabla}\hat{\psi}^v) \\
& + (\quad \hat{\chi}_f B_{16}, \quad \hat{\psi}^p) + (\hat{\chi}_s(B_7 - 1), \quad \hat{\psi}^p) \\
& + (\hat{\alpha}_u \hat{\chi}_f B_3, \widehat{\nabla}\psi^u) + (\quad \hat{\chi}_s B_1, \hat{\psi}^u) \,.
\end{aligned}
$$

(6.11)

Definition 6.4. The directional derivative of the value B_i at the position $\hat{U}$ and only in one "state" direction e.g. the velocity component will be denoted as

$$
B_i'(\hat{U})(\hat{\phi}^v) := \tfrac{d}{d\epsilon}B_i(\hat{U} + \epsilon\hat{\Phi}^v)_{|\epsilon=0},
$$

with $\hat{\Phi}^v := \{\hat{\phi}^v, 0, 0\} \in \hat{W}^{ah,0}$. The derivatives in the u- and p-directions will be referred to in similar fashion. The derivative of B_i in all components will be referred to as $B_i'(\hat{U})(\hat{\Phi})$. ♮

Remark 6.1. The characteristic functions $\hat{\chi}_f, \hat{\chi}_s$ although unsteady at the interface, only depend on the reference position $\hat{x}$. They are independent of the state variables $\{\hat{v}, \hat{u}, \hat{p}\}$ and consequently have no directional derivatives. Hence they have no assigned B_i-definitions.

The reason we take note of this simple point is that this is not the case later in the Eulerian framework, since there the characteristic functions χ_f, χ_s are in part also determined by the displacement u:

$$
\chi_f(x) = \hat{\chi}_f(x - u) \,, \ \chi_s(x) = \hat{\chi}_s(x - u) \,.
$$

♮

Lemma 6.1. The directional derivative of B_7 at $\hat{U}$ in the direction $\hat{\phi}^u$ is

$$
\begin{aligned}
B_7'(\hat{U})(\hat{\phi}^u) = \ & (\widehat{\partial}_1\hat{\phi}_1^u)(1 + \widehat{\partial}_2\hat{u}_2) - \widehat{\partial}_2\hat{\phi}_1^u\widehat{\partial}_1\hat{u}_2 \\
& + (1 + \widehat{\partial}_1\hat{u}_1)(\widehat{\partial}_2\hat{\phi}_2^u) - \widehat{\partial}_2\hat{u}_1\widehat{\partial}_1\hat{\phi}_2^u \,.
\end{aligned}
$$

Proof. We apply the directional derivative in the first and second components of the displacement to B_7 in equation (6.12).

$$
\begin{aligned}
B_7 = \hat{J} \; &= \det F = \det(1 + \widehat{\nabla}\hat{u}) \\
&= \begin{vmatrix} 1 + \widehat{\partial}_1\hat{u}_1 & \widehat{\partial}_2\hat{u}_1 \\ \widehat{\partial}_1\hat{u}_2 & 1 + \widehat{\partial}_2\hat{u}_2 \end{vmatrix} \\
&= (1 + \widehat{\partial}_1\hat{u}_1)(1 + \widehat{\partial}_2\hat{u}_2) - \widehat{\partial}_2\hat{u}_1\widehat{\partial}_1\hat{u}_2 \; .
\end{aligned}
\tag{6.12}
$$

$\square$

Lemma 6.2. The directional derivative of B_5 at $\hat{U}$ in the direction $\hat{\phi}^u$ is

$$
B_5'(\hat{U})(\hat{\phi}^u) \;\; = -B_5 \, B_4'(\hat{U})(\hat{\phi}^u) \, B_5 \; ,
$$

provided the directional derivative of B_4 at $\hat{U}$ in the direction $\hat{\phi}^u$ is known.

Proof. The directional derivative of $B_5 = \hat{F}^{-1}$ is obtained by observing its implicit defining equation. Since B_4 and B_5 are inverse to each other, the definition of B_6 is actually an equation $B_6 = 0$. We apply the chain rule to $B_6 = B_4 B_5 - I$. It follows:

$$
\begin{aligned}
B_6'(\hat{U})(\hat{\phi}^u) \;\; &= B_4'(\hat{U})(\hat{\phi}^u) \, B_5 + B_4 \, B_5'(\hat{U})(\hat{\phi}^u) = 0 \; , \\
\Leftrightarrow \;\; B_5'(\hat{U})(\hat{\phi}^u) \;\; &= -B_5 \, B_4'(\hat{U})(\hat{\phi}^u) \, B_5 \; .
\end{aligned}
$$

$\square$

Lemma 6.3. The directional derivatives of B_i for $i = 1, \ldots, 16$ at $\hat{U}$ in the direction $\hat{\phi}^u$ are:

$$
\left.
\begin{aligned}
B_1 \;\; &= \hat{v} \, , B_2 = \widehat{\nabla}\hat{v} \, , B_3 = \widehat{\nabla}\hat{u} \\
B_4 \;\; &= I + B_3 \\
B_5 \;\; &= B_4^{-1} \\
B_6 \;\; &= B_4 B_5 - I = 0 \\
B_7 \;\; &= \det B_4 \\
\\
B_8 \;\; &= B_7 B_5 B_1 \\
B_9 \;\; &= B_2 B_5 \\
B_{10} \;\; &= B_4 B_4^T \\
B_{11} \;\; &= -\hat{p}I + \rho_f \nu_f (B_9 + B_9^T) \\
B_{12} \;\; &= -\hat{p}I + \mu_s (B_{10} - I) \\
B_{13} \;\; &= \hat{\chi}_f B_{11} + \hat{\chi}_s B_{12} \\
B_{14} \;\; &= B_7 B_{13} B_5^T \\
B_{15} \;\; &= B_7 B_9 B_1 \\
B_{16} \;\; &= \widehat{\mathrm{div}} B_8
\end{aligned}
\right\}
\rightarrow
\left\{
\begin{aligned}
B_1' \;\; &= 0 \, , \; B_2' \;\; = 0 \, , \; B_3' \;\; = \widehat{\nabla}\hat{\phi}^u \\
B_4' \;\; &= B_3' \\
B_5' \;\; &= -B_5 \, B_4' \, B_5 \\
B_6' \;\; &= 0 \\
B_7' \;\; &= (\widehat{\partial}_1\hat{\phi}_1^u)(1 + \widehat{\partial}_2\hat{u}_2) - \widehat{\partial}_2\hat{\phi}_1^u\widehat{\partial}_1\hat{u}_2 \\
&\quad + (1 + \widehat{\partial}_1\hat{u}_1)(\widehat{\partial}_2\hat{\phi}_2^u) - \widehat{\partial}_2\hat{u}_1\widehat{\partial}_1\hat{\phi}_2^u \\
B_8' \;\; &= B_7' \, B_5 B_1 + B_7 \, B_5' \, B_1 \\
B_9' \;\; &= B_2 \, B_5' \\
B_{10}' \;\; &= B_4' \, B_4^T + B_4 \, B_4'^{\;T} \\
B_{11}' \;\; &= \rho_f \nu_f (\, B_9' \;\; + \;\; B_9'^{\;T}) \\
B_{12}' \;\; &= \mu_s \, B_{10}' \\
B_{13}' \;\; &= \hat{\chi}_f \, B_{11}' \;\; + \hat{\chi}_s \, B_{12}' \\
B_{14}' \;\; &= B_7' \, B_{13} B_5^T + B_7 \, B_{13}' \, B_5^T + B_7 B_{13} \, B_5'^{\;T} \\
B_{15}' \;\; &= B_7' \, B_9 B_1 + B_7 \, B_9' \, B_1 \\
B_{16}' \;\; &= \widehat{\mathrm{div}} \, B_8' \;\; .
\end{aligned}
\right.
\tag{6.13}
$$

For brevity all derivatives $B_i'(\hat{U})(\phi^u)$ have been abbreviated to B_i'.

Proof. In two cases we use the Lemmas 6.1 and 6.2. Otherwise all derivates follow directly when applying the rules of derivation to the sums and products, and omitting zero-valued sums. $\square$

Lemma 6.4. The directional derivatives of B_i for $i = 1, \ldots, 16$ at $\hat{U}$ in the direction $\hat{\phi}^v$ are:

$$
\left.\begin{aligned}
B_1 &= \hat{v} \,, B_2 = \widehat{\nabla}\hat{v} \,, B_3 = \widehat{\nabla}\hat{u} \\
B_4 &= I + B_3 \\
B_5 &= B_4^{-1} \\
B_6 &= B_4 B_5 - I \\
B_7 &= \det B_4 \\
B_8 &= B_7 B_5 B_1 \\
B_9 &= B_2 B_5 \\
B_{10} &= B_4 B_4^T \\
B_{11} &= -\hat{p}I + \rho_f \nu_f (B_9 + B_9^T) \\
B_{12} &= -\hat{p}I + \mu_s(B_{10} - I) \\
B_{13} &= \hat{\chi}_f B_{11} + \hat{\chi}_s B_{12} \\
B_{14} &= B_7 B_{13} B_5^T \\
B_{15} &= B_7 B_9 B_1 \\
B_{16} &= \widehat{\operatorname{div}} B_8
\end{aligned}\right\}
\rightarrow
\left\{\begin{aligned}
B_1' &= \hat{\phi}^v \,, \ B_2' = \widehat{\nabla}\hat{\phi}^v \,, \ B_3' = 0 \\
B_4' &= 0 \\
B_5' &= 0 \\
B_6' &= 0 \\
B_7' &= 0 \\
B_8' &= B_7 B_5 \, B_1' \\
B_9' &= B_2' \, B_5 \\
B_{10}' &= 0 \\
B_{11}' &= \rho_f \nu_f (\, B_9' \, + \, B_9'^{\,T}) \\
B_{12}' &= 0 \\
B_{13}' &= \hat{\chi}_f \, B_{11}' \\
B_{14}' &= B_7 \, B_{13}' \, B_5^T \\
B_{15}' &= B_7 \, B_9' \, B_1 + B_7 B_9 \, B_1' \\
B_{16}' &= \widehat{\operatorname{div}} \, B_8' \quad.
\end{aligned}\right.
\tag{6.14}
$$

For brevity all derivatives $B_i'(\hat{U})(\phi^v)$ have been abbreviated to B_i'.

Proof. Analogous to Lemma 6.3. $\qquad\square$

Lemma 6.5. The directional derivatives of B_i for $i = 1, \ldots, 16$ at $\hat{U}$ in the direction $\hat{\phi}^p$ are all zero except for the following four:

$$
\left.\begin{aligned}
B_{11} &= -\hat{p}I + \rho_f \nu_f (B_9 + B_9^T) \\
B_{12} &= -\hat{p}I + \mu_s(B_{10} - I) \\
B_{13} &= \hat{\chi}_f B_{11} + \hat{\chi}_s B_{12} \\
B_{14} &= B_7 B_{13} B_5^T
\end{aligned}\right\}
\rightarrow
\left\{\begin{aligned}
B_{11}' &= -\hat{\phi}^p I \\
B_{12}' &= -\hat{\phi}^p I \\
B_{13}' &= -\hat{\phi}^p I \\
B_{14}' &= -\hat{J}\hat{\phi}^p B_5^T \quad.
\end{aligned}\right.
\tag{6.15}
$$

For brevity all derivatives $B_i'(\hat{U})(\phi^p)$ have been abbreviated to B_i'.

Proof. Analogous to Lemma 6.3. $\qquad\square$

Lemma 6.6. The directional derivatives of $\hat{A}^{ahs}$ at $\hat{U}$ in the directions (respectively) $\hat{\phi}^v, \hat{\phi}^u, \hat{\phi}^p$ are

$$
\begin{aligned}
\hat{A}^{ahs\prime}(\hat{U})(\hat{\phi}^v, \hat{\Psi}) = \ &(\rho_f \hat{\chi}_f \hat{B}_{15}'(\hat{U})(\hat{\phi}^v), \ \hat{\psi}^v) + (\ B_{14}'(\hat{U})(\hat{\phi}^v), \ \widehat{\nabla}\hat{\psi}^v) \\
&+ (\ \hat{\chi}_f B_{16}'(\hat{U})(\hat{\phi}^v), \ \hat{\psi}^p) \\
&\qquad\qquad\qquad\qquad + (\ \hat{\chi}_s B_1'(\hat{U}), \ \hat{\psi}^u) \,, \\
\hat{A}^{ahs\prime}(\hat{U})(\hat{\phi}^u, \hat{\Psi}) = \ &(\rho_f \hat{\chi}_f \hat{B}_{15}'(\hat{U})(\hat{\phi}^u), \ \hat{\psi}^u) + (\ B_{14}'(\hat{U})(\hat{\phi}^u), \ \widehat{\nabla}\hat{\psi}^u) \\
&+ (\ \hat{\chi}_f B_{16}'(\hat{U})(\hat{\phi}^u), \ \hat{\psi}^p) + (\hat{\chi}_s B_7'(\hat{U})(\hat{\phi}^u), \ \hat{\psi}^p) \\
&+ (\ \hat{\alpha}_u \chi_f \widehat{\nabla}\hat{\phi}^u, \widehat{\nabla}\psi^u) \,, \\
\hat{A}^{ahs\prime}(\hat{U})(\hat{\phi}^p, \hat{\Psi}) = \ &\qquad\qquad\qquad\qquad\quad (\ -\hat{J}\hat{\phi}^p B_5^T, \widehat{\nabla}\hat{\psi}^p) \,.
\end{aligned}
$$

Proof. Follows by deriving the Equation (6.11) in the respective direction and applying the Lemmas 6.3, 6.4 and 6.5. $\qquad\square$

6.7.3 Eulerian framework

We demonstrate the method of automatic differentiation for the semilinear form $A^{es}(U)(\Psi)$ (Problem 5.7, in the case of harmonic continuation of u_s). In essence we make the same steps as in the ALE framework. There is one notable difficulty, as already mentioned in Remark 6.1. In the ALE framework the characteristic functions $\hat{\chi}_f, \hat{\chi}_s$ have no directional derivatives, since they depend only on the reference position $\hat{x}$. This is not the case in the Eulerian framework, since

$$\chi_f(x) = \hat{\chi}_f(x - u) \ , \ \chi_s(x) = \hat{\chi}_s(x - u) \ .$$

This difficulty is addressed (and resolved).

As a first step towards 'serialized evaluation' of the form we define the following values.

Definition 6.5.

$$
\begin{aligned}
C_1 \ \ &:= v \ , C_2 := \nabla v \ , C_3 := \nabla u \ , \\
C_4 \ \ &:= I - C_3 \ , &(\ = F &) \ , \\
C_5 \ \ &:= C_4^{-1} \ , &(\ = F^{-1} = \hat{F} &) \ , \\
C_6 \ \ &:= C_4 C_5 - I \ , &(\ = 0 &) \ , \\
C_7 \ \ &:= \det C_4 \ , &(\ = J = \hat{J}^{-1} &) \ , \\
C_8 \ \ &:= C_5 C_5^T \ , &(\ = F^{-1} F^{-T} &) \ , \\
C_9 \ \ &:= -pI + \rho_f \nu_f (C_2 + C_2^T) \ , &(\ = \sigma_f &) \ , \\
C_{10} &:= -pI + \mu_s (C_8 - I) \ , &(\ = \sigma_s &) \ , \\
C_{11} &:= \chi_f \ , &(\ = \hat{\chi}_f(x - u) &) \ , \\
C_{12} &:= \chi_s \ , &(\ = \hat{\chi}_s(x - u) &) \ , \\
C_{13} &:= C_{11} C_9 + C_{12} C_{10} \ , &(\ = \sigma &) \ , \\
C_{14} &:= C_2 C_1 \ , &(\ = (v \cdot \nabla) v &) \ , \\
C_{15} &:= \operatorname{div} C_1 \ , &(\ = \operatorname{div} v &) \ .
\end{aligned}
$$

(6.16)

♮

We express the evaluation of the semilinear form A^{es} in terms of the presented definitions.

$$
\begin{aligned}
A^{es}(U)(\Psi) = \ \ &(\ \rho_f C_{11} C_{14} \ , \ \ \psi^v \ ) + (\ C_{11} C_9 + C_{12} C_{10} \ , \nabla \psi^v \ ) \\
&+ (\ \ \ \ C_{11} C_{15} \ , \ \ \psi^p \ ) + (\ \ \ \ \ C_{12}(1 - C_7) \ , \ \ \psi^p \ ) \\
&+ (\ \alpha_u C_{11} C_3 \ , \nabla \psi^u \ ) + (\ \ \ \ \ \ \ \ \ \ \ C_{12} C_1 \ , \ \ \psi^u \ )
\end{aligned}
$$

(6.17)

Definition 6.6. We define the following directional derivatives of the value C_i at the position U as (in similar fashion as in the Definition 6.4 in previous section)

$$C_i'(U)(\phi^v) := \tfrac{d}{d\epsilon} C_i(U + \epsilon \Phi^v)_{|\epsilon=0} \ ,$$

with $\Phi^v := \{\phi^v, 0, 0\} \in W^{e,0}$. The derivatives in the u- and p-directions will be referred to in similar fashion. The derivative of C_i in all components will be referred to as $C_i'(U)(\Phi)$. ♮

Lemma 6.7. The directional derivative of C_7 at U in the direction ϕ^u is

$$C_7'(U)(\phi^u) = \begin{aligned}&(-\partial_1\phi_1^u)(1-\partial_2 u_2) - \partial_2\phi_1^u\partial_1 u_2\\&+(1-\partial_1 u_1)(-\partial_2\phi_2^u) - \partial_2 u_1\partial_1\phi_2^u\ .\end{aligned}$$

Proof. The statement is similar to that of Lemma 6.1. The proof follows in analogous fashion. □

Lemma 6.8. The directional derivative of C_5 at U in the direction ϕ^u is

$$C_5'(U)(\phi^u)\ \ = -C_5\, C_4'(U)(\phi^u)\, C_5\ ,$$

provided the directional derivative of C_4 at U in the direction ϕ^u exists.

Proof. The statement is equivalent to that of Lemma 6.2. The proof follows in analogous fashion. □

We will also need the derivatives of $C_{11} = \chi_f, C_{12} = \chi_s$ in the direction $-\phi^u$, since

$$\chi_f(x) = \hat{\chi}_f(x-u)\ ,\ \chi_s(x) = \hat{\chi}_s(x-u)\ .$$

Obtaining these directional derivatives is not immediately clear due to the unsteadiness of the otherwise constant characteristic functions. Since we are interested in the influence of χ_f regarding the rest of the integral, we observe the situation with an arbitrary function $g \in H^1(\Omega)$ in the integral:

$$\lim_{\epsilon\to 0}\frac{\int_\Omega \chi_f(x-\epsilon\phi^u)\, g\ dx\ -\ \int_\Omega \chi_f(x)\, g\ dx}{\epsilon}. \tag{6.18}$$

The derivative in Equation (6.18) is an expression typically encountered in the field of shape and structural optimization, see for example [SoZo92, AGJT04]. It is referred to as the *‘directional shape derivative’* of the domain Ω_f in the direction $-\phi^u$. Such problems are sometimes also referred to as ‘shape sensitivity’ or ‘boundary variation problems’ [Pironneau84]. The derivatives lead to integrals of the trace of g on the interface. To be able to refer to the derivatives in the same notational ‘C-framework’ on Ω we define the following Dirac functions.

Definition 6.7. We define the *‘interface Dirac functions’* δ_f and δ_s with a function $g \in L(\Omega) \cap H^1(\Omega_f) \cap H^1(\Omega_s)$ in the following manner:

$$\begin{aligned}\int_\Omega \delta_f g\ dx &:= \int_{\Gamma_i} g_f^-\ dx\ ,\\ \int_\Omega \delta_s g\ dx &:= \int_{\Gamma_i} g_s^-\ dx\ .\end{aligned}$$

The values g_f^-, g_s^- are as defined in Section 2.1. They are the traces of g on the interface Γ_i *as seen from* from the Ω_f or Ω_s side of the interface. If $g \in H^1(\Omega)$, then of course $g_{|\Gamma_i} \in H^{1/2}(\Gamma_i)$ and $g_{|\Gamma_i} = g_f^- = g_s^-$. ♮

Lemma 6.9. The directional derivatives of C_{11}, C_{12} at U in the direction ϕ^u in conjunction with the rest of the integrand $g \in L(\Omega) \cap H^1(\Omega_f) \cap H^1(\Omega_s)$, are

$$\begin{aligned}C_{11}'(U)(\phi^u)\, g &= -n_f\cdot\phi^u\, \delta_f\, g\ ,\\ C_{12}'(U)(\phi^u)\, g &= -n_s\cdot\phi^u\, \delta_s\, g\ .\end{aligned}$$

Proof. By the Hadamard structure theorem (see [Zol79] or any of the shape citations above), it is known that the derivative is carried only by the boundary of the shape $\Omega_f = \chi_f \Omega$ in the following manner

$$\lim_{\epsilon \to 0} \tfrac{1}{\epsilon}(\textstyle\int_\Omega \chi_f(x + \epsilon\phi^u)\, g\, dx \; - \; \int_\Omega \chi_f(x)\, g\, dx) = \int_{\Gamma_i} n_f \cdot \phi^u g_f^-\, dx \,.$$

Finally, the boundary integral on Γ_i is written as an integral in Ω with the Dirac function δ_f as defined in 6.7. We only consider the C_{11} case. The C_{12} follows in analogous fashion. $\qquad\square$

Lemma 6.10. The directional derivatives of C_i for $i = 1, \ldots, 16$ at U in the direction ϕ^u are

$$
\left. \begin{array}{ll}
C_1 & = v\,, C_2 = \nabla v\,, C_3 = \nabla u \\
C_4 & = I - C_3 \\
C_5 & = C_4^{-1} \\
C_6 & = C_4 C_5 - I = 0 \\
C_7 & = \det C_4 \\
\\
C_8 & = C_5 C_5^T \\
C_9 & = -pI + \rho_f \nu_f(C_2 + C_2^T) \\
C_{10} & = -pI + \mu_s(C_8 - I) \\
C_{11} & = \chi_f \\
C_{12} & = \chi_s \\
C_{13} & = C_{11}C_9 + C_{12}C_{10} \\
C_{14} & = C_2 C_1 \\
C_{15} & = \operatorname{div} C_1
\end{array} \right\}
\rightarrow
\left\{ \begin{array}{ll}
C_1' & = 0\,, C_2' = 0\,, C_3' = \nabla\phi^u \\
C_4' & = -\,C_3' \\
C_5' & = -C_5\, C_4'\, C_5 \\
C_6' & = 0 \\
C_7' & = (-\partial_1\phi_1^u)(1 - \partial_2 u_2) - \partial_2\phi_1^u \partial_1 u_2 \\
& \quad + (1 - \partial_1 u_1)(-\partial_2\phi_2^u) - \partial_2 u_1 \partial_1 \phi_2^u \\
C_8' & = C_5'\, C_5^T + C_5\, C_5'^{\,T} \\
C_9' & = 0 \\
C_{10}' & = \mu_s\, C_8' \\
C_{11}' & = -n_f \cdot \phi^u\, \delta_f \\
C_{12}' & = -n_s \cdot \phi^u\, \delta_s \\
C_{13}' & = C_{11}'\, C_9 +\, C_{12}'\, C_{10} + C_{12}\, C_{10}' \\
C_{14}' & = 0 \\
C_{15}' & = 0
\end{array} \right.
$$

$$(6.19)$$

For brevity all derivatives $C_i'(U)(\phi^u)$ have been abbreviated to C_i'.

Proof. For the C_5, C_7, C_{11} and C_{12} we apply the Lemmas 6.7, 6.8 and 6.9. Otherwise all derivates follow directly when applying the rules of derivation to the sums and products, and omitting zero-valued sums. $\qquad\square$

Lemma 6.11. The directional derivatives of C_i for $i = 1, \ldots, 16$ at U in the direction ϕ^v are

$$
\left. \begin{array}{ll}
C_1 & = v\,, C_2 = \nabla v\,, C_3 = \nabla u \\
C_4 & = I - C_3 \\
C_5 & = C_4^{-1} \\
C_6 & = C_4 C_5 - I = 0 \\
C_7 & = \det C_4 \\
C_8 & = C_5 C_5^T \\
C_9 & = -pI + \rho_f \nu_f(C_2 + C_2^T) \\
C_{10} & = -pI + \mu_s(C_8 - I) \\
C_{11} & = \chi_f \\
C_{12} & = \chi_s \\
C_{13} & = C_{11}C_9 + C_{12}C_{10} \\
C_{14} & = C_2 C_1 \\
C_{15} & = \operatorname{div} C_1
\end{array} \right\}
\rightarrow
\left\{ \begin{array}{ll}
C_1' & = \phi^v\,, C_2' = \nabla\phi^v\,, C_3' = 0 \\
C_4' & = 0 \\
C_5' & = 0 \\
C_6' & = 0 \\
C_7' & = 0 \\
C_8' & = 0 \\
C_9' & = \rho_f \nu_f(\, C_2' +\, C_2'^{\,T}) \\
C_{10}' & = 0 \\
C_{11}' & = 0 \\
C_{12}' & = 0 \\
C_{13}' & = C_{11}\, C_9' \\
C_{14}' & = C_2'\, C_1 + C_2\, C_1' \\
C_{15}' & = \operatorname{div} C_1'
\end{array} \right.
$$

$$(6.20)$$

For brevity all derivatives $C_i'(U)(\phi^v)$ have been abbreviated to C_i'.

Proof. Analogous to Lemma 6.10. $\qquad\square$

Lemma 6.12. The directional derivatives of C_i for $i = 1, \ldots, 16$ at U in the direction ϕ^p are all zero except for the following three

$$
\left.
\begin{array}{ll}
C_9 & = -pI + \rho_f \nu_f (C_2 + C_2^T) \\
C_{10} & = -pI + \mu_s (C_8 - I) \\
C_{13} & = C_{11} C_9 + C_{12} C_{10}
\end{array}
\right\}
\rightarrow
\left\{
\begin{array}{ll}
C_9' & = -\phi^p I \\
C_{10}' & = -\phi^p I \\
C_{13}' & = -\phi^p I
\end{array}
\right.
\tag{6.21}
$$

For brevity all derivatives $C_i'(U)(\phi^p)$ have been abbreviated to C_i'.

Proof. Analogous to Lemma 6.10. $\qquad\square$

Lemma 6.13. The directional derivatives of A^{es} at U in the directions (respectively) ϕ^v, ϕ^u, ϕ^p are

$$
\begin{aligned}
A^{es'}(U)(\phi^v, \Psi) = {}& (\ \rho_f \chi_f\, C_{14}'(U)(\phi^v)\ ,\qquad \psi^v\ ) + (\ \chi_f\, C_9'(U)(\phi^v)\ ,\quad \nabla \psi^v\ ) \\
& + (\ \chi_f\, C_{15}'(U)(\phi^v)\ ,\qquad \psi^p\ ) \\
& \qquad\qquad\qquad\qquad\qquad\qquad + (\ \chi_s\, C_1'(U)(\phi^v)\ ,\qquad \psi^u\ )\ ,
\end{aligned}
$$

$$
\begin{aligned}
A^{es'}(U)(\phi^u, \Psi) = {}& -(\quad \rho_f n_f \cdot \phi^u (C_{14})_f^-\ ,\qquad \psi^v\ ) + (\ \chi_s\, C_{10}'(U)(\phi^u)\ ,\quad \nabla\psi^v\ ) \\
& \qquad\qquad\qquad\qquad\qquad\qquad - (\quad n_f \cdot \phi^u C_9\quad ,\ (\nabla\psi^v)_f^-\ )_{\Gamma_i} \\
& \qquad\qquad\qquad\qquad\qquad\qquad - (\quad n_s \cdot \phi^u C_{10}\quad ,\ (\nabla\psi^v)_s^-\ )_{\Gamma_i} \\
& -(\quad n_f \cdot \phi^u (C_{15})_f^-\ ,\qquad \psi^p\ ) - (\ \chi_s\, C_7'(U)(\phi^u)\ ,\qquad \psi^p\ ) \\
& \qquad\qquad\qquad\qquad\qquad\qquad + (\quad n_s \cdot \phi^u (C_7)_s^-\ ,\qquad \psi^p\ ) \\
& +(\qquad \alpha_u \chi_f \nabla \phi^u\ ,\qquad \nabla \psi^u\ ) \\
& -(\quad \alpha_u n_f \cdot \phi^u (C_3)_f^-\ ,\ (\nabla\psi^u)_f^-\ ) - (\quad n_s \cdot \phi^u (C_1)_s^-\ ,\qquad \psi^u\ )\ ,
\end{aligned}
$$

$$
A^{es'}(U)(\phi^p, \Psi) = \qquad\qquad\qquad\qquad\qquad\qquad (\quad C_{13}'(U)(\phi\ )\ ,\quad \nabla\psi^v\ )\ .
$$

Proof. Follows by deriving the semilinear form (6.17) in the respective directions and applying the Lemmas 6.10, 6.11 and 6.12. $\qquad\square$

6.7.4 Similarities and differences

An obvious difference between the Eulerian directional derivative $A^{es'}(U)(\Phi, \Psi)$ and the ALE directional derivative $\hat{A}^{ahsi'}(\hat{U})(\hat{\Phi}, \hat{\Psi})$ are the differences of the directional derivatives concerning the displacement $\phi^u, \hat{\phi}^u$. In the Eulerian framework we obtain the 'interface Dirac functions', whereas in the ALE framework the transformation acting on fluid equations are 'derived'. In fact, if we assume $\hat{U} = \{\hat{v}, \hat{u}, \hat{p}\}$ and $U = \{v, u, p\}$ to be strong solutions of the Problems 5.3 and 5.7, then this difference is actually the *only* difference, since the directional derivatives for the velocity and pressure are then *equal*.

Lemma 6.14. Let $\hat{U} = \{\hat{v}, \hat{u}, \hat{p}\}$ and $U = \{v, u, p\}$ to be strong solutions of the Problems 5.3 and 5.7, so that $\hat{U}(\hat{x}) = U(\hat{x} + \hat{u}(\hat{x}))$ for all $\hat{x} \in \Omega$. For given test functions $\{\hat{\Phi}, \hat{\Psi}\}$ and

respectively $\{\Phi, \Psi\} = \{\hat{\Phi}(\hat{T}(\hat{x})), \Psi(\hat{T}(\hat{x}))\}$, the directional derivatives for the velocity and pressure are then equal:

$$\hat{A}^{ahs'}(\hat{U})(\hat{\phi}^v, \hat{\Psi}) = A^{es'}(U)(\phi^v, \Psi) \quad , \quad \hat{A}^{ahs'}(\hat{U})(\hat{\phi}^p, \hat{\Psi}) = A^{es'}(U)(\phi^p, \Psi) .$$

Proof. We list and 'expand' all considered ALE parts:

$$(\rho_f \hat{\chi}_f \hat{B}'_{15}(\hat{U})(\hat{\phi}^v), \hat{\psi}^v) = (\rho_f \hat{\chi}_f \hat{J}(\widehat{\nabla}\hat{\phi}^v \hat{F}^{-1}\hat{v} + \widehat{\nabla}\hat{v}\hat{F}^{-1}\hat{\phi}^v), \hat{\psi}^v) , \tag{6.22}$$

$$(\hat{\chi}_f B'_{14}(\hat{U})(\hat{\phi}^v), \widehat{\nabla}\hat{\psi}^v) = (\hat{\chi}_f \rho_f \nu_f \hat{J}(\widehat{\nabla}\hat{\phi}^v \hat{F}^{-T} + \hat{F}^{-1}\widehat{\nabla}\hat{\phi}^{vT})\hat{F}^{-T}, \widehat{\nabla}\hat{\psi}^v) , \tag{6.23}$$

$$(\hat{\chi}_f B'_{16}(\hat{U})(\hat{\phi}^v), \hat{\psi}^p) = (\hat{\chi}_f \widehat{\mathrm{div}}(\hat{J}\hat{F}^{-1}\hat{\phi}^v), \hat{\psi}^p) , \tag{6.24}$$

$$(\hat{\chi}_s B'_1(\hat{U})(\hat{\phi}^v), \hat{\psi}^u) = (\hat{\chi}_s \hat{\phi}^v, \hat{\psi}^u) = (\hat{\chi}_s \hat{J}\hat{\phi}^v, \hat{\psi}^u) \ , \ (\text{since } J = 1) , \tag{6.25}$$

$$(B'_{14}(\hat{U})(\hat{\phi}^p), \widehat{\nabla}\hat{\psi}^p) = (-\hat{J}\hat{\phi}^p \hat{F}^{-T}, \widehat{\nabla}\hat{\psi}^p) . \tag{6.26}$$

We list and 'expand' all considered Eulerian parts:

$$(\rho_f \chi_f C'_{14}(U)(\phi^v), \psi^v) = (\rho_f \chi_f (\nabla\phi^v v + \nabla v \phi^v), \psi^v) , \tag{6.27}$$

$$(\chi_f C'_9(U)(\phi^v), \nabla\psi^v) = (\chi_f \rho_f \nu_f (\nabla\phi^v + \nabla\phi^{vT}), \nabla\psi^v) , \tag{6.28}$$

$$(\chi_f C'_{15}(U)(\phi^v), \psi^p) = (\chi_f \mathrm{div}(\phi^v), \psi^p) , \tag{6.29}$$

$$(\chi_s C'_1(U)(\phi^v), \psi^u) = (\chi_s \phi^v, \psi^u) , \tag{6.30}$$

$$(C'_{13}(U)(\phi^p), \nabla\psi^p) = (-\phi^p I, \nabla\psi^p) . \tag{6.31}$$

With (3.12), (3.2), (3.1) and (3.13) it follows that the equations (6.22)-(6.26) are (respectively) equal to (6.27)-(6.31). We note that for the tensors A, B and C the identity $(AB, C) = (A, CB^T)$ holds. $\qquad\square$

Thus for this special case the diagram commutes:

$$
\begin{array}{ccc}
\hat{A}^{ahs}(\hat{U})(\hat{\Psi}) & \xleftarrow{\quad\text{framework change}\quad} & A^{es}(U)(\Psi) \\
\Big\downarrow{\text{derivative}} & & \Big\downarrow{\text{derivative}} \\
\hat{A}^{ahs'}(\hat{U})(\hat{\Phi}^{v,p}, \hat{\Psi}) & \xleftarrow{\quad\text{framework change}\quad} & A^{es'}(U)(\Phi^{v,p}, \Psi)
\end{array}
\tag{6.32}
$$

with $\hat{\Phi}^{v,p} = \{\hat{\phi}^v, 0, \hat{\phi}^p\} \in \hat{W}^{ah,0}$ and $\Phi^{v,p} = \{\phi^v, 0, \phi^p\} \in W^{e,0}$

Remark 6.2. The directional derivatives play a direct role in the determination of the 'dual solution'. The dual solution is needed for a posteriori error estimation and goal-oriented mesh adaption, described in the next Chapter 7. Later in the Chapters 8 and 9 we display for various examples all second derivatives of the components of the dual solution for both frameworks. In Chapter 8 we first consider basic 'structure-structure interaction' problems. In this case no obvious differences can be seen. In the later case of stationary fluid-structure

interaction in Chapter 9 though there are visible effects. In these results it can be seen that in the velocity and pressure components the dual solutions of the different frameworks are similar. Whereas obvious differences in displacement component can be seen. ♮

Remark 6.3. In the Eulerian framework, we encounter in the directional derivative of the displacement boundary integrals as a result of the 'shape derivative'. This key difference, although it follows from the Eulerian framework, can also occur in an ALE framework.

This can be achieved by switching the reference frame of the characteristic functions. We ignore the key function of the characteristic functions in the FSI problem, and just treat them as 'step functions'. If the characteristic functions χ_f, χ_s are explicitly *only* known in the spatial reference frame Ω and no longer depend on $\hat{\chi}_f, \hat{\chi}_s$, then they have no directional derivatives and there are no boundary integrals. Consequently $\hat{\chi}_f, \hat{\chi}_s$ must now be defined in terms of χ_f, χ_s:

$$\hat{\chi}_f(\hat{x}) = \chi_f(\hat{x} + \hat{u}) \ , \ \hat{\chi}_s(\hat{x}) = \chi_s(\hat{x} + \hat{u}) \ .$$

Hence the functions have directional derivatives in the ALE framework. That means that by switching the reference frames the boundary integrals now only occur in the ALE framework.

Changing the reference frames of the functions χ_f, χ_s is 'odd', since their natural reference frames are 'material'. A more fitting example of step functions in an Eulerian framework are force-density functions, that have spatial cut-offs. In the Eulerian framework such a function, $f(x)$, is independent of all state variables and has no directional derivative. In the ALE framework the function has to be evalued as $f(\hat{x} + \hat{u})$, and consequently has a directional derivative. ♮

Remark 6.4. In the Eulerian framework such boundary integrals will occur when splitting a domain at an interface Γ_i with characteristic functions χ_1, χ_2. But if (in the context of Definition 6.7) the left- and right-sided traces of the function g on the interface Γ_i are equal, then the respective left and right-sided boundary integrals cancel each other out and can thus be neglected. ♮

Chapter 7

Adaptivity and error estimation

Now, we come to the main issues of this thesis, namely the automatic mesh adaptation within the finite element solution of the FSI problem. The computations shown in the Chapters 8, 9 and 10 below, have been done on three different types of meshes:

- globally refined meshes obtained using several steps of uniform (edge) bisection of a coarse initial mesh,

- locally refined meshes obtained using a purely geometry-based criterion by marking all cells for refinement, which have certain prescribed distances from the fluid-structure interface,

- locally refined meshes obtained using a systematic residual-based criteria by marking all cells for refinement, which have error indicators above a certain threshold.

The main goal of this thesis is to employ the 'dual weighted residual method' (DWR method) for the adaptive solution of FSI problems. This method has been developed in [BeRa95] (see also [BeRa01] and [BaRa03]) as an extension of the duality technique for a posteriori error estimation described by Eriksson et al in [ErEs+95]. The DWR method provides a general framework for the derivation of 'goal-oriented' a posteriori error estimates together with criteria of mesh adaptation for the Galerkin discretization of general linear and nonlinear variational problems, including optimization problems. It is based on a complete variational formulation of the problem, such as (6.6) for the FSI problem. In fact, this was one of the driving factors for deriving the Eulerian formulation underlying (6.6). In order to incorporate also the time discretization into this framework, we have to use a fully space-time Galerkin method, i.e., a standard finite element method in space combined with the dG(r) or cG(r) ('discontinuous' Galerkin or 'continuous' Galerkin) method in time. The following discussion assumes such a space-time Galerkin discretization, though in our test computations, we have used the fractional-step-θ scheme, which is a difference scheme. Accordingly, in this thesis the DWR method is used only in its stationary form in computing either steady states or intermediate quasi-steady states within the time stepping process.

7.1 Dual weighted residual method

We consider as the basis for the description of the DWR method any of the stationary FSI problems.

For notational purposes we will simply refer to the problems and the function spaces in the following manner. *Find $U \in U^D + X$, such that*

$$A(U)(\Psi) = 0 \quad \forall \Psi \in X. \tag{7.1}$$

The corresponding Galerkin approximation reads: *Find $U_h \in U_h^D + X_h$, such that*

$$A(U_h)(\Psi_h) = 0 \quad \forall \Psi_h \in X_h. \tag{7.2}$$

The goal of the calculation is to use the result U_h for calculating an approximation $J(U_h)$ of the goal-functional $J(U)$. To estimate the respective *'approximation error'* $J(U) - J(U_h)$, we use the method of Euler-Lagrange. We introduce the 'dual' variable $Z \in X$ and define the Lagrangian functional:

$$\mathcal{L}(U, Z) := J(U) - A(U)(Z) . \tag{7.3}$$

For this we seek the stationary point, which leads to the following nonlinear variational Karush-Kuhn-Tucker (KKT) system:

$$\mathcal{L}'(U, Z)(\Phi, \Psi) = \left\{ \begin{array}{cc} J_U'(U)(\Phi) & -A_U'(U)(\Phi, Z) \\ & -A(U)(U, \Psi) \end{array} \right\} = 0 \quad \forall \{\Phi, \Psi\} \in X \times X . \tag{7.4}$$

The first equation is referred to as the *'dual problem'*, whereas the second equation of (7.4), the *'primal problem'*, is equivalent to (7.1).

The respective Galerkin approximations $\{U_h, Z_h\} \in X_h \times X_h$ are obtained by solving the system in the discrete subspaces $X_h \times X_h$:

$$\mathcal{L}'(U_h, Z_h)(\Phi_h, \Psi_h) = \left\{ \begin{array}{cc} J_U'(U_h)(\Phi_h) & -A_U'(U_h)(\Phi_h, Z_h) \\ & -A(U_h)(U_h, \Psi_h) \end{array} \right\} = 0 \quad \forall \{\Phi_h, \Psi_h\} \in X_h \times X_h . \tag{7.5}$$

As in the continuous system, the discrete 'primal problem' of (7.5) is equivalent to (7.2). As above, the first equation is referred to as the discrete 'dual problem'.

For given solutions $\{U, Z\}, \{U_h, Z_h\}$ of the systems (7.4) and (7.5) we obtain the following identity for the approximation error:

$$J(U) - J(U_h) = \mathcal{L}(U, Z) - \mathcal{L}(U_h, Z_h) . \tag{7.6}$$

To approximate (7.6) we recall a general result from [BeRa01], which expresses the approximation error of the goal functional in terms of residuals of the discrete system (7.5). Later we use this as the basis of the a posteriori error estimation.

Proposition 7.1. Let the functional $L(\cdot)$ on the function space X be three times Gâtaux differentiable, with the stationary point $x \in X$, thus

$$L'(x)(y) = 0 \quad \forall y \in X . \tag{7.7}$$

We assume that on a finite dimensional subspace $X_h \subset X$, the respective Galerkin approximation

$$L'(x_h)(y_h) = 0 \quad \forall y_h \in X_h , \tag{7.8}$$

has the respective discrete solution $x_h \in X_h$. With this we obtain the following error representation

$$L(x) - L_h(x_h) = \tfrac{1}{2}L'(x_h)(x - y_h) + \mathcal{R}_h \quad \forall y_h \in X_h . \tag{7.9}$$

The remainder $\mathcal{R}_h$ is cubic in the error $e := x - x_h$:

$$\mathcal{R}_h := \tfrac{1}{2} \int_0^1 L'''(x_h + se)(e, e, e)s(s - 1) \, ds . \tag{7.10}$$

Proof. From the Fundamental Theorem of Calculus we have

$$L(x) - L(x_h) = \int_0^1 L'(x_h + se)(e) \, ds . \tag{7.11}$$

The integral in (7.11) is replaced with it's equal by the trapezoidal rule:

$$\int_0^1 f(s) \, ds = \tfrac{1}{2}(f(0) + f(1)) + \tfrac{1}{2} \int_0^1 f''(s)s(s - 1) \, ds . \tag{7.12}$$

Thus, it follows

$$L(x) - L(x_h) = \tfrac{1}{2}L'(x_h)(e) + \tfrac{1}{2}L'(x_h + e)(e) + \mathcal{R}_h . \tag{7.13}$$

From (7.7) it follows in (7.13) that $L'(x_h + e)(e) = L'(x)(e) = 0$. From (7.8) we have $L'(x_h)(y_h) = 0$ for all $y_h \in X_h$. Hence for (7.13) it follows:

$$L(x) - L(x_h) = \tfrac{1}{2}L'(x_h)(x - y_h) + \mathcal{R}_h \quad \forall y_h \in X_h . \tag{7.14}$$

$$\square$$

As a consequence we apply Proposition 7.1 to the Lagrangian functional $\mathcal{L}$, with (7.6) this leads to error estimation of the goal functional $J(U)$.

Lemma 7.1. For given solutions $\{U, Z\}, \{U_h, Z_h\}$ of the systems (7.4) and (7.5) we obtain the following identity:

$$J(U) - J(U_h) = \tfrac{1}{2}\rho(U_h)(Z - \Psi_h) + \tfrac{1}{2}\rho^*(U_h, Z_h)(U - \Phi_h) + \mathcal{R}_h^{(3)} , \tag{7.15}$$

for all $\{\Phi_h, \Psi_h\} \in X_h \times X_h$ and with the 'primal' and 'dual' residuals:

$$\begin{array}{rclcl} \rho(U_h)(\cdot) & := & & -A(U_h)(\cdot) & , \\ \rho^*(U_h, Z_h)(\cdot) & := & J'(U_h)(\cdot) & -A'(U_h)(\cdot, Z_h) & . \end{array} \tag{7.16}$$

The remainder $\mathcal{R}_h^{(3)}$ is cubic in the 'primal' and 'dual' errors $e := \{E, E^*\} := \{U - U_h, Z - Z_h\}$:

$$\mathcal{R}_h^{(3)} := \tfrac{1}{2} \int_0^1 \tilde{\mathcal{R}}_h^{(3)} s(s - 1) \, ds , \tag{7.17}$$

with

$$\begin{array}{rcl} \tilde{\mathcal{R}}_h^{(3)} & := & J'''(U_h + sE)(E, E, E) - A'''(E, E, E, Z_h + sE^*) \\ & & -3A''(U_h + sE)(E, E, E^*) . \end{array} \tag{7.18}$$

Proof. By defining the spaces $Y := X \times X$, $Y_h := X_h \times X_h \subset Y$, and the solution of (7.4) as $x := \{U, Z\} \in Y$ we can define the Lagrangian functional $\mathcal{L}$ as the functional $L(x) := \mathcal{L}(U, Z)$. Thus (7.6) can be written as

$$J(U) - J(U_h) = L(x) - L(x_h) \tag{7.19}$$

To (7.19) we apply Proposition 7.1:

$$J(U) - J(U_h) = \tfrac{1}{2} L'(x_h)(x - y_h) + \mathcal{R}_h \quad \forall y_h \in Y_h \ . \tag{7.20}$$

In (7.20) we 'expand' $L'(x_h)(x - y_h)$ with $y_h = \{\Phi_h, \Psi_h\}$:

$$
\begin{aligned}
L'(x_h)(x - y_h) &= \mathcal{L}'_Z(U_h, Z_h)(Z - \Psi_h) + \mathcal{L}'_U(U_h, Z_h)(U - \Phi_h) \\
&= -A(U_h)(Z - \Psi_h) + J'(U_h)(U - \Phi_h) - A'(U_h)(U - \Phi_h, Z_h) \\
&= \rho(U_h)(Z - \Psi_h) + \rho^*(U_h, Z_h)(U - \Phi_h) \ .
\end{aligned}
\tag{7.21}
$$

Since $\mathcal{L}(U, Z)$ is only linear in Z we obtain for $L'''(x_h + se)(e, e, e)$

$$
\begin{aligned}
L'''(x_h + se)(e, e, e) &= J'''(U_h + sE)(E, E, E) - A'''(E, E, E, Z_h + sE^*) \\
&\quad - 3A''(U_h + sE)(E, E, E^*) \ .
\end{aligned}
\tag{7.22}
$$

Since $L'''(x_h + se)(e, e, e) = \tilde{\mathcal{R}}_h^{(3)}$ equation (7.17) follows. $\qquad\square$

To obtain a usable version of the error identity as shown in (7.15) for FSI problems in the ALE and Eulerian frameworks we make the following approximations.

First we neglect the remaining term $\mathcal{R}_h^{(3)}$. Then the primal and dual problems are augmented with the usual stabilization terms as described in Section 6.4. We note again that the local projection scheme is only 'weakly consistent', which means that when the strong solutions U, Z are applied, it does not vanish, but creates an error, which is of the same order of the discretization.

Finally, we approximate the differences $U - \Phi_h$ and $Z - \Psi_h$ respectively with $I_{2h}^{(2)} U_h - U_h$ and $I_{2h}^{(2)} Z_h - Z_h$:

$$J(U) - J(U_h) \approx \tfrac{1}{2} \rho(U_h)(I_{2h}^{(2)} Z_h - Z_h) + \tfrac{1}{2} \rho^*(U_h, Z_h)(I_{2h}^{(2)} U_h - U_h) := \tilde{E}(U_h, Z_h) \ . \tag{7.23}$$

Here $I_{2h}^{(2)}$ represents a higher-order interpolation of the bilnear solutions. From U_h and Z_h, we generate improved approximations of U and Z in a post-processing step by patchwise higher-order interpolation. For this we require that the triangulation $\mathbb{T}_h$ be organized in a patch-wise manner as explained in Section 6.1. In two dimensions this is done on 2×2-patches of cells in $\mathbb{T}_h$ the 9 nodal values of the piecewise bilinear functions are used to construct patchwise biquadratic functions. [BeRa96, BaRa03].

The solvability of the primal and dual problems in the system (7.5) is not for granted. This is a difficult task in view of the rather few existence results in the literature for general FSI problems. For the primal problem the Gâtaux derivative of the complete FSI problem does not need to be exact, it only needs to be 'good enough' for the Newton iteration to ensure

convergence, leading to a reduction of the residuals of the nonlinear system. Thus for the primal problem the nonlinear system is used to measure the 'quality' of the solution.

For the dual problem though things may initially seem less clear, since the dual problem is simply a *linear* problem directly based on the Gâteaux derivative. Of course, an immediate 'measure of quality' of the discrete dual solution is the residual of the linear system. But there is no immediate measure for the quality of the discrete dual solution in relation to the *continuous* dual solution. This uncertainty stems from highly nonlinear (unusual) influence of the displacement u in the Gâteaux derivative. For the ALE framework this is seen in the transformed fluid equations. For the Eulerian framework this is seen in additional boundary Dirac integrals, which stem from the shape derivatives. This seemingly lack of clarity though is not typical to fluid-structure interaction problems. It is only more obvious in such problems since everything *visibly* depends on the position of the interface. Generally though this uncertainty concerning the discrete dual solution is present in *all* nonlinear problems, since in such problems the Gâteaux derivatives depend on the primal solution and can only be approximated by using the discrete primal solutions.

In the case of fluid-structure interaction we assume that the interface obtained on the current mesh is already in good agreement with the correct one, $\Gamma_{ih} \approx \Gamma_i$, and set up the dual problem formally with Γ_{ih} as a fixed interface. This approach has proven very successful in similar situations, e.g., for Hencky elasto-plasticity [RaSu02].

In all test calculations, we did not encounter difficulties in obtaining the discrete solutions. In fact the performance of the error-estimator for a given goal-functional was always good for both the ALE and Eulerian frameworks. A common measure of the accuracy of the error estimator is the *'effectivity index'* defined by

$$I_{eff} := \left| \frac{\tilde{E}(U_h, Z_h)}{J(U) - J(U_h)} \right| \, , \tag{7.24}$$

which is the overestimation factor of the error estimator. It should desirably be close to one.

A second measure for the error-estimator is how effective its results are as error indicators, that are used for adaptive mesh refinement. The error indicators η_K are the cell-wise contributions of the error estimator:

$$\tilde{E}(U_h, Z_h) = \sum_{K \in \mathbb{T}_h} \eta_K =: \eta \, , \tag{7.25}$$

which one invariably obtains in the process of calculating $\tilde{E}(U_h, Z_h)$. Again, in all test calculations the error-estimator performed well for both the ALE and Eulerian frameworks. This could be seen in the improved convergence of the goal-functionals.

Remark 7.1. The above assumption of differentiability may cause concerns in treating the FSI problems in the Eulerian framework since the dependence of the characteristic function $\chi_f(x - u)$ on the deflection u is generically not differentiable (only Lipschitzian). However, this non-differentiability can be resolved by the 'Hadamard structure theorem', on the assumption that the interface between fluid and structure forms a lower dimensional manifold and the differentiation is done in context of an integral, see Lemma 6.9 and

[Zol79, SoZo92, AGJT04]. In essence this has the same effect as discretizing along the interface and replacing the directional derivative by a mesh-size dependent difference quotient, a pragmatic approach that has proven itself in similar situations, e.g., for Hencky elastoplasticity [RaSu02]. ♮

Remark 7.2. The actual computation of the directional derivatives can become quite involved, especially when one considers the nonlinear expressions encountered in structure mechanics. To alleviate this problem we use an approach that is also used in the method of 'automatic differentiation'. This is explained in Section 6.7.1. ♮

7.2 Mesh adaptation algorithm.

The approach we use for the adaptive refinement of the spatial mesh is straightforward. Particularly, for the refinement criteria there exist much more sophisticated versions, which are not used in this thesis for sake of simplicity. Let an error tolerance TOL be give. Then, on the basis of the (approximate) a posteriori error estimate (7.25), the mesh adaptation proceeds as follows:

1. Compute the primal solution U_h from (7.2) on the current mesh, starting from some initial state, e.g., that with zero deformation.

2. Compute the solution $\tilde{Z}_h$ of the approximate discrete dual problem (7.5).

3. Evaluate the cell-error indicators η_K.

4. If $\eta < TOL$ then accept U_h and evaluate $J(U_h)$, otherwise proceed to the next step.

5. Determine the 30% cells with largest and the 10% cell-patches with smallest values of η_K. The cells of the first group are refined and those of the second group coarsened. Then, continue with Step 1. (Coarsening usually means canceling of an earlier refinement. Further refinement may be necessary to prevent the occurrence of too many hanging nodes. In two dimensions this strategy leads to about a doubling of the number of cells in each refinement cycle. By a similar strategy it can be achieved that the number of cells stays about constant during the adaptation process within a time stepping procedure.)

7.3 Numerical quadrature along the interface

As described at the beginning of this chapter we will be using three methods of mesh adaptation:

- globally refined meshes obtained using several steps of uniform (edge) bisection of a coarse initial mesh,

- locally refined meshes obtained using a purely geometry-based criterion by marking all cells for refinement, which have certain prescribed distances from the fluid-structure interface,

- locally refined meshes obtained using a systematic residual-based criteria by marking all cells for refinement, which have error indicators above a certain threshold.

In the Eulerian framework, in all three cases, regardless of the refinement technique, the interface line will be intersecting element cells. In these interface cells equations, e.g. the constitutive equations of the stress tensor, change. In two structure-structure interaction examples below only the material parameter of the structure changes. In the fluid-structure examples the constitutive equation of the stress tensor changes entirely.

The primal approach for coping with the error at the interface is to increase the refinement. This is either done by employing zonal refinement along the whole interface or using sensitivity analysis as a guide for local refinement.

Of course the first reason for an error at the inteface cells is when the discrete variables do not approximate the continuous values well enough. This error can only be resolved with cell refinement. If the error at the interface cells is in large parts only caused by quadrature errors, then refinement along the inteface cells *solely* on this basis is expensive, since this increases the number of unknowns in the complete system. Additionaly, even if the discrete variables *do* approximate the continuous values well, the quadrature error will still occur, due to the change of equations. Consider for example in Problem 5.7 the incompressibility condition for the fluid:

$$0 = (\chi_f \, \mathrm{div}_h v_h, \psi_h^p) = \int_\Omega \chi_f \, \mathrm{div}_h v_h \, \psi_h^p \, dx = \sum_{K \in \mathbb{T}_h} \int_K \chi_f \, \mathrm{div} v_h \, \psi_h^p \, dx \, . \qquad (7.26)$$

Generally we will be using the Gauss rule of quadrature. This quadrature though is only good for smooth functions. For cells that are either completely in the fluid domain or in the structure domain the use of the Gauss quadrature is appropriate. But for interface cells (assumming that the characteristic function χ_f is exact and not regularized by $\tanh(\alpha_h \phi)$, see below), this will lead to the cell integrals being weighted wrong. In the context of Equation (7.26) and Problem 5.7 it will lead to the incompressibility condition either having a strong and unnecessary influence on the structure velocity or on the other hand being influenced by the structure velocity. In Figure 7.1 some extremes are shown. In the cell K_1 the incompressibility condition has an appropriate 50% part of the quadrature, since the fluid occupies approximately 50% of the area. In the next cell K_2 though the structure has a 50% part, although it only occupies approximately two sevenths of the cell. Alternatively in K_3 the structure part occupies approximately the same area, but is completely neglected in the quadrature.
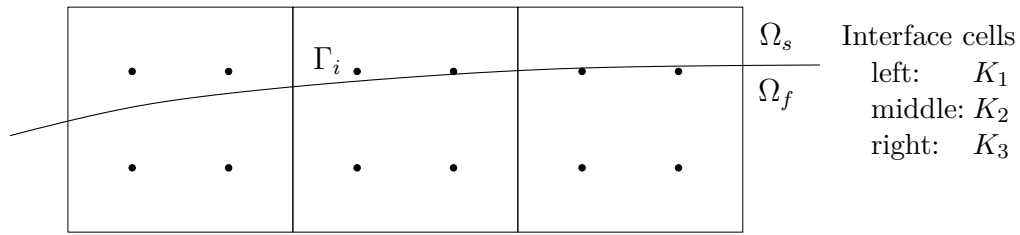
Figure 7.1: Interface Γ_i crossing through different cells; in each cell the Gauss(4) quadrature points are shown.

To reduce this error we use an adaptive quadrature. On cells, that are not cut by the interface, we continue to use the Gauss rule. On cells containing the interface we use a more appropriate summed quadrature rule, which is based on the elementary midpoint rule.
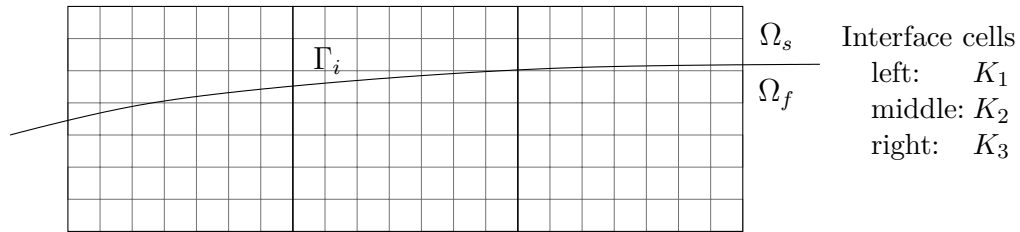

Figure 7.2: Interface Γ_i crossing through different interface cells; in each cell the a composite quadrature rule is used.

Thus the immediate errors that stem from using an unsuitable quadrature rule on interface cells are avoided.

An additional source of unsteady behavior is the exact evaluation of the characteristic functions. This stems from the way the basis functions on the cells couple. As a coupling value we consider the contribution of $\chi_f \mathrm{div} v$ to the system matrix. Entries in the system matrix are of the form $(\chi_f \mathrm{div} \varphi_{h,i}, \varphi_{h,j})$ for discrete Lagrangian bilinear node-based and -numbered test functions $\varphi_{h,i} \in V_h$. Since we are using bilinear finite element functions only nodes, that are on a common cell, couple. Due to the χ_f factor, only cells contribute, that have at least one 'fluid' node.

In the left diagram of Figure 7.3 the value of v_h on node 5 (black) couples with (itself and) the nodes $\{1, 2, 4, 7, 8\}$ (green). It does not couple with the nodes $\{3, 6, 9\}$ (red), regardless of how close *from the left* the interface Γ_i comes to the cell nodes. Only once the inteface crosses one of the right cells' nodes does coupling with the right-hand side nodes occur. This leads to a sudden on- and off-switching of the coupling between the nodes of interface cells and their neighbors, which in turn leads to sudden unsteady behavior of node values. An effect, that could (albeit rarely) be seen in the instationary experiments in Chapter 10, when using exact characteristic functions.
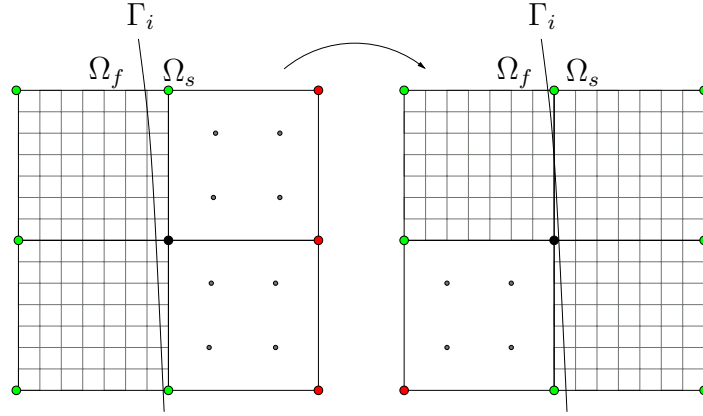
Figure 7.3: Interface Γ_i crossing through different cells; Nodes are numbered 1 to 9, left to right, top to bottom.

To alleviate this problem we regularize the characteristic functions χ_f, χ_s :

$$\chi_{f,h} := \frac{1 + \tanh(\alpha_\chi \phi(x))}{2} \; , \chi_{s,h} := 1 - \chi_{f,h} \; ,$$

with the smoothing parameter α_χ and the signed distance function $\phi(x) := (\chi_f - \chi_s) \, \mathrm{dist}(x, \Gamma_i)$. The smoothing parameter is chosen accordingly to the mesh size h. We only use ϕ as a parameter to the tanh function, thus it is only necessary, that it roughly approximate the distance. In the examples below material deformations at the interface were regular enough to allow the Eulerian distance function $\phi(x)$ to be approximated with the reference domain distance $\phi(x) \approx \hat{\phi}(x - u)$ with $\hat{\phi}(\hat{x}) := (\hat{\chi}_f - \hat{\chi}_s) \, \mathrm{dist}(\hat{x}, \hat{\Gamma}_i)$. This approach has similarity to the Volume-of-Fluid method [HiNi81] or Variable-Density method, since both use a "fraction of equation" variable similar to our approximation of χ_f.

In the driven cavity numerical tests (Chapter 9) the interface will be a smooth line, as shown in Figure 7.5. There we seek the stationary solution to an FSI problem using a pseudo time-stepping method. The fluid and structure are both incompressible, thus as a final stationary result the structure will be deformed, but with the same volume (=1). Since we are using an Eulerian framework, it is not immediately clear, due to the coupling with the fluid, how well (or badly) the mass of the structure is conserved. In Figure 7.4 we display the general conservation of mass regardless of which quadrature rule is used. Additionally the improvement of conservation of mass is shown when using a composite quadrature rule on the interface cells.

In later experiments (Chapter 10) the structure is surrounded by a fluid and has corners as shown in Figure 7.6. It is especially in the cells with the interface corners that the summed rule improves accuracy.
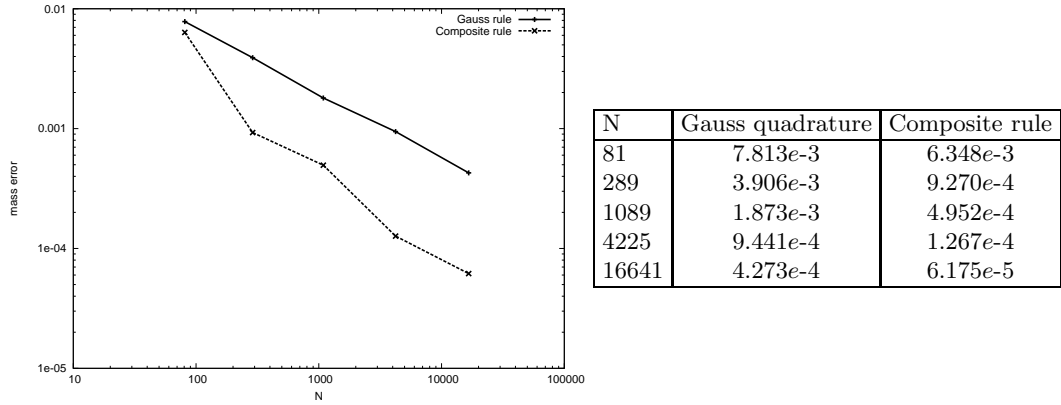
Figure 7.4: Based on which quadrature rule is used, we display the mass errors of the final domain Ω_s of the stationary FSI problem, when using a pseudo time-stepping scheme.

N	Gauss quadrature	Composite rule
81	7.813e-3	6.348e-3
289	3.906e-3	9.270e-4
1089	1.873e-3	4.952e-4
4225	9.441e-4	1.267e-4
16641	4.273e-4	6.175e-5

☐ Composite rule   ☐ Gauss (4) rule
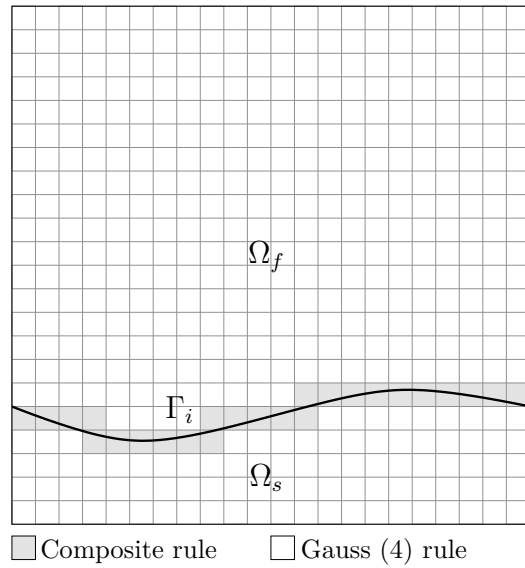
Figure 7.5: Summed quadrature along the interface Γ_i.

☐ Composite rule   ☐ Gauss (4) rule
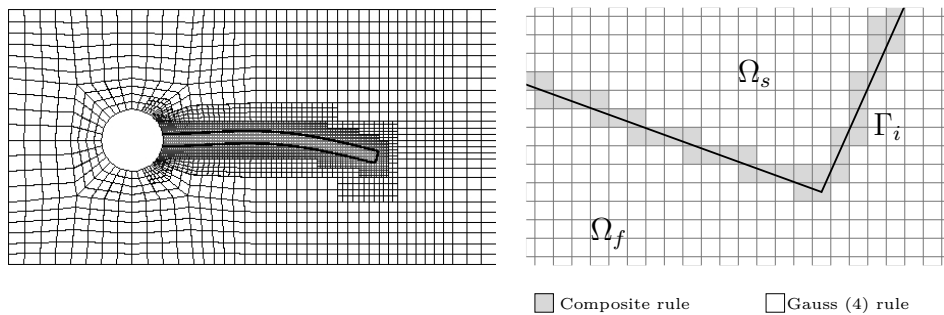
Figure 7.6: Summed quadrature along the interface Γ_i.

Chapter 8

Numerical test: elastic materials

As a validation of the Eulerian approach to structure mechanics we do some numerical studies based on a basic structure with a piecewise constant material elasticity parameter. All calculations are done using both the conventional Lagrangian approach and the alternative Eulerian approach. These tests are done using a model based on the St. Venant Kirchhoff law for compressible materials.

In the first part we show that for a given known solution both approaches display similar errors and an equal rate of convergence.

In the second part the material elasticity parameter is piecewise constant and assumes two different values. The material and domain are split into two parts connected by an interface where the elasticity parameter jumps. This is done for two different geometries.

We show that both the Lagrangian and Eulerian approach converge to same functional values and apply the 'dual weighted residual' method to estimate the error of the functional values. Based on this method we apply a mesh adaption scheme and compare the resulting meshes.

Since we are only observing structure problems in this chapter we will for brevity usually omit the 's' suffix on the domains and variables. It will be used though on occasions, when a problem or definitions from previous chapters are used.

8.1 Convergence results for a known solution

We investigate a stationary problem on a two-by-two material domain $\hat{\Omega} = (0,2)^2$. We use the St. Venant-Kirchhoff law for compressible materials (Section 4.6.1). For compressible materials the Poisson ratio is $\nu_s = 0.4$. For the first Lamé coefficient we use the value $\mu_s = 1$. For the second it follows from Equations (4.20) $\lambda_s = 4\mu_s$. We set the density to $\rho_s = 1$.

As a boundary condition we prescribe a homogeneous Dirichlet value of zero on all of $\partial\hat{\Omega}$. Thus $\Omega = \hat{\Omega}$. The Lagrangian and Eulerian problems are the stationary versions of the Problems 4.3 and 4.5

Problem 8.1 (Stationary variational structure problem, St. Venant-Kirchhoff, Lagrangian framework). *Find $\hat{u}_s \in \hat{V}_s^0$, such that*

$$(\hat{J}_s \, \hat{\sigma}_s \, \hat{F}_s^{-T}, \widehat{\nabla}\hat{\psi}^u) = (\hat{f}_s, \psi^u) \, , \tag{8.1}$$

for all $\hat{\psi}^u \in \hat{V}_s^0$ where all definition and notations as in Problem 4.3. ♮

Problem 8.2 (Stationary variational structure problem, St. Venant-Kirchhoff, Eulerian framework). *Find $u_s \in V_s^0$, such that*

$$(\sigma_s, \nabla \psi^u) = (J_s f_s, \psi^u) \, , \tag{8.2}$$

for all $\hat{\psi}^u \in \hat{V}_s^0$ where all definition and notations as in Problem 4.5. ♮

In the 'strong' form the Lagrangian and Eulerian problems are (respectively):

$$
\begin{array}{c|c}
\text{Find } \hat{u}, \text{ such that} & \text{Find } u, \text{ such that} \\
-\widehat{\text{div}}(\hat{J}\hat{\sigma}\hat{F}^{-T}) = \hat{f}(\hat{x}) \, . & -\text{div}\sigma = Jf(x) \, .
\end{array}
\tag{8.3}
$$

We prescribe an explicit displacement $\hat{u}(\hat{x})$. In the Lagrangian case we can use this displacement directly to calculate the respective right-hand side $\hat{f}(\hat{x})$ by explicitly calculating the value $\widehat{\text{div}}(\hat{J}\hat{\sigma}\hat{F}^{-T})$. This is done by using the method of automatic differentiation (see Section 6.7.1).

In the Eulerian case this is not immediately possible, since the framework is Eulerian, thus the provided coordinate is the end point $x = \hat{x} + \hat{u}$ and not the starting point $\hat{x}$, for which we have the provided displacement $\hat{u}(\hat{x})$. For each evaluation of the right-hand side function $Jf(x)$, we solve the reverse problem of determining the start position $\hat{x}$ using a Newton iteration (Find $\hat{x}$, such that $x = \hat{x} + \hat{u}(\hat{x})$). Once the displacement $u = \hat{u}$ is known (to a satisfactory tolerance), we use this to calculate the respective right-hand side $Jf(x)$ by explicitly calculating the value $\text{div}\sigma$. Again, this is done by using the method of automatic differentiation (see Section 6.7.1).

As a prescribed displacement we use

$$\hat{u}(\hat{x}) = \begin{pmatrix} A_1 \sin(2\pi\omega_1\hat{x}_1) \sin(2\pi\omega_1\hat{x}_2) \\ A_2 \sin(2\pi\omega_2\hat{x}_1) \sin(2\pi\omega_2\hat{x}_2) \end{pmatrix} \, , \tag{8.4}$$

with $A = (-0.02, -0.2)^T$ and $\omega = (1/2, 1/4)^T$. This displacement was chosen, since it is similar to the resulting displacement when applying a small gravitational force.
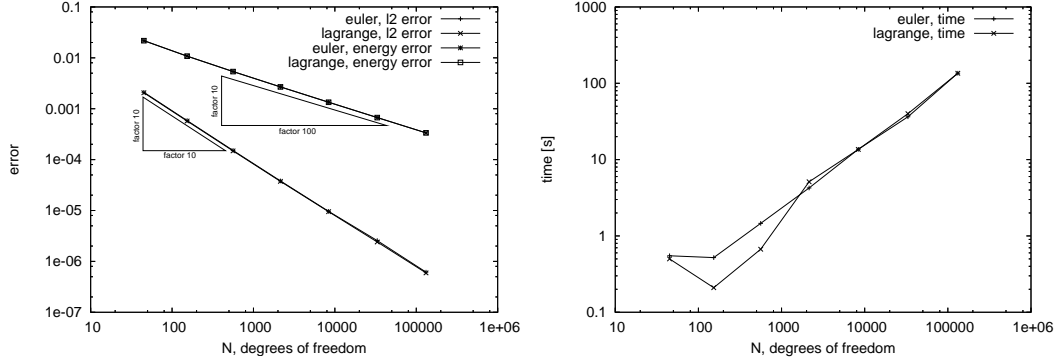
Figure 8.1: (left) Comparison of L^2- and H^1-seminorm -Errors when using the Lagrangian or Eulerian approaches for a given known displacement. (right) Comparison of the run-times.

The convergence results are shown in the left chart of Figure 8.1. Both approaches have the same convergence behavior. The H^1-seminorm-errors converge uniformly of the order $O(N^{1/2}) = O(h)$ whereas the L^2-errors converge with the order $O(N) = O(h^2)$. In the right chart of Figure 8.1 we can see that both approaches are of equal speed (and that the time consumption is of the order O(N)).

8.2 Convergence results for solid-solid interaction

In these tests the domain $\hat{\Omega} = (0,2)^2$ is split into two domains $\hat{\Omega}_1, \hat{\Omega}_2$ with a common interface $\hat{\Gamma}_i$.

$$\hat{\Omega} = \hat{\Omega}_1 \cup \hat{\Omega}_2 \cup \hat{\Gamma}_i \;.$$

A material parameter, the first Lamé coefficient $\hat{\mu}(\hat{x})$, is assigned a different constant value μ_i, depending on which domain $\hat{\Omega}_i$ it is in. Specifically in the Lagrangian and Eulerian frameworks:

$$\hat{\mu}(\hat{x}) = \hat{\chi}_1 \mu_1 + \hat{\chi}_2 \mu_2 \quad , \quad \mu(x) = \chi_1 \mu_1 + \chi_2 \mu_2 \;,$$

with $\hat{\chi}_1$ being the characteristic function of $\Omega_1 \cup \Gamma_i$, $\hat{\chi}_2$ that of Ω_2, and the Eulerian functions defined in reference $\chi_i := \hat{\chi}_i(x - u)$. We use the St. Venant-Kirchhoff law for compressible materials (Section 4.6.1). For compressible materials the Poisson ratio is $\nu_s = 0.4$. For the second Lamé coefficient it follows from Equations (4.20) $\hat{\lambda}_i = 4\hat{\mu}_i$ (or respectively $\lambda_i = 4\mu_i$).

The problems we observe are similar to those in the previous section, with the discontinuity of $\hat{\mu}$ and μ being the only difference. We used the problems in the previous section for the Lagrangian framework (Problem 8.1) and the Eulerian framework (Problem 8.2). The difference is that the displacement is no longer explicitly provided. Instead an explicit force density is used on the right-hand side.

For the distribution of the material constant in the reference configuration we use two different scenarios.

- In the first scenario (Fig. 8.2 left) the domain is split horizontally into two parts. In this case the cell borders match with the change of the material constant on the reference grid. This setting suggests that the Lagrangian approach should have an advantage, since in the Eulerian approach the interface will always be intersecting cells.

- In the second scenario (Fig. 8.2 right) the domain is split diagonally into two equal parts. This would lead one to assume that the Lagrangian and Eulerian approaches will more likely behave in similar fashion.
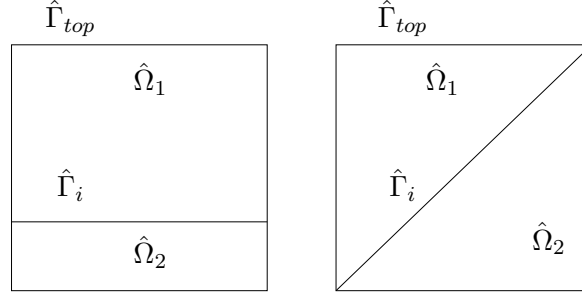
Figure 8.2: The two basic scenarios with a horizontal and diagonal interface.

Based on these scenarios we compare the results of the Lagrangian and the Eulerian approaches. We use the results to calculate the goal functional,

$$\hat{G}(\hat{\Gamma}_{top})(\hat{U})(\varphi) := \int_{\hat{\Gamma}_{top}} \hat{J}\hat{\sigma}\hat{F}^{-1} \cdot \hat{n} \; \varphi \; d\hat{x} = \int_{\Gamma_{top}} \sigma \cdot n \; \varphi \; dx =: G(\Gamma_{top})(U)(\varphi) \;, \qquad (8.5)$$

with $\varphi = (1,0)^T$. This is the horizontal component of the force along the upper boundary of the domain. We denote the semilinear forms of the Problems 8.1 (Lagrangian framework) and 8.2 (Eulerian framework) as (respectively),

$$\hat{A}(\hat{U})(\hat{\psi}) := (\hat{J}\hat{\sigma}\hat{F}^{-1}, \widehat{\nabla}\hat{\psi}) \quad , \quad A(U)(\psi) := (\sigma, \nabla\psi) \quad , \qquad (8.6)$$

where $\{\hat{\psi}, \psi\} \in \hat{V}_s \times V_s$. The functional values $\hat{G}$ and G can also be obtained using a so-called 'residual based method', which we explain in the following in the Eulerian framework for G. For the Lagrangian framework this can be done in the same fashion. The following identity follows by integrating in A by parts (as in Section 4.7.2):

$$A(U)(\psi) \;=\; (-\mathrm{div}\sigma, \psi) \;\; + G(\partial\Omega)(U)(\psi) \;.$$

If U is a strong solution of the Problem 8.2 and $\psi \in \{v \in V_s | v_{|\Gamma_{top}} = \varphi\}$, then

$$G(\Gamma_{top})(U)(\psi) = A(U)(\psi) - (Jf, \psi) \;. \qquad (8.7)$$

Based on this, we approximate the goal functional by evaluating the residuals of the discrete problems:

$$G_h(\Gamma_{top})(U_h)(\psi_h) := A(U_h)(\psi_h) - (Jf, \psi_h) \;, \qquad (8.8)$$

where $\psi_h \in \{v \in V_{s,h} \mid v_{|\Gamma_{top}} = \varphi\}$. This residual based method has been shown to have an improved rate of convergence compared to the direct evaluation of $\hat{G}$ and G, see [BrRi05].

We compare the convergence results of both approaches. Additionally we approximate the error of the goal functional using the DWR method. We determine the efficiency of the error estimator by comparing the approximation of the error with the 'actual' error. The actual error is obtained by extrapolating the discrete goal functional values to the limit.

Based on the DWR method we adaptively refine the grid with the aim of calculating the goal functional to the same degree of precision as when refining globally, but with less degrees of freedom and less CPU-time. We show that also here the Lagrangian and Eulerian approaches have the same results and that the error estimator works equally well.

To solve the primal and dual problems we will need the directional derivatives of the semilinear forms $\hat{A}(\hat{U})(\psi), A(U)(\psi)$. In the Lagrangian and Eulerian frameworks these derivatives for a given direction can be obtained by using the method of automatic differentiation as explained in Section 6.7.1.

In the Eulerian framework we define the stress tensor in the two domains as,

$$\sigma_1 := JF^{-1}(\lambda_1(\mathrm{tr}E)I + 2\mu_1 E)F^{-T} ,$$
$$\sigma_2 := JF^{-1}(\lambda_2(\mathrm{tr}E)I + 2\mu_2 E)F^{-T} ,$$

and use these to express the stress tensor as a composite stress tensor $\sigma = \chi_1\sigma_1 + \chi_2\sigma_2$. From Section 6.7.3 we know that in the Eulerian framework the directional derivative of the displacements will contain additional boundary integrals on the interface, e.g. for the stress tensors:

$$-(\sigma_1^- n_1 \cdot \phi, (\nabla\psi)_1^-)_{\Gamma_i} - (\sigma_2^- n_2 \cdot \phi, (\nabla\psi)_2^-)_{\Gamma_i} . \tag{8.9}$$

We approximate the boundary integrals in the discrete form by expressing them as domain integrals with a discrete regularized boundary Dirac function δ_h,

$$\begin{aligned}(\sigma_1^- n_1 \cdot \phi, (\nabla\psi)_1^-)_{\Gamma_i} &\approx \int_\Omega \delta_h \, n_1 \cdot \phi_h \, (\sigma_{1,h}^- : (\nabla\psi_h)_1^-) \, dx , \\ (\sigma_2^- n_2 \cdot \phi, (\nabla\psi)_2^-)_{\Gamma_i} &\approx \int_\Omega \delta_h \, n_2 \cdot \phi_h \, (\sigma_{2,h}^- : (\nabla\psi_h)_2^-) \, dx ,\end{aligned}$$

with $\delta_h := \max(0, h - \mathrm{dist}(x - u, \hat{\Gamma}_i))/h^2$. In the discrete form we will either be using the Gauss or summed quadrature formulas for the quadrature on each cell K of the triangulation, see Section 7.3. In both cases all quadrature points will be inside each triangulation cell K. Since we are using bilinear fem functions, it follows that at all such inner points, the left and right traces of $\sigma_{1,h}, \sigma_{2,h}$ and $\nabla\psi_h$ will be equal. The sum in (8.9) in the discrete form then is approximated as a function of the jump of σ around the interface,

$$(\delta_h \, (\sigma_1 - \sigma_2) \, n_1 \cdot \phi_h, \nabla\psi_h) . \tag{8.10}$$

8.2.1 Horizontal interface

The material interface is set as a horizontal line through the reference configuration with the height 0.5. The material parameters are $\mu_1 = 0.15$, $\mu_2 = 0.30$.
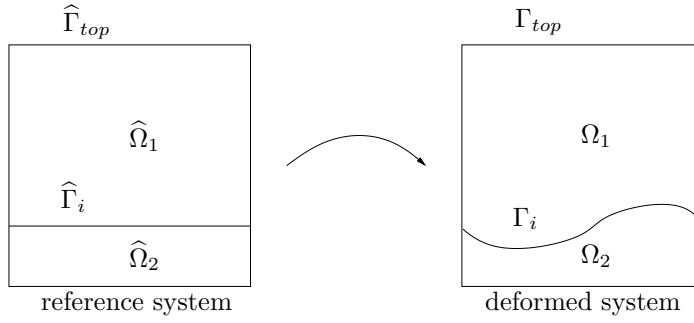
Figure 8.3: Configuration and deformation of the structure-structure interface test with a horizontal reference-grid matching interface

As a driving force we supply a right-hand side, that is chosen so, that the left and right halves of the material are 'pulled' down and up leading to a deformation as in Figure 8.3. Since we are primarily interested in comparing the convergence behavior of the Lagrangian and Eulerian frameworks, the force density is modified to improve overall convergence. To this end, we multiply the right-hand side with the square of a 'bubble function' $b(x) := x_1 x_2 (2 - x_1)(2 - x_2)$. As a right-hand side we use the force density $f : \Omega \to \mathbb{R}^2$,

$$f(x) := b(x)^2 (\frac{x_1}{2}(-e_2) + \frac{2 - x_1}{2} e_2) \ .$$

Due to the square bubble function, the function f and its normal gradient are zero on the boundary: $f_{|\partial\Omega} = \partial_n f_{|\partial\Omega} = 0$.

We extrapolate the goal functional values ($\hat{G}(\hat{\Gamma}_{top})(\hat{U})(e_1)$, $G(\Gamma_{top})(U)(e_1)$) for the Lagrangian and Eulerian frameworks below (Tables 8.1, 8.2) to the limit and use a value that fits both limits best. This we use as the reference goal functional value and refer to as g_∞. The calculated goal functional values we simply refer to as g_N, with N being the number of degrees of freedom. In the first simulations we calculate the goal functional errors $g_N - g_\infty$ in both approaches. The errors of both approaches are shown in the Tables 8.1, 8.2. The convergence of the error in both frameworks is displayed in Figure 8.6 (left).

For both approaches we also apply the 'dual weighted residual' method to approximate the error of the goal functional (column 'Estimate'). The *'efficiency index'* of the estimator is in the column 'Efficiency'. This value defined by

$$I_{eff} := \left| \frac{\tilde{E}(U_h, Z_h)}{J(U) - J(U_h)} \right| \ , \tag{8.11}$$

is the overestimation factor of the error estimator and serves as a measure of the accuracy of the error estimator. It should desirably be close to one. As can be seen in Figure 8.7 the efficiency of the error estimator is good for both frameworks. As a means of visualizing and comparing the sensitivity of the problem to the goal functional, we show the square norms of second derivatives of the components of z in the Figures 9.12 and 8.9 for both frameworks. Since the values $\|\nabla^2 z_i\|^2$ vary greatly, we display the values on a logarithmic scale.

Based on these results we use the error estimator to adaptively refine the grid using the mesh refinement method described in Section 7.1. We compare the errors of both approaches in the Tables 8.3, 8.4. The convergence of the error and the approximation of the error for both frameworks and refinement methods is shown in the Figures 8.10. The Figures 8.11 and 8.12 show the evolution of adaptive mesh refinement for both frameworks. Finally in Figure 8.13 the errors of the goal functional are compared in a chart for both frameworks and global and local mesh refinement.
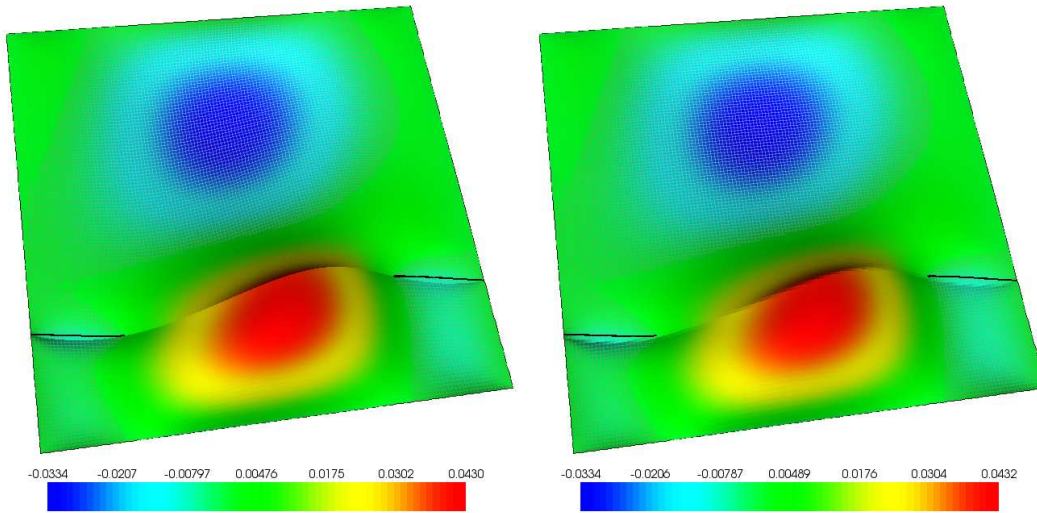
Figure 8.4: Comparison of the horizontal displacements ($N = 16,641$) for the Lagrangian (left, displayed in the deformed system) and Eulerian (right) frameworks.
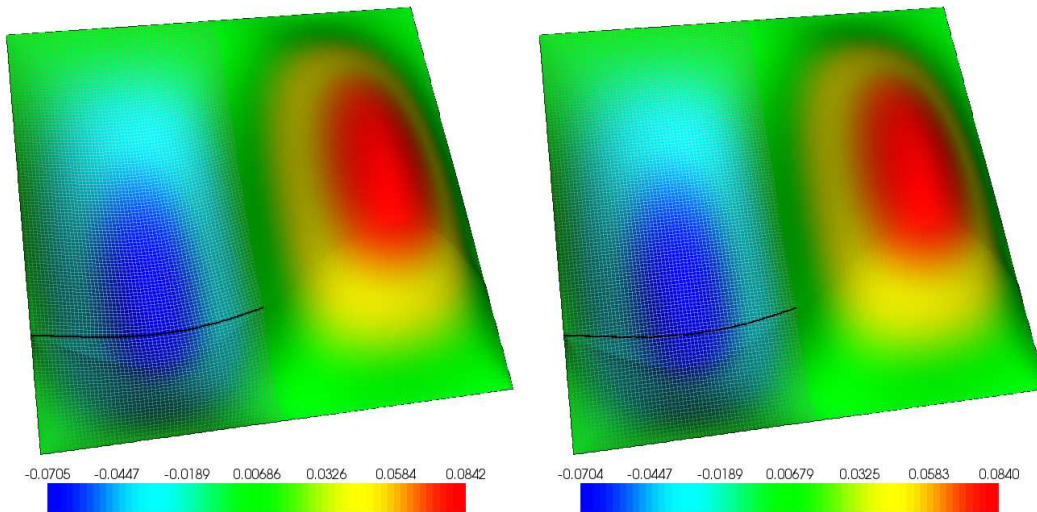
Figure 8.5: Comparison of the vertical displacements ($N = 16,641$) for the Lagrangian (left, displayed in the deformed system) and Eulerian (right) frameworks.

N	g_N	Error	Estimate	Efficiency
81	$-2.15295e\text{-}2$	$-7.76303e\text{-}3$	$-7.56227e\text{-}3$	$9.74138e\text{-}1$
289	$-2.60619e\text{-}2$	$-3.23056e\text{-}3$	$-3.87201e\text{-}3$	$1.19856e\text{-}0$
1089	$-2.79782e\text{-}2$	$-1.31433e\text{-}3$	$-1.71405e\text{-}3$	$1.30412e\text{-}0$
4225	$-2.87579e\text{-}2$	$-5.34604e\text{-}4$	$-7.16383e\text{-}4$	$1.34002e\text{-}0$
16641	$-2.90743e\text{-}2$	$-2.18167e\text{-}4$	$-2.94380e\text{-}4$	$1.34934e\text{-}0$
66049	$-2.92035e\text{-}2$	$-8.89730e\text{-}5$	$-1.20774e\text{-}4$	$1.35743e\text{-}0$
263169	$-2.92566e\text{-}2$	$-3.58874e\text{-}5$	$-4.96606e\text{-}5$	$1.38379e\text{-}0$
∞	$-2.92925e\text{-}2$	$-$	$-$	$-$

Table 8.1: Lagrangian framework, convergence behavior of error of goal functional, only global refinement.

N	g_N	Error	Estimate	Efficiency
81	$-2.08546e\text{-}2$	$-8.43794e\text{-}3$	$-7.54122e\text{-}3$	$8.93728e\text{-}1$
289	$-2.56065e\text{-}2$	$-3.68599e\text{-}3$	$-4.09141e\text{-}3$	$1.10999e\text{-}0$
1089	$-2.77214e\text{-}2$	$-1.57107e\text{-}3$	$-1.88268e\text{-}3$	$1.19834e\text{-}0$
4225	$-2.86234e\text{-}2$	$-6.69121e\text{-}4$	$-8.09636e\text{-}4$	$1.21000e\text{-}0$
16641	$-2.90057e\text{-}2$	$-2.86821e\text{-}4$	$-3.41711e\text{-}4$	$1.19137e\text{-}0$
66049	$-2.91689e\text{-}2$	$-1.23569e\text{-}4$	$-1.44373e\text{-}4$	$1.16835e\text{-}0$
263169	$-2.92392e\text{-}2$	$-5.32636e\text{-}5$	$-6.14130e\text{-}5$	$1.15300e\text{-}0$
∞	$-2.92925e\text{-}2$	$-$	$-$	$-$

Table 8.2: Eulerian framework, convergence behavior of error of goal functional, only global refinement.
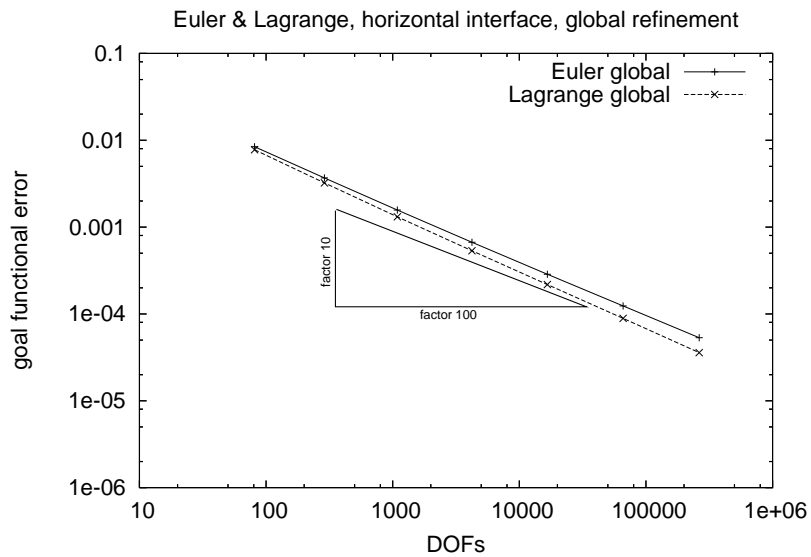
Figure 8.6: Both frameworks, convergence behavior of error of goal functional, only global refinement.
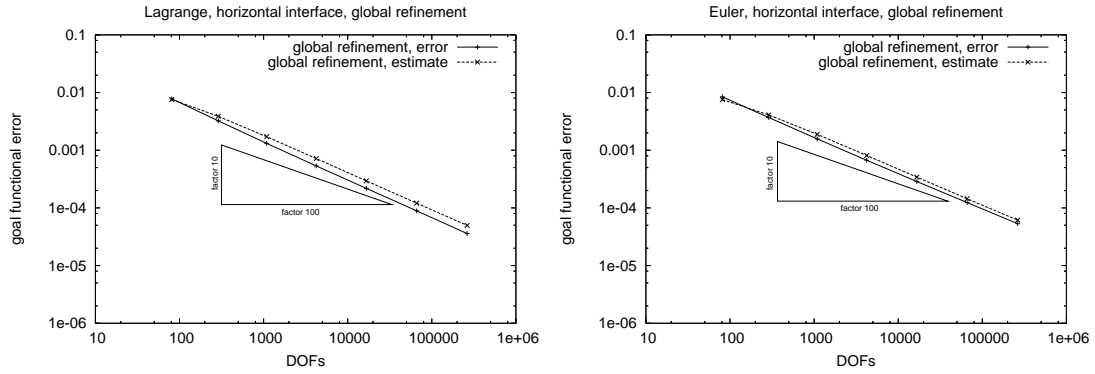
Figure 8.7: Both frameworks, comparison of error and approximation of error, only global refinement.

N	g_N	Error	Estimate	Efficiency
81	$-2.15295e\text{-}2$	$-7.76303e\text{-}3$	$-7.56227e\text{-}3$	$9.74138e\text{-}1$
239	$-2.58715e\text{-}2$	$-3.42097e\text{-}3$	$-3.86199e\text{-}3$	$1.12892e\text{-}0$
637	$-2.78243e\text{-}2$	$-1.46825e\text{-}3$	$-1.71114e\text{-}3$	$1.16543e\text{-}0$
1771	$-2.86829e\text{-}2$	$-6.09629e\text{-}4$	$-7.15764e\text{-}4$	$1.17410e\text{-}0$
4555	$-2.90315e\text{-}2$	$-2.60990e\text{-}4$	$-2.94240e\text{-}4$	$1.12740e\text{-}0$
11415	$-2.91857e\text{-}2$	$-1.06838e\text{-}4$	$-1.20751e\text{-}4$	$1.13022e\text{-}0$
28259	$-2.92493e\text{-}2$	$-4.31882e\text{-}5$	$-4.96563e\text{-}5$	$1.14977e\text{-}0$
66545	$-2.92743e\text{-}2$	$-1.82039e\text{-}5$	$-2.04639e\text{-}5$	$1.12415e\text{-}0$
151489	$-2.92855e\text{-}2$	$-6.98734e\text{-}6$	$-8.44616e\text{-}6$	$1.20878e\text{-}0$
∞	$-2.92925e\text{-}2$	$-$	$-$	$-$

Table 8.3: Lagrangian framework, convergence behavior of error of goal functional, adaptive refinement.

N	g_N	Error	Estimate	Efficiency
81	$-2.08546e\text{-}2$	$-8.43794e\text{-}3$	$-7.54122e\text{-}3$	$8.93728e\text{-}1$
239	$-2.53933e\text{-}2$	$-3.89917e\text{-}3$	$-4.08318e\text{-}3$	$1.04719e\text{-}0$
649	$-2.75412e\text{-}2$	$-1.75125e\text{-}3$	$-1.87642e\text{-}3$	$1.07148e\text{-}0$
1853	$-2.85579e\text{-}2$	$-7.34571e\text{-}4$	$-8.08376e\text{-}4$	$1.10047e\text{-}0$
5305	$-2.89823e\text{-}2$	$-3.10183e\text{-}4$	$-3.41436e\text{-}4$	$1.10076e\text{-}0$
13905	$-2.91563e\text{-}2$	$-1.36224e\text{-}4$	$-1.44335e\text{-}4$	$1.05954e\text{-}0$
34311	$-2.92324e\text{-}2$	$-6.01314e\text{-}5$	$-6.13948e\text{-}5$	$1.02101e\text{-}0$
84419	$-2.92667e\text{-}2$	$-2.58315e\text{-}5$	$-2.63232e\text{-}5$	$1.01903e\text{-}0$
196433	$-2.92814e\text{-}2$	$-1.10571e\text{-}5$	$-1.13736e\text{-}5$	$1.02863e\text{-}0$
∞	$-2.92925e\text{-}2$	$-$	$-$	$-$

Table 8.4: Eulerian framework, convergence behavior of error of goal functional, adaptive refinement.
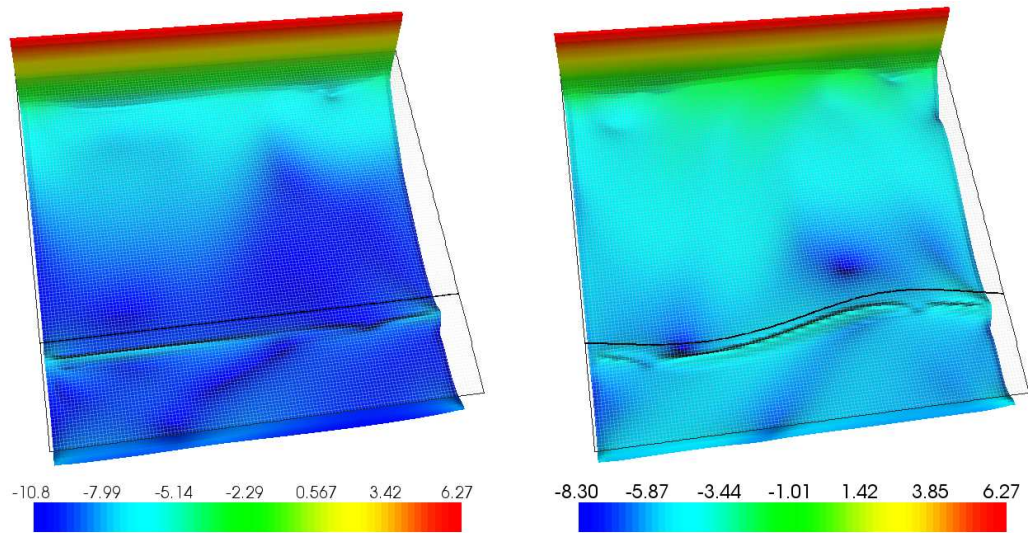
Figure 8.8: Comparison of $\log\|\nabla^2 z_1\|^2$ ($N = 16{,}641$) for the Lagrangian (left, displayed in the reference system) and Eulerian (right) frameworks.
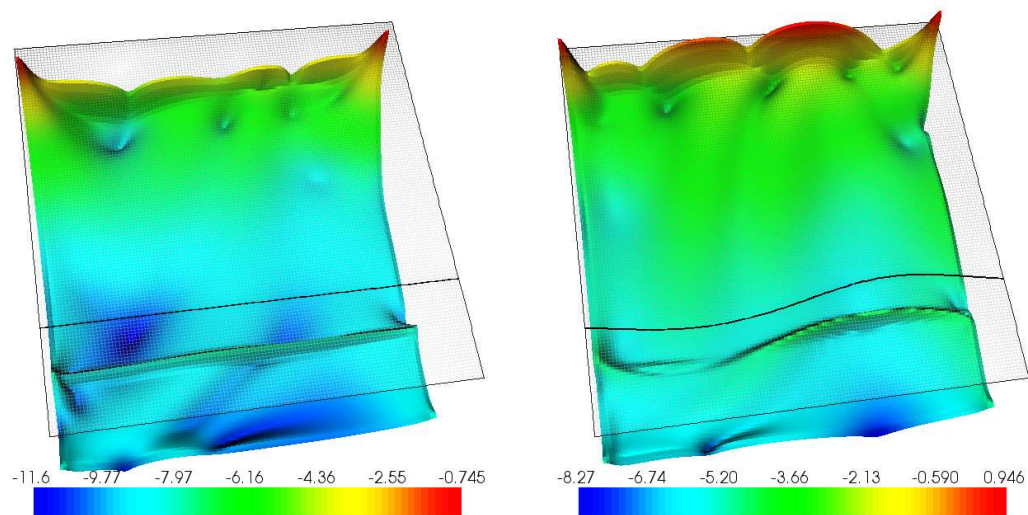
Figure 8.9: Comparison of $\log\|\nabla^2 z_2\|^2$ ($N = 16{,}641$) for the Lagrangian (left, displayed in the reference system) and Eulerian (right) frameworks.
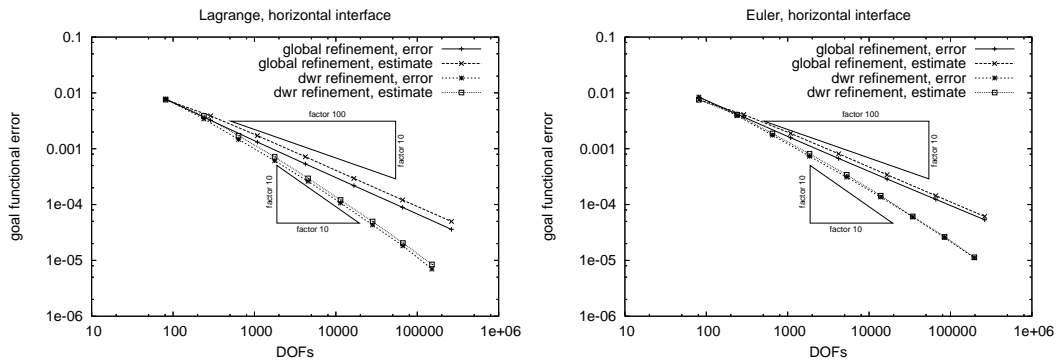
Figure 8.10: Both frameworks, comparison of error and approximation of error, both local and global refinement.

$$N = 4{,}555 \qquad\qquad N = 28{,}259$$

$$N = 66{,}545 \qquad\qquad N = 151{,}489$$
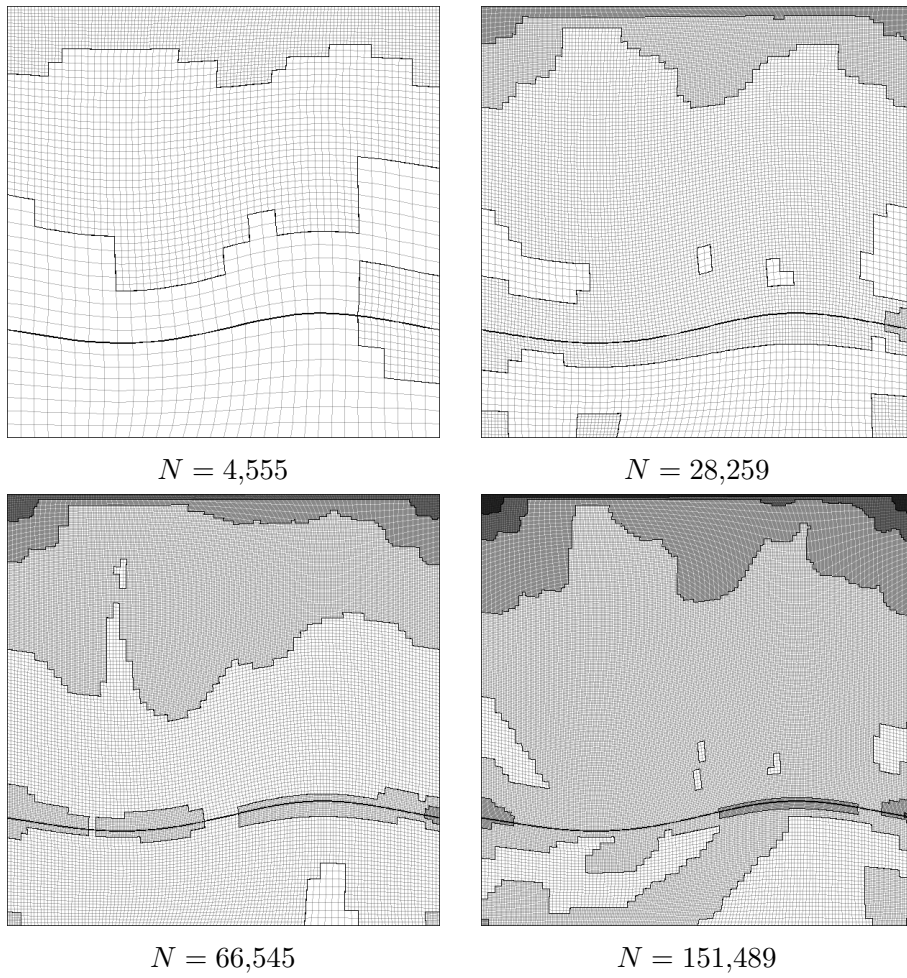
Figure 8.11: Lagrangian framework, adaptively refined mesh, displayed in the deformed system.

$N = 5{,}303$

$N = 34{,}311$

$N = 84{,}419$

$N = 196{,}433$
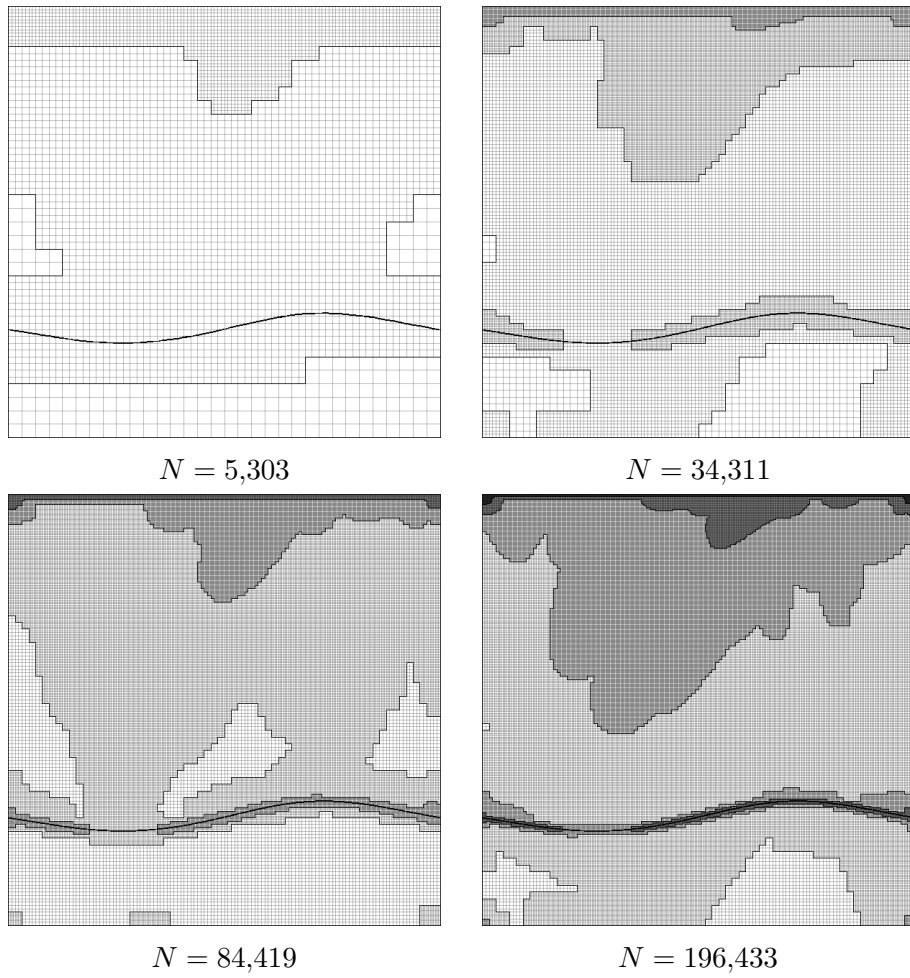
Figure 8.12: Eulerian framework, adaptively refined mesh.
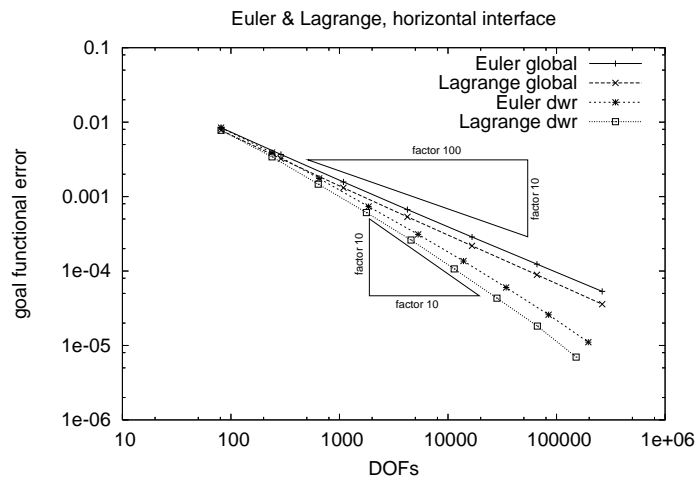
Figure 8.13: Both frameworks, convergence behavior of error of goal functional, both local and global refinement.

8.2.2 Diagonal interface

The material interface is set as a diagonal line through the reference configuration. The material parameters are $\mu_1 = 0.15$, $\mu_2 = 0.30$.

Similar to the previous section, as a driving force we supply a right-hand side, that is chosen so that the top-left and bottom-right halves of the material are 'pulled' to the lower-right and upper-left leading to a deformation as shown in Figure 8.14. Again, the force density is modified to improve overall convergence. To this end, we multiply the right-hand side with the square of a *'bubble function'* $b(x) := x_1 x_2 (2 - x_1)(2 - x_2)$. As a right-hand side we use the force density $f : \Omega \to \mathbb{R}^2$,

$$f(x) := b(x)^2 (\frac{x_1}{2}(-e_1 - e_2) + \frac{2 - x_1}{2}(e_1 + e_2)) \, ,$$
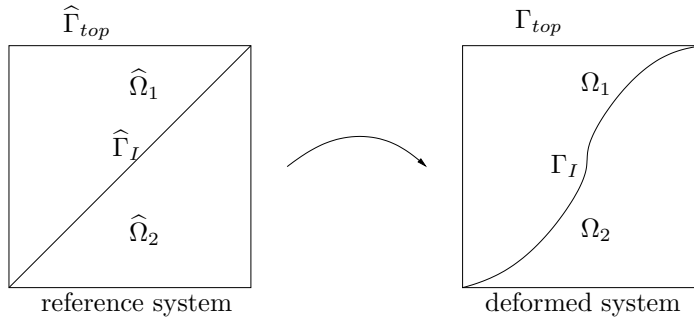
Figure 8.14: Configuration of the structure tests.

Again, just as in the previous section, we extrapolate the goal functional values ($\hat{G}(\hat{\Gamma}_{top})(\hat{U})(e_1)$, $G(\Gamma_{top})(U)(e_1)$) for the Lagrangian and Eulerian frameworks below (Tables 8.5, 8.6) to the limit and use a value that fits both limits the best. This we use as the reference goal functional value and refer to as g_∞. The calculated goal functional values we simply refer to as g_N, with N being the number of degrees of freedom. In the first simulations we calculate the goal functional errors $g_N - g_\infty$ in both approaches. The convergence of the error in both frameworks is displayed in the Tables 8.5, 8.6 and visually compared in Figure 8.17 (left).

For both approaches we also apply the 'dual weighted residual' method to approximate the error of the goal functional (column 'Estimate'). The efficiency of the estimator is in the column 'Efficiency', which is |Estimate/Error|. As can be seen in the plots in Figure 8.18 the efficiency of the error estimator is good. As a means of visualizing and comparing the sensitivity of the problem to the goal functional, we show the square norms of second derivatives of the components of z in the Figures 9.12 and 8.9 for both frameworks. Since the values $\|\nabla^2 z_i\|^2$ vary greatly, we display the values on a logarithmic scale.

Based on these results we use the error estimator to adaptively refine the grid using the mesh refinement method described in Chapter 7. We compare the errors of both approaches in the Tables 8.7, 8.8. The convergence of the error and the approximation of the error for

both frameworks and refinement methods is shown in the Figures 8.21. There we compare these values with the values in the when using global refinement. The Figures 8.22 and 8.23 show the evolution of adaptive mesh refinement for both frameworks. Finally in Figure 8.24 the errors of the goal functional are compared in a chart for both frameworks and global and local mesh refinement.
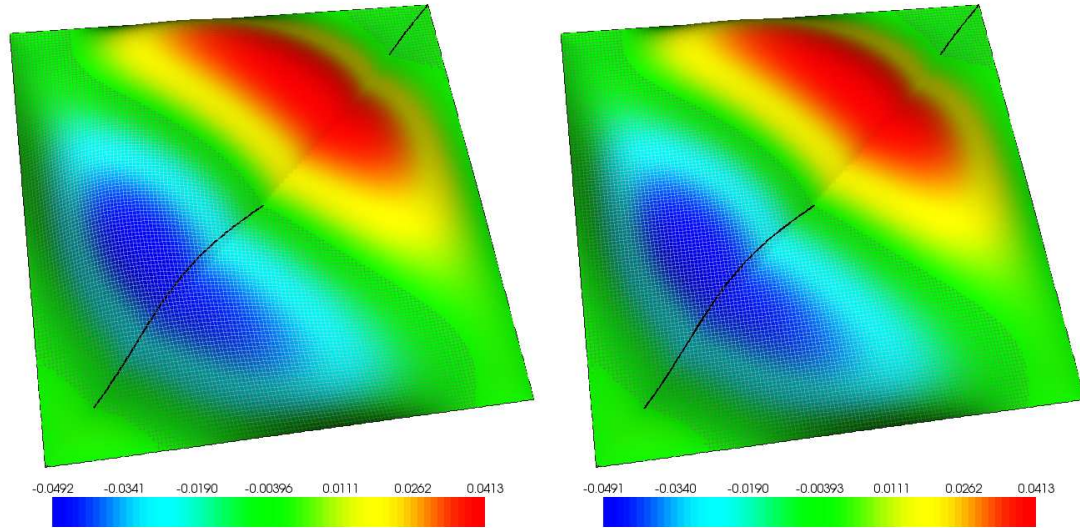
Figure 8.15: Comparison of the horizontal displacements ($N = 16{,}641$) for the Lagrangian (left, displayed in the deformed system) and Eulerian (right) frameworks.
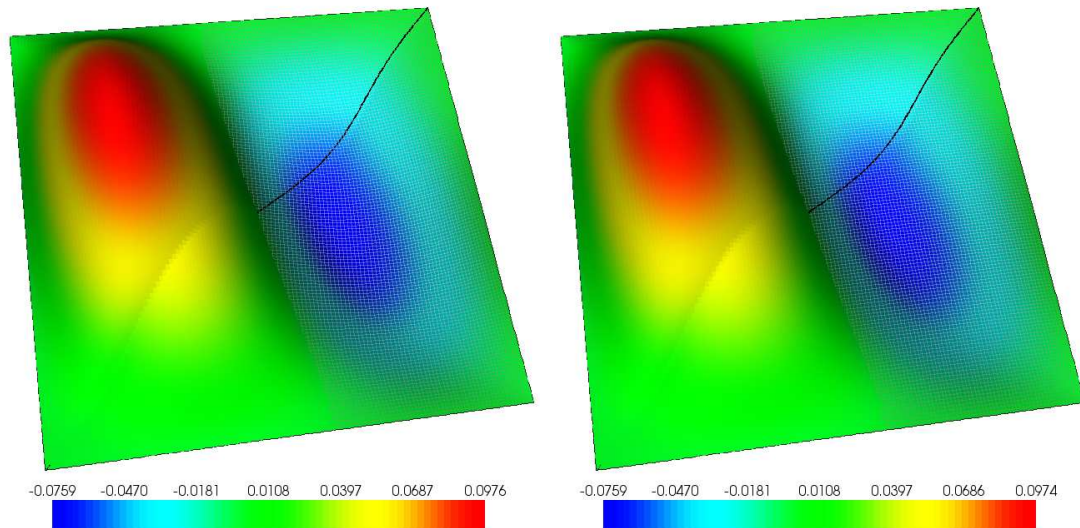
Figure 8.16: Comparison of the vertical displacements ($N = 16{,}641$) for the Lagrangian (left, displayed in the deformed system) and Eulerian (right) frameworks.

N	g_N	Error	Estimate	Efficiency
81	1.42849e-2	6.66014e-3	7.15751e-3	1.07468e-0
289	1.80919e-2	2.85306e-3	3.77811e-3	1.32423e-0
1089	1.97466e-2	1.19840e-3	1.65076e-3	1.37747e-0
4225	2.04450e-2	5.00019e-4	6.78556e-4	1.35706e-0
16641	2.07334e-2	2.11556e-4	2.77842e-4	1.31333e-0
66049	2.08567e-2	8.83052e-5	1.14336e-4	1.29479e-0
263169	2.09075e-2	3.74890e-5	4.74495e-5	1.26569e-0
∞	2.09450e-2	—	—	—

Table 8.5: Lagrangian framework, convergence behavior of error of goal functional, only global refinement.

N	g_N	Error	Estimate	Efficiency
81	1.35624e-2	7.38265e-3	6.78366e-3	9.18866e-1
289	1.74914e-2	3.45361e-3	4.04085e-3	1.17004e-0
1089	1.93778e-2	1.56720e-3	1.96629e-3	1.25465e-0
4225	2.02470e-2	6.97956e-4	8.75275e-4	1.25405e-0
16641	2.06356e-2	3.09435e-4	3.81162e-4	1.23180e-0
66049	2.08076e-2	1.37406e-4	1.66544e-4	1.21205e-0
263169	2.08838e-2	6.12193e-5	7.34431e-5	1.19967e-0
∞	2.09450e-2	—	—	—

Table 8.6: Eulerian framework, convergence behavior of error of goal functional, only global refinement.
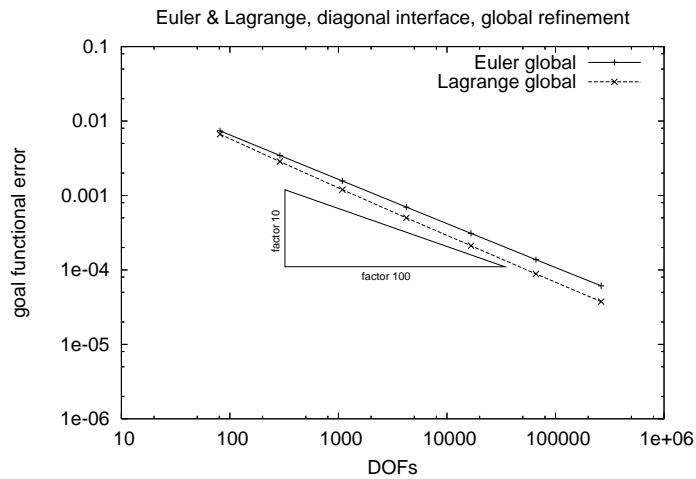
Figure 8.17: Both frameworks, convergence behavior of error of goal functional, only global refinement.
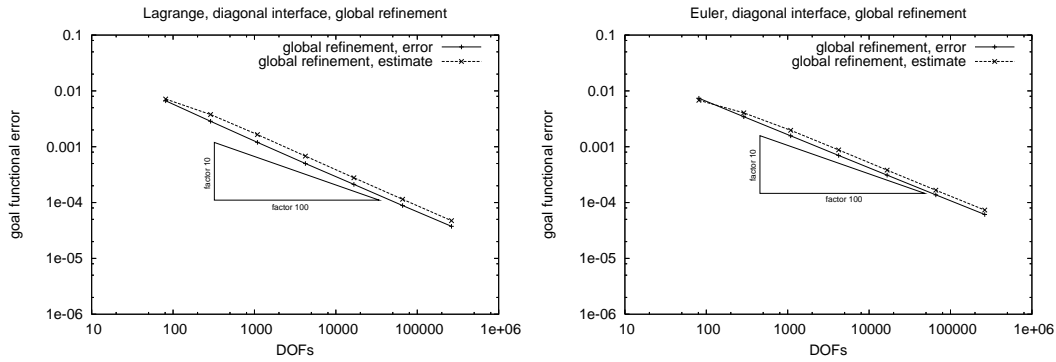
Figure 8.18: Both frameworks, comparison of error and approximation of error, only global refinement.

N	g_N	Error	Estimate	Efficiency
81	1.42849e-2	6.66014e-3	7.15751e-3	1.07468e-0
239	1.79383e-2	3.00674e-3	3.76958e-3	1.25371e-0
687	1.96396e-2	1.30537e-3	1.64584e-3	1.26082e-0
1989	2.04036e-2	5.41418e-4	6.78363e-4	1.25294e-0
5637	2.07113e-2	2.33729e-4	2.77422e-4	1.18694e-0
14241	2.08466e-2	9.83783e-5	1.14313e-4	1.16197e-0
36633	2.09034e-2	4.16487e-5	4.74305e-5	1.13882e-0
89403	2.09269e-2	1.81088e-5	1.97641e-5	1.09141e-0
203191	2.09375e-2	7.54264e-6	8.25049e-6	1.09385e-0
∞	2.09450e-2	—	—	—

Table 8.7: Lagrangian framework, convergence behavior of error of goal functional, adaptive refinement.

N	g_N	Error	Estimate	Efficiency
81	1.35624e-2	7.38265e-3	6.78366e-3	9.18866e-1
239	1.73354e-2	3.60960e-3	4.02342e-3	1.11464e-0
649	1.91330e-2	1.81204e-3	1.95082e-3	1.07659e-0
1621	2.01380e-2	8.06958e-4	8.72447e-4	1.08115e-0
4315	2.05892e-2	3.55757e-4	3.80333e-4	1.06908e-0
11693	2.07863e-2	1.58742e-4	1.66380e-4	1.04812e-0
30677	2.08729e-2	7.21171e-5	7.34062e-5	1.01788e-0
74707	2.09127e-2	3.23053e-5	3.26850e-5	1.01175e-0
183233	2.09305e-2	1.45488e-5	1.46824e-5	1.00918e-0
∞	2.09450e-2	—	—	—

Table 8.8: Eulerian framework, convergence behavior of error of goal functional, adaptive refinement.
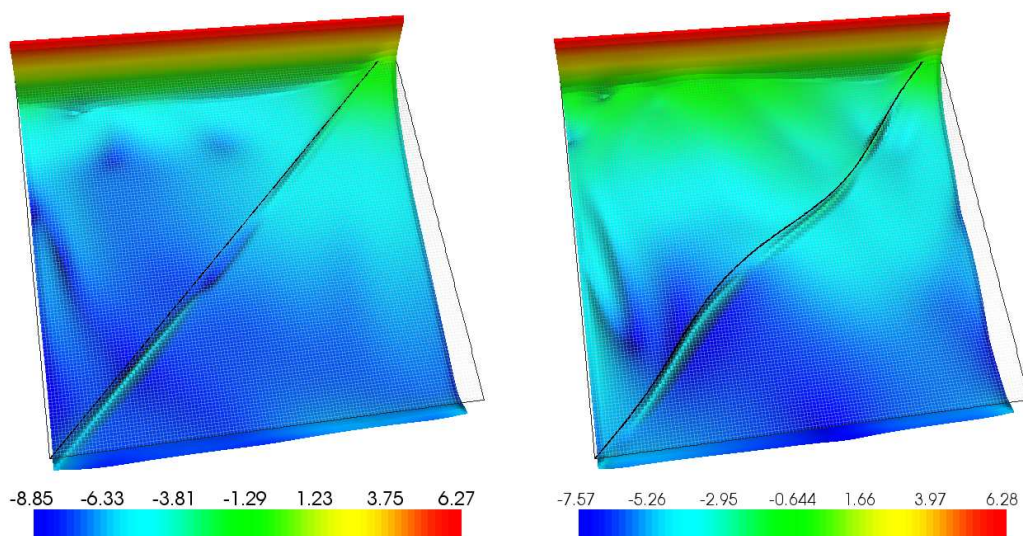
Figure 8.19: Comparison of $\log\|\nabla^2 z_1\|^2$ ($N = 16{,}641$) for the Lagrangian (left, displayed in the reference system) and Eulerian (right) frameworks.
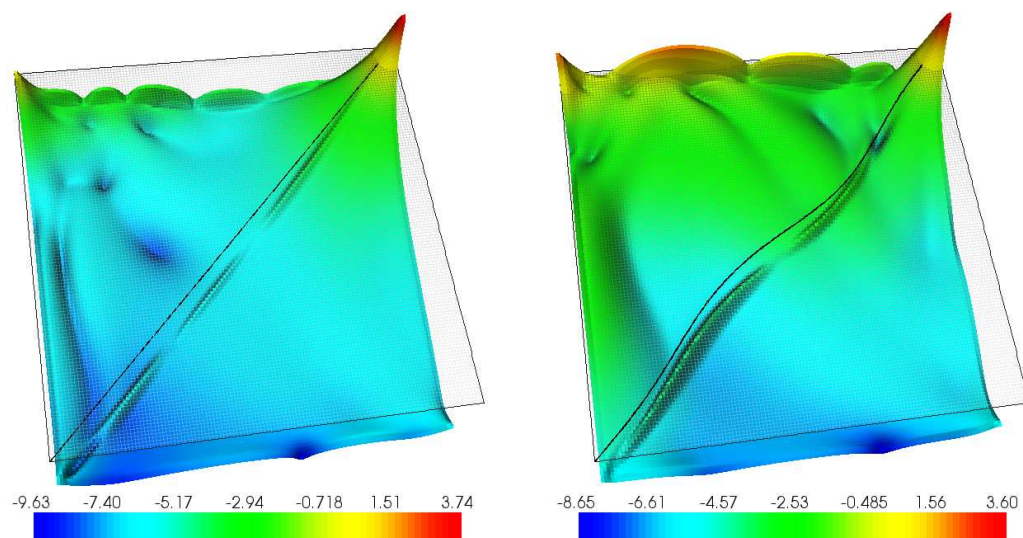
Figure 8.20: Comparison of $\log\|\nabla^2 z_2\|^2$ ($N = 16{,}641$) for the Lagrangian (left, displayed in the reference system) and Eulerian (right) frameworks.
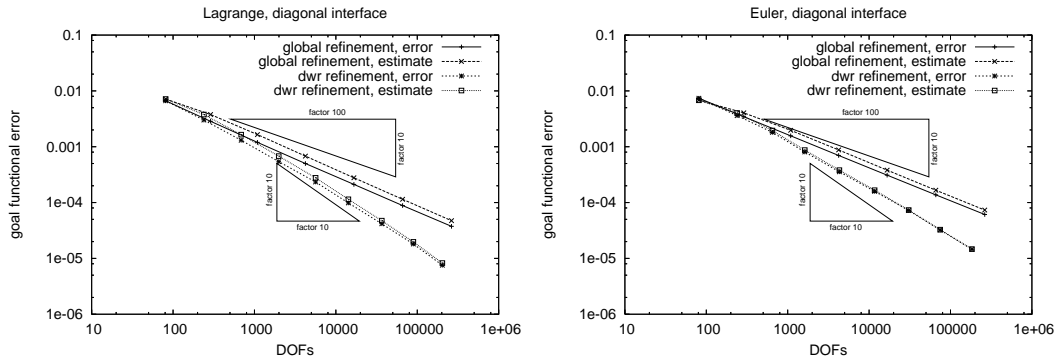
Figure 8.21: Both frameworks, comparison of error and approximation of error, both local and global refinement.

$N = 14{,}241$

$N = 36{,}633$

$N = 89{,}403$

$N = 203{,}191$
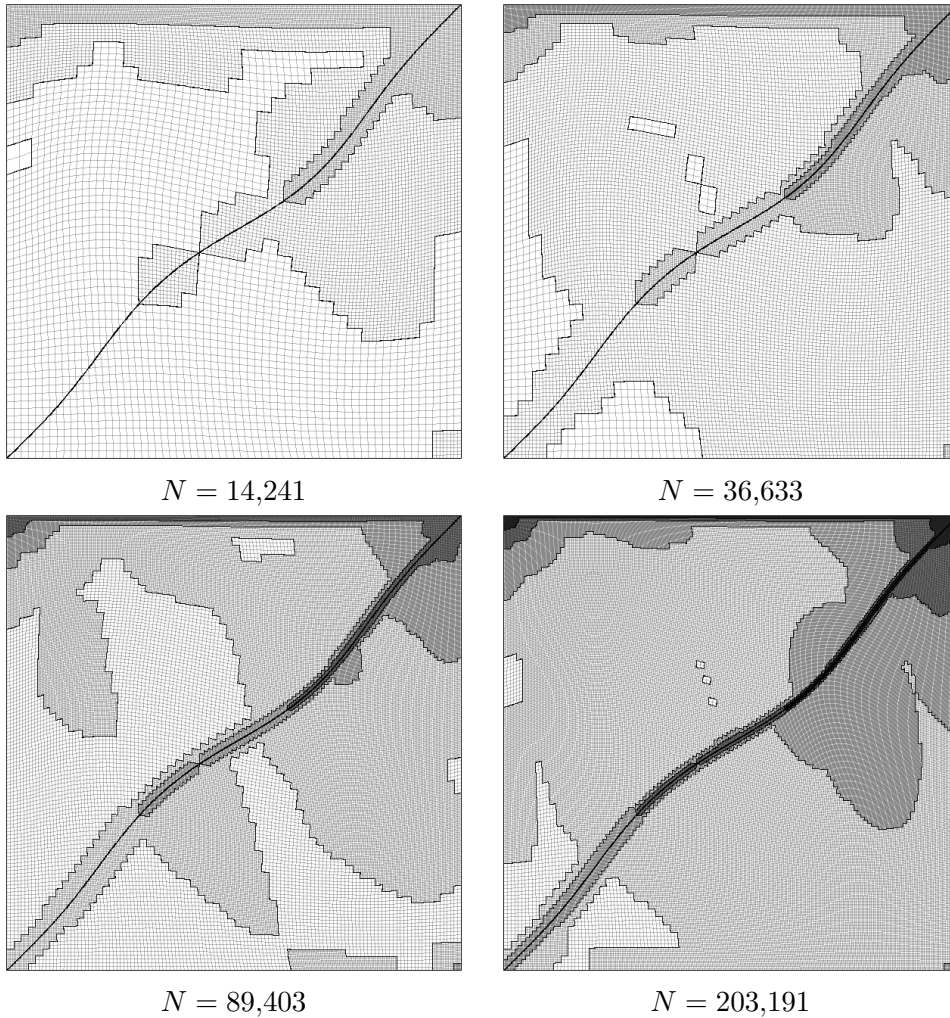
Figure 8.22: Lagrangian framework, adaptively refined mesh, displayed in the deformed system.
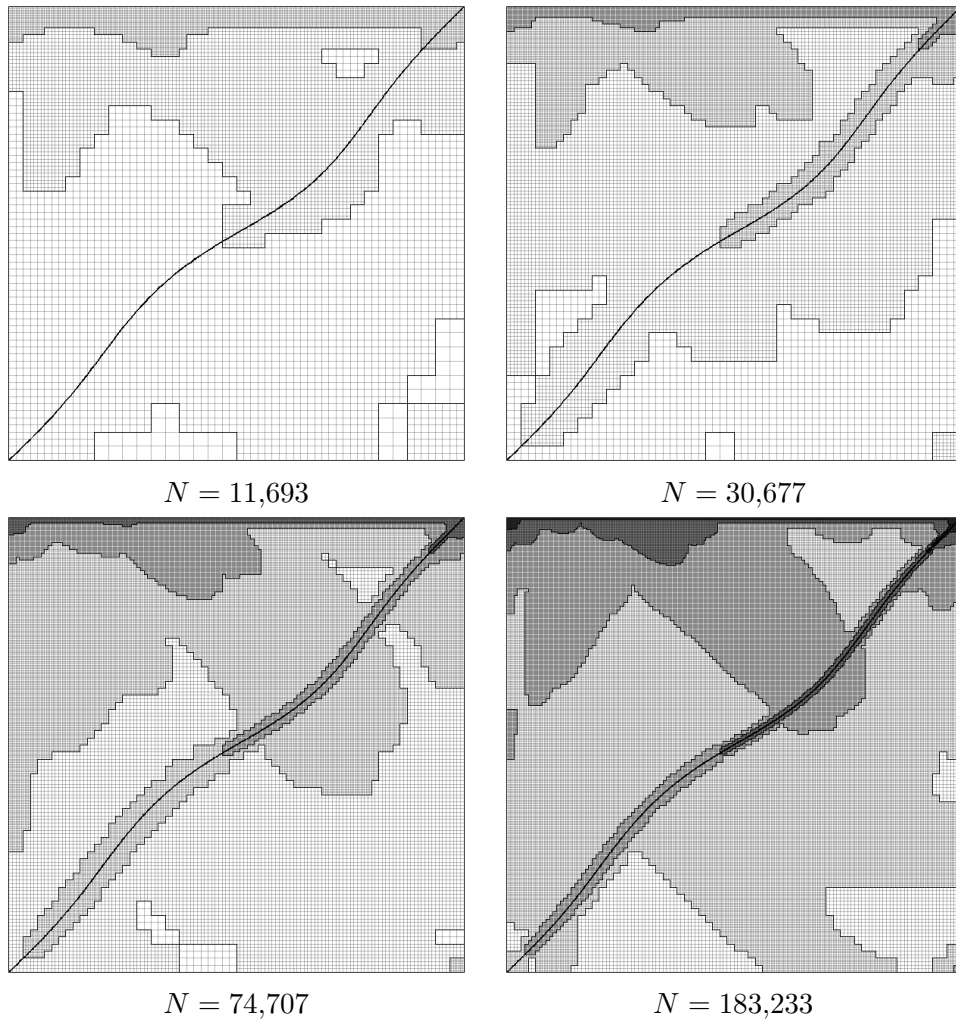
Figure 8.23: Eulerian framework, adaptively refined mesh.
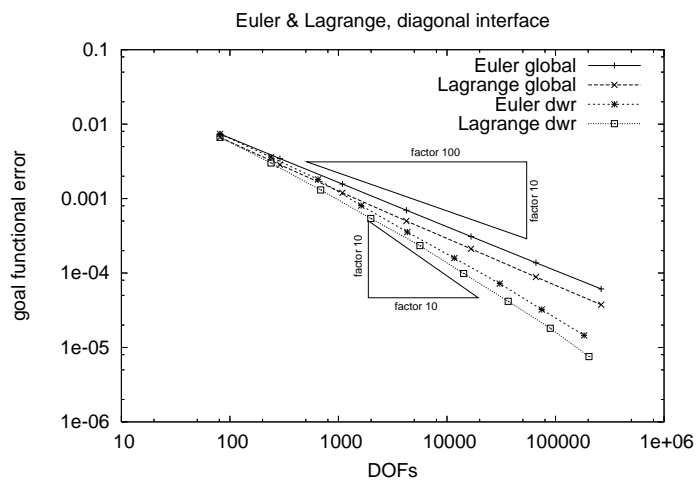
Figure 8.24: Both frameworks, convergence behavior of error of goal functional, both local and global refinement.

8.3 Influence of the boundary integrals

From Section 6.7.3 we know that in the Eulerian framework the directional derivative of the displacements will contain additional boundary integrals on the interface, e.g. for the stress tensors:

$$-(\sigma_1^- n_1 \cdot \phi, (\nabla \psi)_1^-)_{\Gamma_i} - (\sigma_2^- n_2 \cdot \phi, (\nabla \psi)_2^-)_{\Gamma_i} \, . \tag{8.12}$$

The values n_1, n_2 are to be understood as the normal-fields on the interface Γ_i, with n_1 'pointing out of' Ω_1 and $n_2 = -n_1$. We explained at the beginning of Section 8.2 how the expressions in (8.12) are then approximated by

$$(\delta_h \, (\sigma_1 - \sigma_2) \, n_1 \cdot \phi_h, \nabla \psi_h) \, , \tag{8.13}$$

with $\delta_h := \max(0, h - \mathrm{dist}(x - u, \hat{\Gamma}_i))/h^2$.

The material parameters where selected so that the solution would be sensitive to the material discontinuity at the interface.

This led to adaptive refinement along the interface for both Eulerian cases (horizontal and diagonal) and for the Lagrangian diagonal case (where the cell borders in the mesh did not match the interface). This can been seen respectively in the final meshes of the Figures 8.12, 8.23, and 8.22.

In Lagrangian diagonal case the refinement was similar to that using the Eulerian framework. This implies that for the Eulerian framework the directional derivatives of the characteristic functions only play an effectively minor role in the complete directional derivative, and that the sensitivity is largely influenced by the interface not matching the cell borders of the mesh.

To substantiate the negligible role of the jump terms in the directional derivatives, we repeat all calculations (horizontal and diagonal, global and adaptive) in the Eulerian framework and omit all mentioned boundary integrals.

We compare the convergence results in the following tables with their respective counterparts in the previous sections – the tables 8.9 with 8.2 (horizontal, global), 8.10 with 8.4 (horizontal, adaptive), 8.11 with 8.6 (diagonal, global), and 8.12 with 8.8 (diagonal, adaptive). It can been seen that the functional errors of the globally refined primal problems are unchanged. It can also be seen that the changes only lead to marginal differences in error estimator and the consequently adaptively refined meshes.

Both results are as expected, since the jump terms (8.12) only appear in the directional derivatives. Thus the omission of the jump terms affects results that directly depend on the directional derivatives.

In the case of the globally refined primal problems, the functional errors depend on the discrete solution. By changing the directional derivatives, only the convergence behavoir of the Newton iteration is changed. The change will not affect the final results (provided the iteration still converges).

In the case of the error estimates, there are differences, as should be expected, since the calculations of these estimates require the solutions of the linear dual problems, which themselves require the directional derivatives.

8.3.1 Horizontal interface

N	g_N	Error	Estimate	Efficiency
81	$-2.08546e$-2	$-8.43794e$-3	$-7.54123e$-3	8.93729e-1
289	$-2.56065e$-2	$-3.68599e$-3	$-4.09142e$-3	1.10999e-0
1089	$-2.77214e$-2	$-1.57107e$-3	$-1.88268e$-3	1.19834e-0
4225	$-2.86234e$-2	$-6.69121e$-4	$-8.09637e$-4	1.21000e-0
16641	$-2.90057e$-2	$-2.86821e$-4	$-3.41711e$-4	1.19138e-0
66049	$-2.91689e$-2	$-1.23569e$-4	$-1.44373e$-4	1.16835e-0
263169	$-2.92392e$-2	$-5.32636e$-5	$-6.14131e$-5	1.15300e-0
∞	$-2.92925e$-2	$-$	$-$	$-$

Table 8.9: Eulerian framework, convergence behavior of error of goal functional, only global refinement, without boundary integrals.

N	g_N	Error	Estimate	Efficiency
81	$-2.08546e$-2	$-8.43794e$-3	$-7.54123e$-3	8.93729e-1
239	$-2.53933e$-2	$-3.89917e$-3	$-4.08304e$-3	1.04716e-0
649	$-2.75412e$-2	$-1.75125e$-3	$-1.87642e$-3	1.07147e-0
1853	$-2.85579e$-2	$-7.34571e$-4	$-8.08377e$-4	1.10047e-0
5305	$-2.89823e$-2	$-3.10183e$-4	$-3.41437e$-4	1.10076e-0
13955	$-2.91564e$-2	$-1.36130e$-4	$-1.44335e$-4	1.06027e-0
34519	$-2.92324e$-2	$-6.01427e$-5	$-6.13951e$-5	1.02082e-0
84697	$-2.92667e$-2	$-2.58199e$-5	$-2.63232e$-5	1.01950e-0
196903	$-2.92814e$-2	$-1.10529e$-5	$-1.13736e$-5	1.02902e-0
∞	$-2.92925e$-2	$-$	$-$	$-$

Table 8.10: Eulerian framework, convergence behavior of error of goal functional, adaptive refinement, without boundary integrals.

$N = 196{,}433$ $\qquad\qquad\qquad$ $N = 196{,}903$
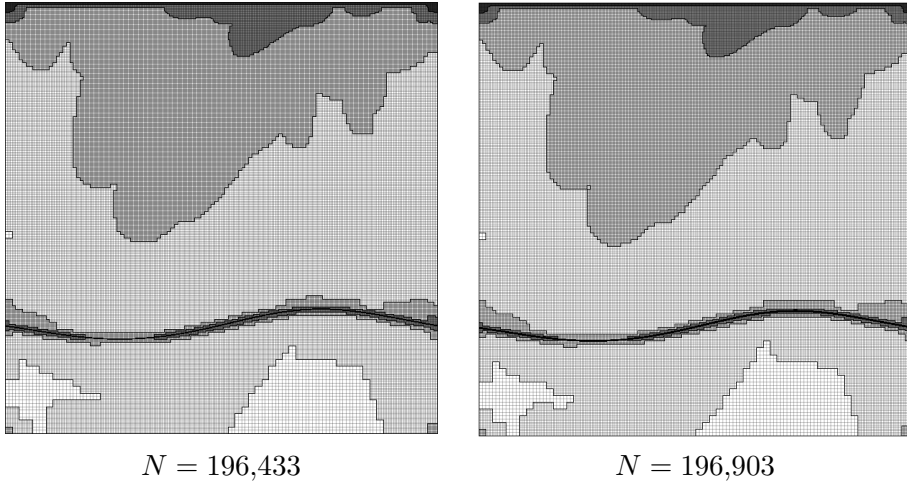
Figure 8.25: Eulerian framework, adaptively refined mesh.

8.3.2 Diagonal interface

N	g_N	Error	Estimate	Efficiency
81	1.35624e-2	7.38265e-3	6.79054e-3	9.19798e-1
289	1.74914e-2	3.45361e-3	4.04125e-3	1.17015e-0
1089	1.93778e-2	1.56720e-3	1.96656e-3	1.25482e-0
4225	2.02470e-2	6.97956e-4	8.75330e-4	1.25413e-0
16641	2.06356e-2	3.09435e-4	3.81175e-4	1.23184e-0
66049	2.08076e-2	1.37406e-4	1.66548e-4	1.21208e-0
263169	2.08838e-2	6.12193e-5	7.34442e-5	1.19969e-0
∞	2.09450e-2	—	—	—

Table 8.11: Eulerian framework, convergence behavior of error of goal functional, only global refinement, without boundary integrals.

N	g_N	Error	Estimate	Efficiency
81	1.35624e-2	7.38265e-3	6.79054e-3	9.19798e-1
239	1.73354e-2	3.60960e-3	4.02407e-3	1.11482e-0
649	1.91330e-2	1.81204e-3	1.95132e-3	1.07687e-0
1621	2.01380e-2	8.06958e-4	8.72565e-4	1.08130e-0
4279	2.05884e-2	3.56555e-4	3.80329e-4	1.06668e-0
11477	2.07850e-2	1.60010e-4	1.66380e-4	1.03981e-0
30005	2.08727e-2	7.22605e-5	7.34057e-5	1.01585e-0
73487	2.09127e-2	3.23354e-5	3.26852e-5	1.01082e-0
180277	2.09304e-2	1.45805e-5	1.46824e-5	1.00699e-0
∞	2.09450e-2	—	—	—

Table 8.12: Eulerian framework, convergence behavior of error of goal functional, adaptive refinement, without boundary integrals.

$$N = 183{,}233 \qquad\qquad N = 180{,}277$$
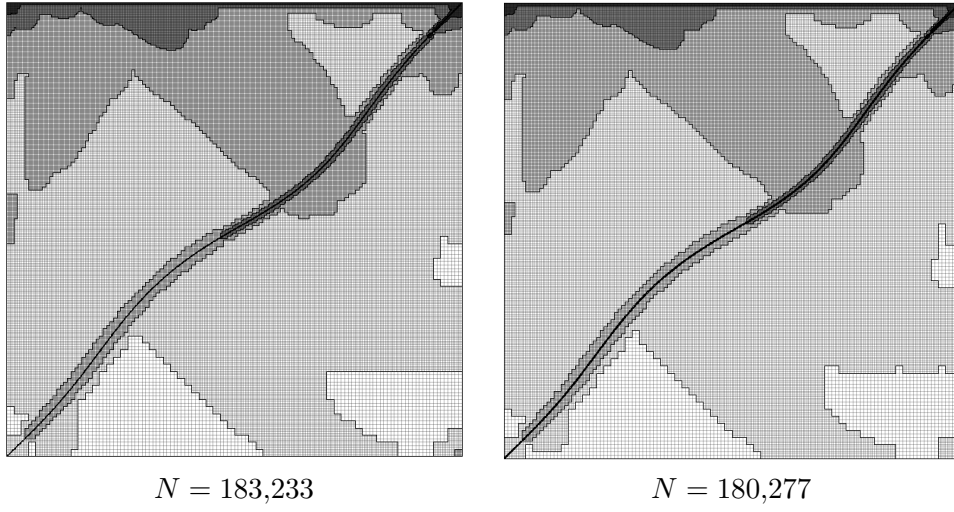
Figure 8.26: Eulerian framework, adaptively refined mesh.

Chapter 9

Numerical test: elastic flow cavity

As a starting test of the monolithic models described in Chapter 5 we use a simple stationary test example, the lid-driven cavity with an elastic bottom wall, as shown in Figure 9.1. The problems to be solved will be based on the Problems 5.3 and 5.7. For simplicity, for modeling the fluid the (linear) Stokes equations are used and the material of the bottom wall is assumed to be neo-Hookean and incompressible. Since we are modelling an incompressible fluid and structure, there will be a scalar pressure field for the fluid and structure domains. Since we are using a bilinear equal order approach, the pressure field on the cells at the interface will be bilinear and steady, although this is not to be expected. To enhance the accuracy of the pressure field at the interface, we decouple the fluid and structure pressure fields into two separate fields, p_f and p_s. The fluid pressure field p_f is used as a Lagrange-multiplier in the fluid domain, its value in the structure domain though is determined by harmonic continuation. The same approach is used for the structure pressure field p_s, only from the other side. The structure material is taken as very soft such that a visible deformation of the fluid-structure interface can be expected. Then, the other material parameters are chosen such that flow and solid deformation velocity are small enough to allow for a stationary solution of the coupled systems. This solution is computed by a pseudo-time stepping method employing the implicit Euler scheme. A steady state is reached once the kinetic energy of the structure is below a prescribed small tolerance, here $\|v_s\|^2 \leq 10^{-7}$.
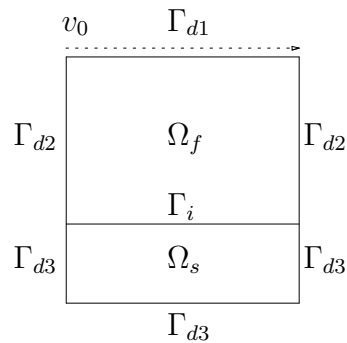
Figure 9.1: Configuration of the 'elastic' lid-driven cavity.

The cavity has a size of 2×2, and its elastic part has a height of 0.5. The material constants are $\rho_f = \rho_s = 1$, $\nu_f = 0.2$, and $\mu_s = 2.0$. At the top boundary Γ_{d1} the regularized tangential flow profile

$$v_0 = 0.5 \begin{cases} 4x, & x \in [0.0, 0.25], \\ 1, & x \in (0.25, 1.75), \\ 4(2 - x), & x \in [1.75, 2.0], \end{cases}$$

is prescribed, in order to avoid problems due to pressure singularities.

9.1 Computations on globally refined meshes

The left halves of the Figures 9.3 (ALE) and 9.4 (Eulerian) show the development of $\|v_s\|^2$ during the pseudo-time stepping process depending on the number of cells of the mesh. As expected the kinetic energy tends to zero. The multiple 'bumps' occur due to the way the elastic structure reaches its stationary state by 'swinging' back and forth a few times. At the extreme point of each swing the kinetic energy has a local minimum. Figures 9.5 (ALE) and 9.6 (Eulerian) show the final stationary states computed on globally uniform meshes.

In the Eulerian framework it is not immediately clear, due to the coupling with the fluid, how well (or bad) the mass of the structure is conserved. In Figure 9.2, we display the mass error of the structure at the stationary state. Additionally we show the improvement by using an adaptive quadrature rule, based on a simple rule. This consists of using a summed quadrature rule on all cells that contain the interface. On all other cells we use a Gauss quadrature rule. When we only use the Gauss quadrature the mass error is approximately of the order $O(h)$. In contrast, when we use the adaptive quadrature, the order of the mass error is between $O(h^{1.5})$ and $O(h^2)$.

The right halves of the Figures 9.3 (ALE) and 9.4 (Eulerian) show the errors of the discrete approximation of the goal functional value $\hat{G}(\hat{\Gamma}_{top})(\hat{U})(\varphi) = G(\Gamma_{top})(U)(\varphi)$ as defined in (8.5). The discrete values are calculated using the residual based method (8.8). Additionally we also display the approximation of the error using the simplified stationary version of the DWR method as described in Section 7.1.
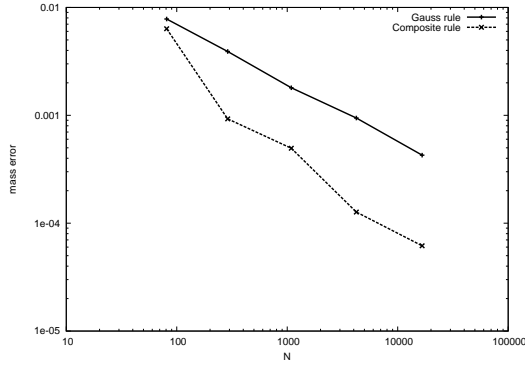
N	Gauss quadrature	Composite rule
81	7.813e-3	6.348e-3
289	3.906e-3	9.270e-4
1089	1.873e-3	4.952e-4
4225	9.441e-4	1.267e-4
16641	4.273e-4	6.175e-5

Figure 9.2: Based on which quadrature rule is used, we display the mass errors of the final domain Ω_s of the stationary FSI problem, when using a pseudo time-stepping scheme.

N	g_N	Error	Estimate	Efficiency
81	$-6.6651e$+0	3.8849e+0	2.2771e+0	5.8614e-1
289	$-8.0599e$+0	2.4901e+0	2.8200e+0	1.1325e+0
1089	$-9.0360e$+0	1.5140e+0	1.1628e+0	7.6802e-1
4225	$-9.7051e$+0	8.4486e-1	4.6624e-1	5.5185e-1
16641	$-1.0118e$+1	4.3174e-1	2.3096e-1	5.3495e-1
∞	$-1.055e$+1	—	—	—

Table 9.1: Lagrangian framework, convergence behavior of error of goal functional, adaptive refinement.

N	g_N	Error	Estimate	Efficiency
81	$-8.2869e$+0	2.2631e+0	3.9409e+0	1.7413e+0
289	$-8.1463e$+0	2.4037e+0	1.6642e+0	6.9235e-1
1089	$-9.0927e$+0	1.4573e+0	9.5076e-1	6.5240e-1
4225	$-9.7693e$+0	7.8071e-1	4.9527e-1	6.3439e-1
16641	$-1.0188e$+1	3.6249e-1	2.2385e-1	6.1753e-1
∞	$-1.055e$+1	—	—	—

Table 9.2: Eulerian framework, convergence behavior of error of goal functional, adaptive refinement.
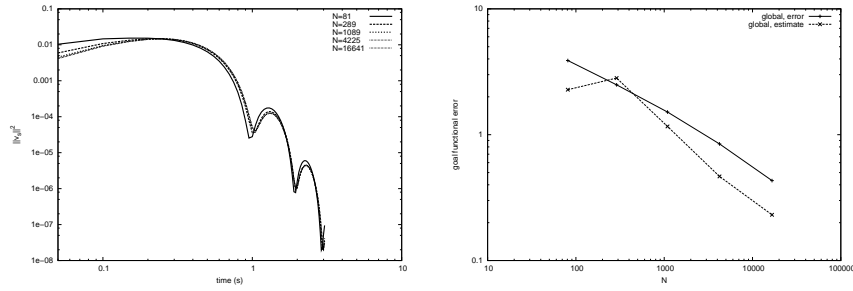
Figure 9.3: (left) Variation of $\|v_s\|^2$ in time for different numbers N of mesh cells. (right) The error of the goal functional $\hat{G}(\hat{\Gamma}_{top})(\hat{U}_h)(\varphi)$ and error estimate.
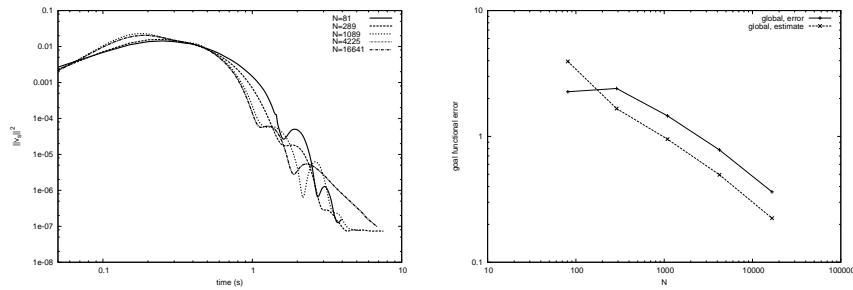
Figure 9.4: (left) Variation of $\|v_s\|^2$ in time for different numbers N of mesh cells. (right) The error of the goal functional $G(\Gamma_{top})(U_h)(\varphi)$ and error estimate.

$N = 16{,}641$ $N = 16{,}641$
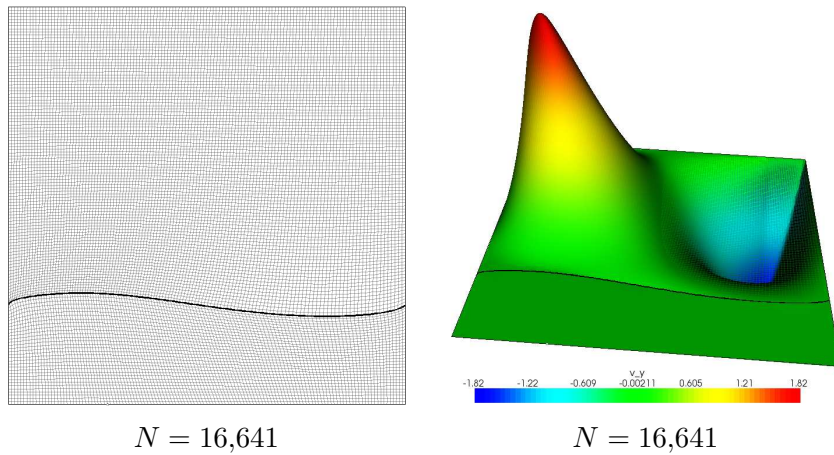
Figure 9.5: Globally refined mesh (left) and vertical velocity field (right) with the ALE approach, both displayed in the deformed system.
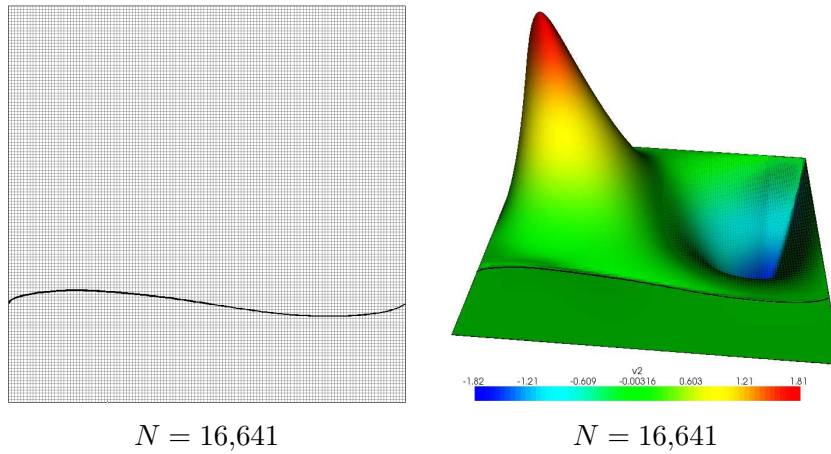
$N = 16{,}641$ $N = 16{,}641$

Figure 9.6: Globally refined mesh and vertical velocity with the Eulerian approach.
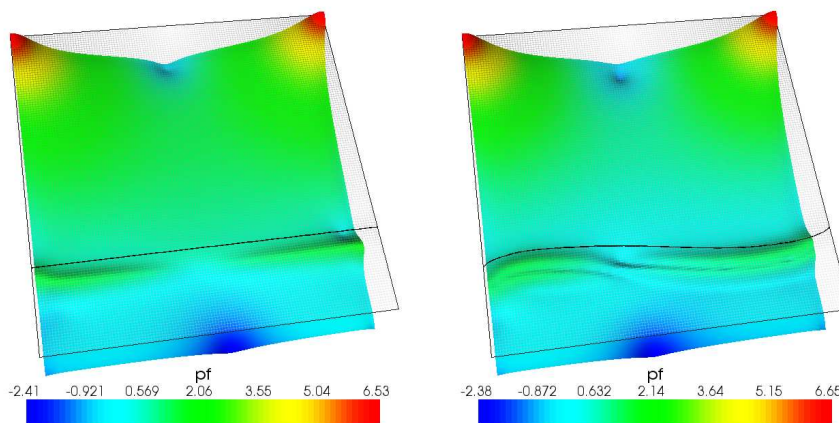
Figure 9.7: Comparison (N=16,641) of $\log\|\nabla^2 z_f^p\|^2$ for the Lagrangian (left, displayed in the reference system) and Eulerian (right) frameworks.
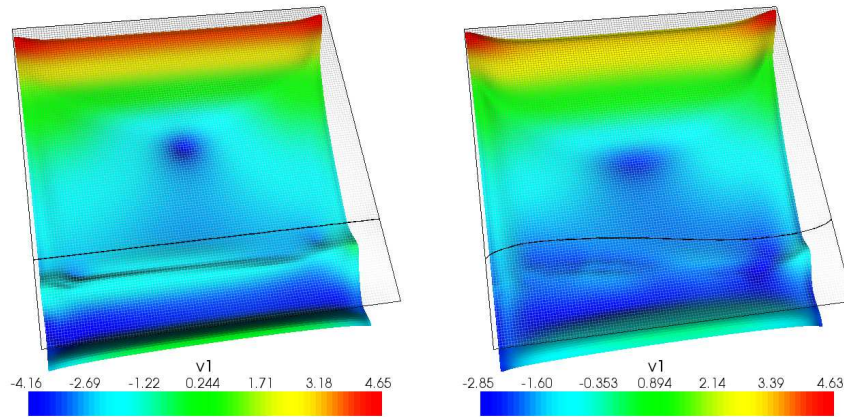
Figure 9.8: Comparison (N=16,641) of $\log\|\nabla^2 z_1^v\|^2$ for the Lagrangian (left, displayed in the reference system) and Eulerian (right) frameworks.
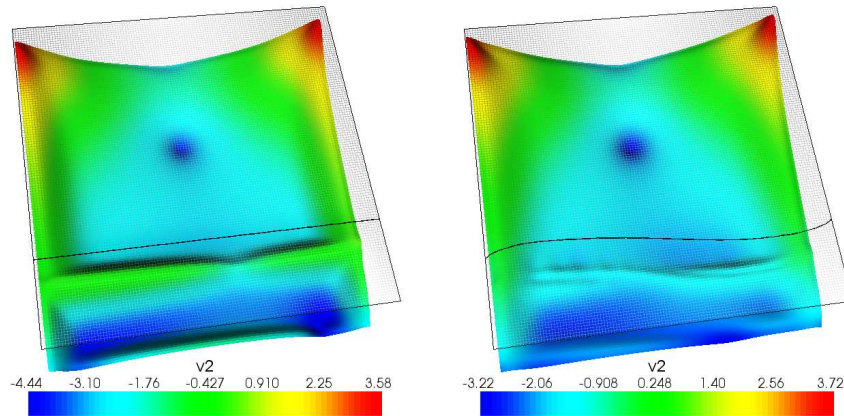
Figure 9.9: Comparison (N=16,641) of $\log\|\nabla^2 z_2^v\|^2$ for the Lagrangian (left, displayed in the reference system) and Eulerian (right) frameworks.
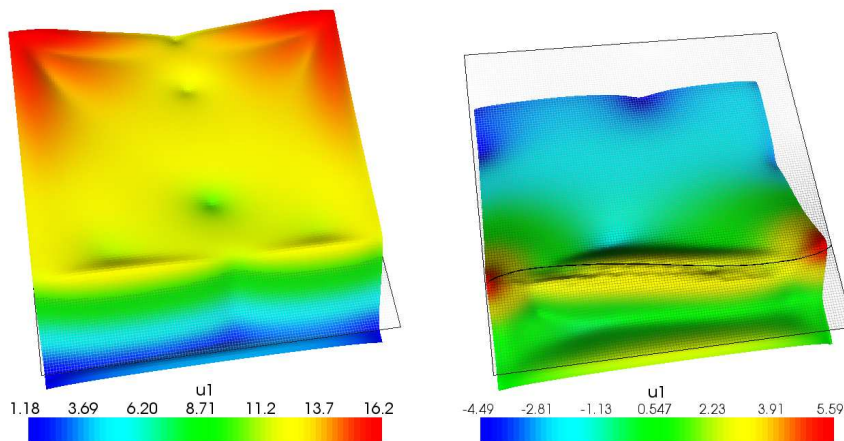
Figure 9.10: Comparison (N=16,641) of $\log\|\nabla^2 z_1^u\|^2$ for the Lagrangian (left, displayed in the reference system) and Eulerian (right) frameworks.
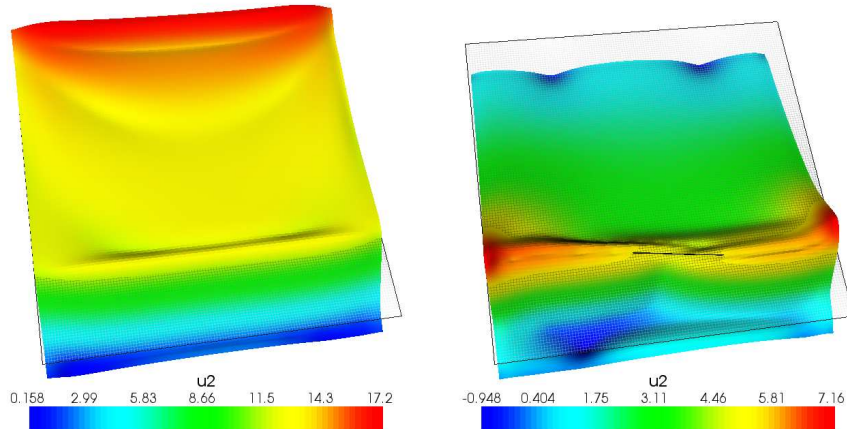
Figure 9.11: Comparison (N=16,641) of $\log\|\nabla^2 z_2^u\|^2$ for the Lagrangian (left, displayed in the reference system) and Eulerian (right) frameworks.
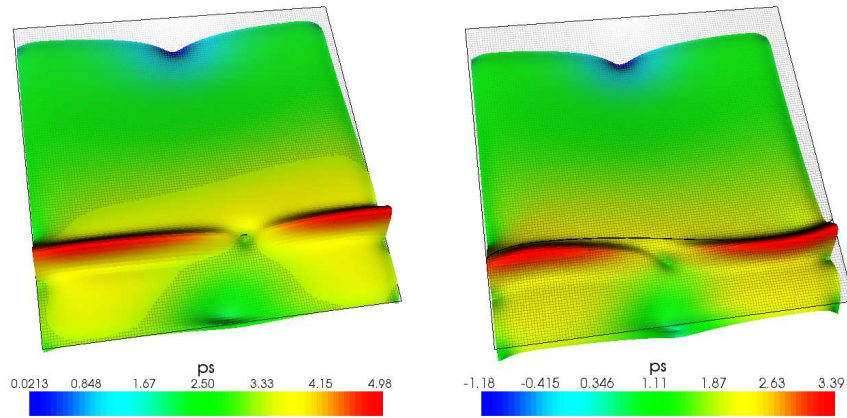
Figure 9.12: Comparison (N=16,641) of $\log\|\nabla^2 z_s^p\|^2$ for the Lagrangian (left, displayed in the reference system) and Eulerian (right) frameworks.

9.2 Computations on locally adapted meshes

We apply the stationary version of the DWR method as described in Chapter 7 for local mesh adaptation in the present test problem. For the a posteriori error estimation, we use the same goal functional as when we were refining the mesh globally. In Figure 9.13 the resulting error is displayed as a function of the number of mesh cells. The Figures 9.14 (ALE) and 9.15 (Eulerian) show sequences of adapted meshes. As expected two effects can be seen. There is local refinement around the area of interest Γ_{top} and since the position of the fluid-structure interface is a decisive factor, local refinement also occurs along the interface.

N	g_N	Error	Estimate	Efficiency
81	$-6.6652e{+}0$	$3.8848e{+}0$	$2.2773e{+}0$	$5.8620e{-}1$
153	$-8.1077e{+}0$	$2.4423e{+}0$	$2.7836e{+}0$	$1.1397e{+}0$
353	$-9.0980e{+}0$	$1.4520e{+}0$	$1.1908e{+}0$	$8.2011e{-}1$
991	$-9.7414e{+}0$	$8.0857e{-}1$	$5.0181e{-}1$	$6.2062e{-}1$
2613	$-1.0138e{+}1$	$4.1165e{-}1$	$1.9285e{-}1$	$4.6849e{-}1$
6451	$-1.0367e{+}1$	$1.8292e{-}1$	$7.3242e{-}2$	$4.0040e{-}1$
15203	$-1.0494e{+}1$	$5.6379e{-}2$	$2.7436e{-}2$	$4.8664e{-}1$
∞	$-1.055e{+}1$	$-$	$-$	$-$

Table 9.3: Lagrangian framework, convergence behavior of error of goal functional, adaptive refinement.

N	g_N	Error	Estimate	Efficiency
81	$-6.7473e{+}0$	$3.8027e{+}0$	$3.3051e{+}0$	$8.6916e{-}1$
155	$-8.2217e{+}0$	$2.3283e{+}0$	$3.7663e{+}0$	$1.6176e{+}0$
349	$-9.1994e{+}0$	$1.3506e{+}0$	$1.4344e{+}0$	$1.0620e{+}0$
845	$-9.8437e{+}0$	$7.0626e{-}1$	$6.5256e{-}1$	$9.2396e{-}1$
2293	$-1.0212e{+}1$	$3.3808e{-}1$	$2.9596e{-}1$	$8.7542e{-}1$
5915	$-1.0413e{+}1$	$1.3743e{-}1$	$1.0255e{-}1$	$7.4623e{-}1$
15069	$-1.0488e{+}1$	$6.1560e{-}2$	$4.6671e{-}2$	$7.5814e{-}1$
∞	$-1.055e{+}1$	$-$	$-$	$-$

Table 9.4: Lagrangian framework, convergence behavior of error of goal functional, adaptive refinement.
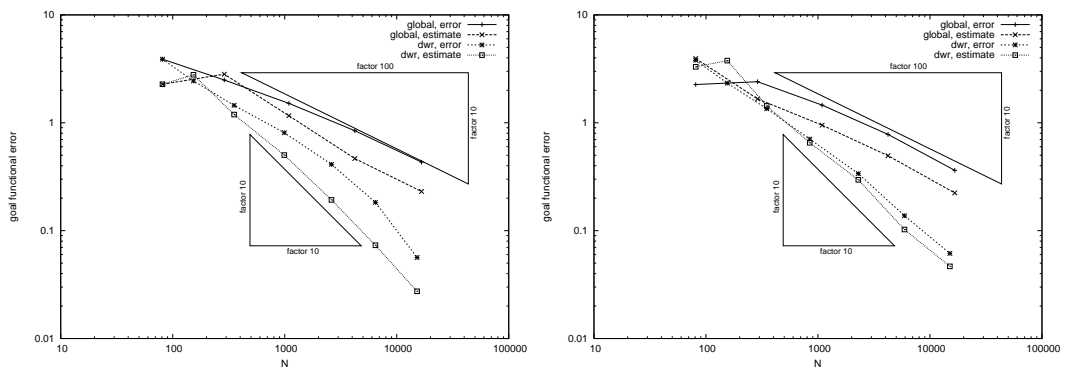
Figure 9.13: The error of the goal functional and respective error estimates for the ALE (left) and Eulerian (right) frameworks.

$$N = 81 \qquad\qquad N = 153 \qquad\qquad N = 353$$

$$N = 991 \qquad\qquad N = 2,613 \qquad\qquad N = 6,451$$

$$N = 15,203$$
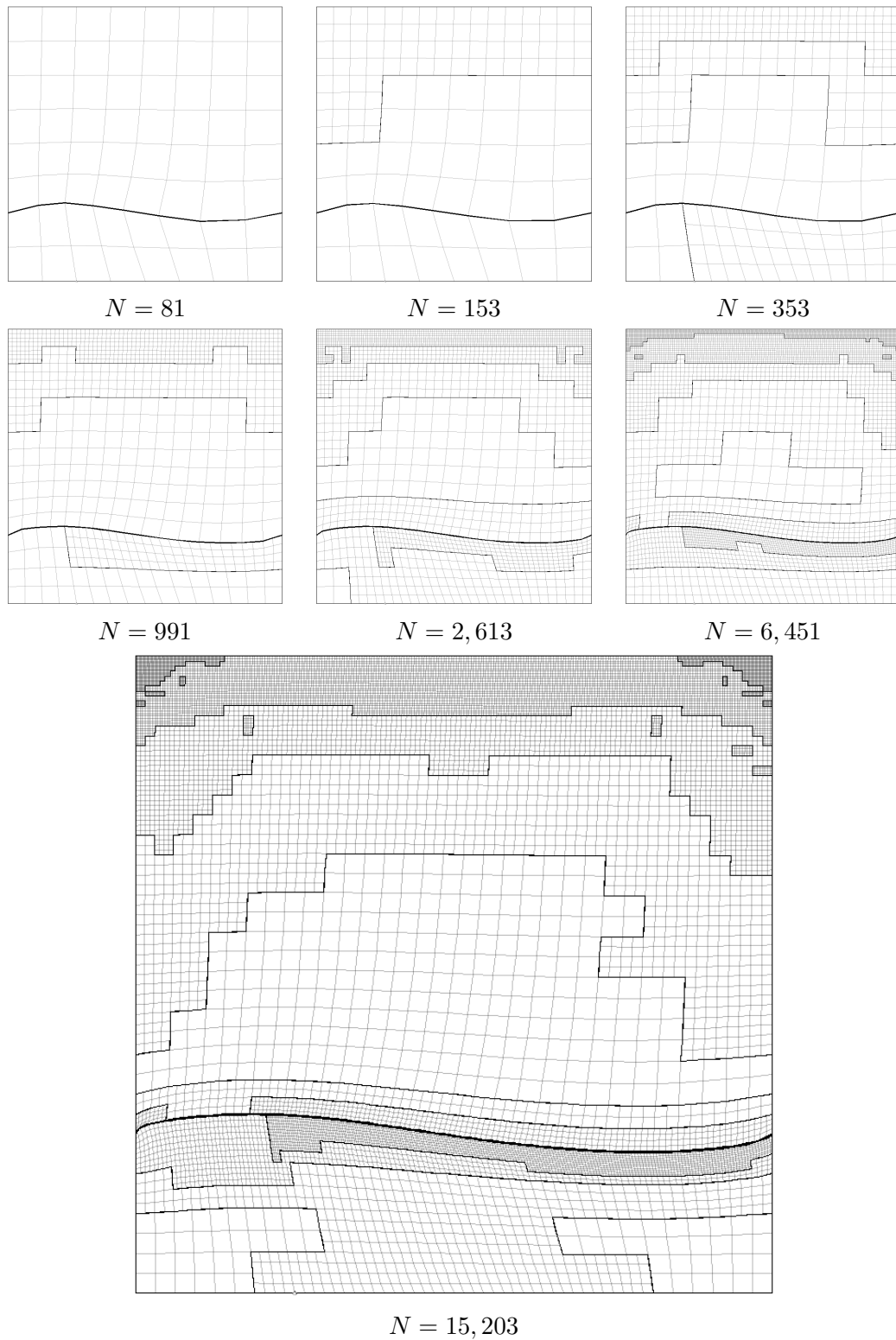
Figure 9.14: Adaptively refined meshes with the ALE approach, all meshes displayed in the deformed system.

$N = 81$ $N = 155$ $N = 349$

$N = 845$ $N = 2,293$ $N = 5,915$

$N = 15,069$
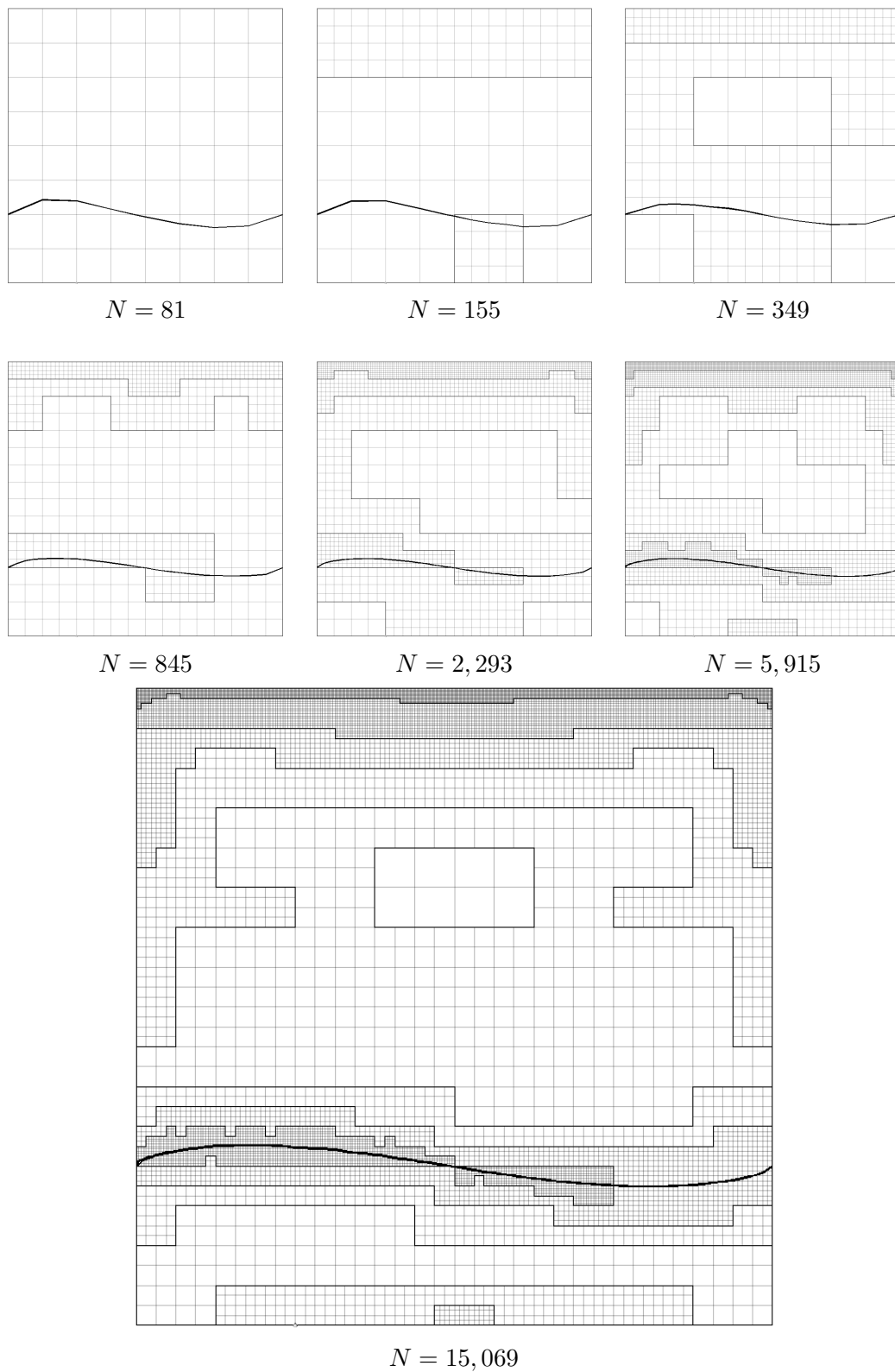
Figure 9.15: Adaptively refined meshes with the Eulerian approach.

Chapter 10

Numerical test: FSI benchmark FLUSTRUK-A

The final example is the FSI benchmark FLUSTRUK-A described in [TuHr06]. A thin elastic bar immersed in an incompressible fluid develops self-induced time-periodic oscillations of different amplitude depending on the material properties assumed. This benchmark has been defined to validate and compare the different computational approaches and software implementations for solving FSI problems. In order to have a fair comparison of our Eulerian-based method with the traditional arbitrary Eulerian-Lagrangian approach, we have also implemented an ALE method for this benchmark problem.

The configuration of this benchmark shown in Figure 10.1 is based on the successful CFD benchmark 'flow around a cylinder', [TurSchae96].
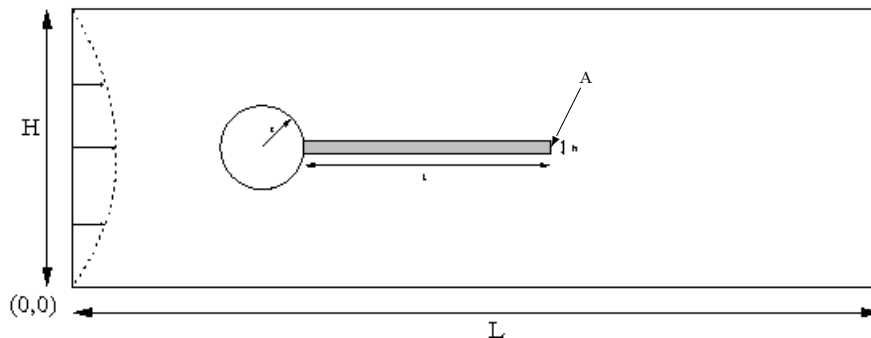
Figure 10.1: Configuration of the FSI benchmark 'FLUSTRUK-A'.

Configuration: The computational domain has length $L = 2.5$, height $H = 0.41$, and left bottom corner at $(0,0)$. The center of the circle is positioned at $C = (0.2, 0.2)$ with radius $r = 0.05$. The elastic bar has length $l = 0.35$ and height $h = 0.02$. Its right lower end is positioned at $(0.6, 0.19)$ and its left end is clamped to the circle. Control points are $A(t)$ fixed at the trailing edge of the structure with $A(0) = (0.6, 0.20)$, and $B = (0.15, 0.2)$ fixed at the cylinder (stagnation point).

Boundary and initial conditions: The boundary conditions are as follows: Along the upper and lower boundary the usual 'no-slip' condition is used for the velocity. At the (left) inlet

a constant parabolic inflow profile,

$$v(0, y) = 1.5\,\bar{U}\,\frac{4y(H - y)}{H^2},$$

is prescribed which drives the flow, and at the (right) outlet zero-stress $\sigma \cdot n = 0$ is realized by using the 'do-nothing' approach in the variational formulation, [HeRaTu92, Rannacher00]. This implicitly forces the pressure to have zero meanvalue at the outlet. The initial condition is zero flow velocity and structure displacement.

Material properties: The fluid is assumed as incompressible and Newtonian, the cylinder as fixed and rigid, and the structure as (compressible) St. Venant-Kirchhoff (STVK) type.

Discretization: The first set of computations is done on globally refined meshes for validating the proposed method and its software implementation. Then, for the same configuration adaptive meshes are used where the refinement criteria are either purely heuristic, i.e., based on the cell distance from the interface, or are based on a simplified stationary version of the DWR approach (at every tenth time step) as already used before for the cavity example. In all cases a uniform time-step size of $0.005\,s$ is used. The curved cylinder boundary is approximated to second order by polygonal mesh boundaries as can be seen in Figure 10.2.

The following four different test cases are considered:

- *Computational fluid dynamics test (CFD Test):* The structure is made very stiff, to the effect that we can compare the computed drag and lift coefficients with those obtained for a pure CFD test (with rigid structure).

- *Computational structure mechanics test (CSM Test):* The fluid is set to be initially in rest around the bar. The deformation of the bar under a vertical gravitational force is compared to the deformation of the same bar in a pure CSM test.

- *FSI tests:* Three configurations are treated corresponding to different inflow velocities and material stiffness parameters, and the Eulerian approach is compared to the standard ALE method.

- *FSI with large deflections:* The fluid is set to be initially in rest around the bar. The gravitational force on the bar is very large, causing a large deformation of the bar and eventually it reaching and running up against the channel wall. This case is difficult for the ALE method but can easily be handled by the Eulerian approach.

10.1 CFD test

Here, the structure is set to be very stiff, to the effect that we can compare derived drag and lift values with those obtained with a pure CFD approach. The forces are calculated based on the closed path S around the whole structure, cylinder and bar,

$$J(u, p) := \int_S \sigma_f n_f \, dx \, . \tag{10.1}$$

The CFD test has been done with the parameters listed in Table 10.1.

Table 10.1: Parameters for the CFD test.

Parameters	CFD test
$\rho_f [10^3 kg\, m^{-3}]$	1
$\nu_f [10^{-3} m^2 s^{-1}]$	1
ν_s	0.4
$\rho_s [10^6 kg\, m^{-3}]$	1
$\mu_s [10^{12} kg\, m^{-1} s^{-2}]$	1
$U [m\, s^{-1}]$	1

For the chosen parameters there is a steady state solution. The reference values for the drag and lift forces are calculated using a pure CFD approach on globally refined meshes (see also [TuHr06]). The results are shown in Table 10.2. Using the Eulerian FSI approach, we calculate the same forces again. As a method of mesh adaption we use a heuristic approach as described above.

Table 10.2: CFD test: Results of CFD computation on uniform meshes (left), and by the Eulerian FSI approach on heuristically adapted meshes (right).

N	dof	drag	lift
1278	3834	145.75	10.042
4892	14676	133.91	10.239
19128	57384	136.00	10.373
75632	226896	136.54	10.366
300768	902304	136.67	10.369
∞	∞	136.70	10.530

N	dof	drag	lift
1300	9100	122.66	12.68
2334	16338	126.13	11.71
9204	64428	131.77	10.53
36680	256760	134.47	10.45
∞	∞	136.70	10.530

10.2 CSM test

Here, the inflow velocity is set to zero and the fluid is initially at rest. A vertical gravitational force is applied, which causes the bar to slowly sink in the fluid filled volume. Due to the viscous effect of the fluid the bar will eventually come to rest. The value of final displacement can be compared to the results calculated with a pure CSM approach in a Lagrangian framework. The quantity of interest is the displacement of the point A at the middle of the trailing tip. The corresponding reference values are taken from [TuHr06]. The CSM test has been done with the parameters listed in Table 10.3. Using the Eulerian FSI approach, we calculate the displacements with mesh adaption by the heuristic approach described above. The final stationary positions and the heuristically adapted meshes can be seen in Figure 10.2.

Table 10.3: Parameters for the CSM test.

parameter	CSM test
$\rho_f[10^3 kg\, m^{-3}]$	1
$\nu_f[10^{-3}m^2 s^{-1}]$	1
ν_s	0.4
$\rho_s[10^3 kg\, m^{-3}]$	1
$\mu_s[10^6 kg\, m^{-1}s^{-2}]$	0.5
$\bar{U}[m\, s^{-1}]$	0
$g[m\, s^{-2}]$	2
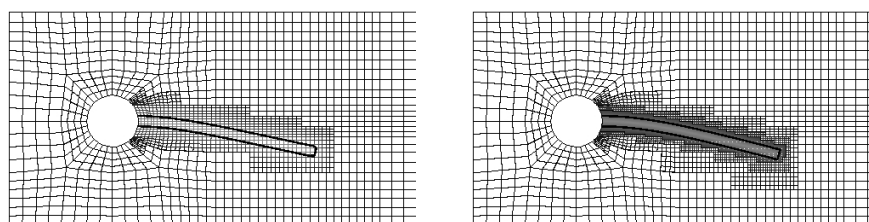
Figure 10.2: CSM test: Stationary position of the control point A on heuristically refined meshes with $N = 1952$ and $N = 7604$ cells.

Table 10.4: CSM test: Displacement of the control point A for three levels of heuristic mesh adaption.

N	dof	$u_x(A)\ [10^{-3}m]$	$u_y(A)\ [10^{-3}m]$
1952	13664	-5.57	-59.3
3672	25704	-6.53	-63.4
7604	53228	-6.74	-64.6
∞	∞	-7.187	-66.10

Next, we apply the DWR method as described in Chapter 7 to the CSM test case. For the dual problem, we construct the Jacobi matrix of the model as explained in Section 6.7.1. In the first example the DWR method was always applied to the final stationary state. The results were used for mesh adaption. The generated mesh was then used with the initially unperturbed problem to determine a new final stationary state. In contrast to that approach, we now apply the DWR method at periodic intervals without restarting. To control the resulting mesh adaption at each interval we try to keep the number of nodes N below a certain threshold N_t. This is achieved by reducing refinement and/or increasing coarsening at each interval. As an example we calculate the point-value of the component sum of $u(A)$ at the control point A. The position x_A is determined from $x_A - u(x_A) = A(0) = (0.6, 0.2)^T$.

As a error control functional, we use a regularized delta function at x_A applied to $(e_1+e_2)^T u$,

$$J(u) = |K_A|^{-1} \int_{K_A} (e_1 + e_2)^T u(x) \, dx \ ,$$

where K_A is the cell in the Mesh $\mathbb{T}_h$ containing the point A.
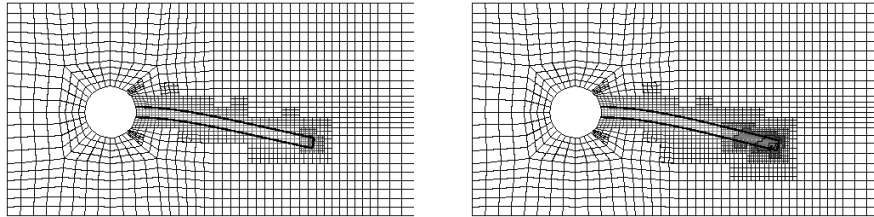
Figure 10.3: CSM Test: Stationary position of the bar computed on locally refined meshes (DWR method) with $N = 2016$ and $N = 4368$ cells.

Table 10.5: CSM Test: Displacements of the control point A for three levels of locally refined meshes (DWR method).

N_t	N	dof	$u_x(A) \ [10^{-3}m]$	$u_y(A) \ [10^{-3}m]$
2000	2016	14112	-5.73	-59.8
3000	2614	18298	-6.54	-63.2
4500	4368	30576	-6.88	-64.6
	∞	∞	-7.187	-66.10

10.3 FSI tests

Three test cases, FSI-2, FSI-3, and FSI-3*, are treated with different inflow velocities and material stiffness values as stated in Table 10.6. The parameters are chosen such that a visible transient behavior of the bar can be seen. To ensure a 'fair' comparison of results, we calculate the comparison values using the ALE method. Using the Eulerian FSI approach, we calculate the displacements on three mesh levels, where the heuristic approach as described above is used for mesh refinement.

Table 10.6: Parameter settings for the FSI test cases.

parameter	FSI-2	FSI-2*	FSI-3	FSI-3*
structure model	STVK	STVK	STVK	INH
$\rho_f [10^3 kg\,m^{-3}]$	1	1	1	1
$\nu_f [10^{-3} m^2 s^{-1}]$	1	1	1	1
ν_s	0.4	0.4	0.4	0.5
$\rho_s [10^3 kg\,m^{-3}]$	10	20	1	1
$\mu_s [10^6 kg\,m^{-1}s^{-2}]$	0.5	0.5	2	2
$U [m\,s^{-1}]$	1	0	2	2

We begin with the FSI-2 and FSI-3 test cases. Some snapshots of the resulting deformations of these simulations are shown in Figures 10.4 and 10.12. The time-dependent behavior of the displacements for the tests are shown in Figures 10.5 and 10.13.
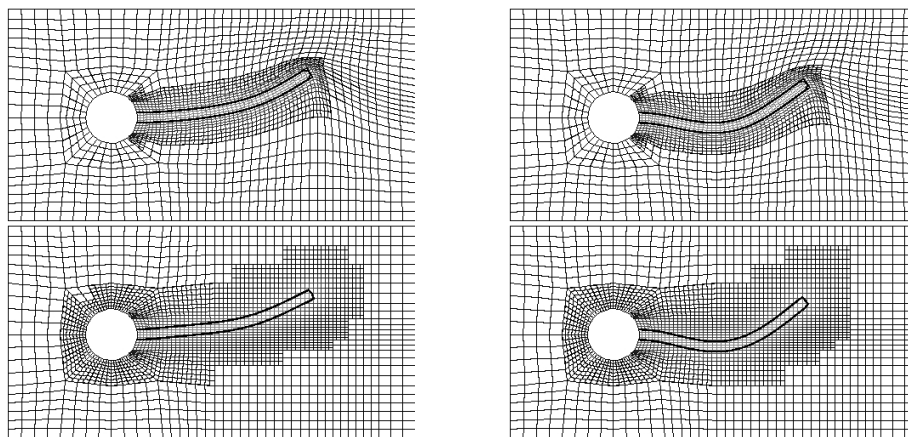
Figure 10.4: FSI-2: Snapshots of results obtained by the ALE (top two, displayed in the deformed system) and by the Eulerian (bottom two) approaches.
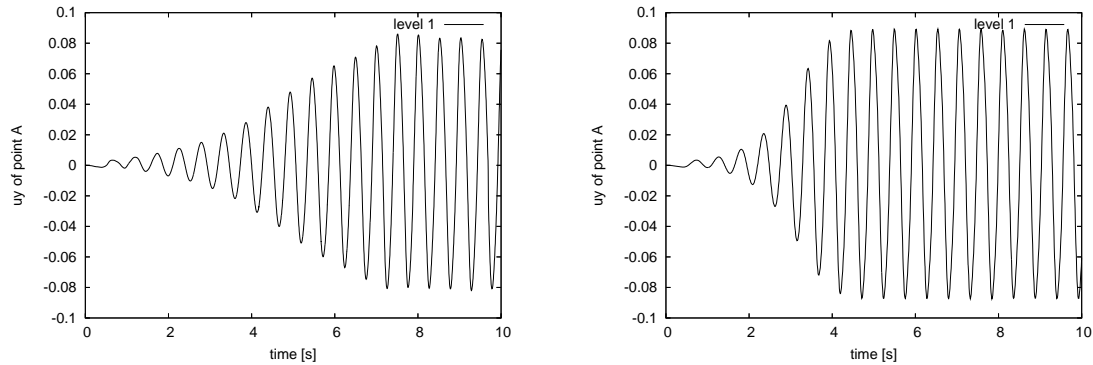
Figure 10.5: FSI-2: Vertical displacement of the control point A, obtained by the Eulerian approach (left, $N = 2082$ cells) with maximum amplitude $2.226 \cdot 10^{-2}$ and frequency $1.92\,s^{-1}$, and by the ALE approach (right, $N = 2784$ cells) with maximum amplitude $2.68 \cdot 10^{-2}$ and frequency $1.953\,s^{-1}$.

Figure 10.5 shows that both the Eulerian and ALE frameworks reach similar states of periodic regular behavior after an initial starting phase. The Eulerian framework needs approximately $0.12s$ longer then the ALE framework to reach this periodic state. Once reached both frameworks display similar periodic movement as shown in the Figures 10.6-10.11.
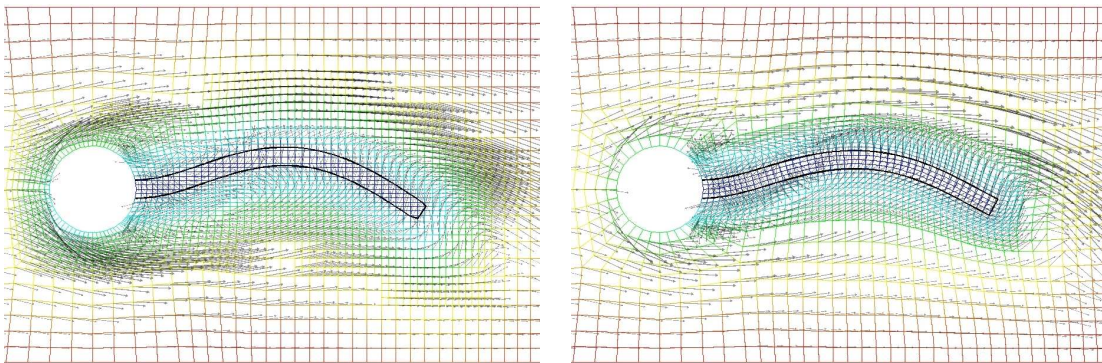
Figure 10.6: FSI-2: Snapshots of Eulerian (left, t=7.8800s) and ALE (ALE, t=8.0000s) results.
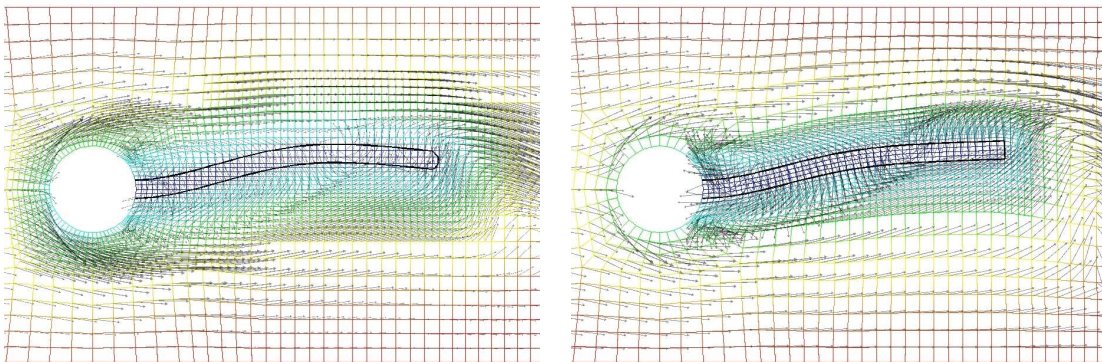
Figure 10.7: FSI-2: Snapshots of Eulerian (left, t=7.9406s) and ALE (ALE, t=8.0600s) results.
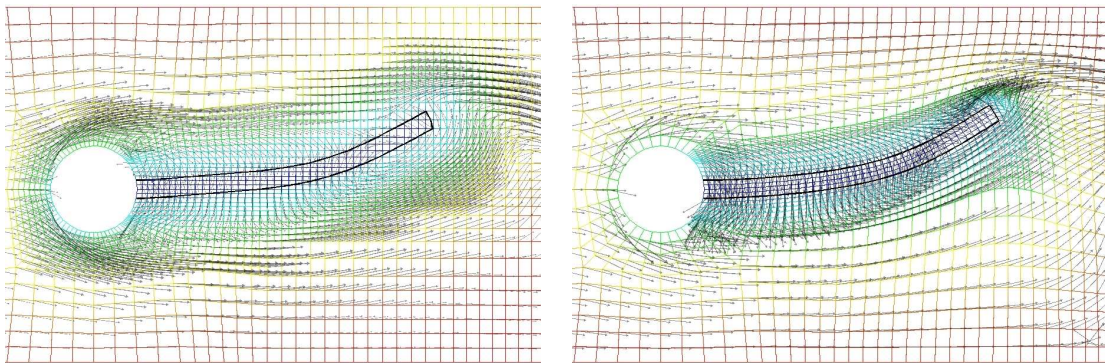
Figure 10.8: FSI-2: Snapshots of Eulerian (left, t=8.0000s) and ALE (ALE, t=8.1200s) results.
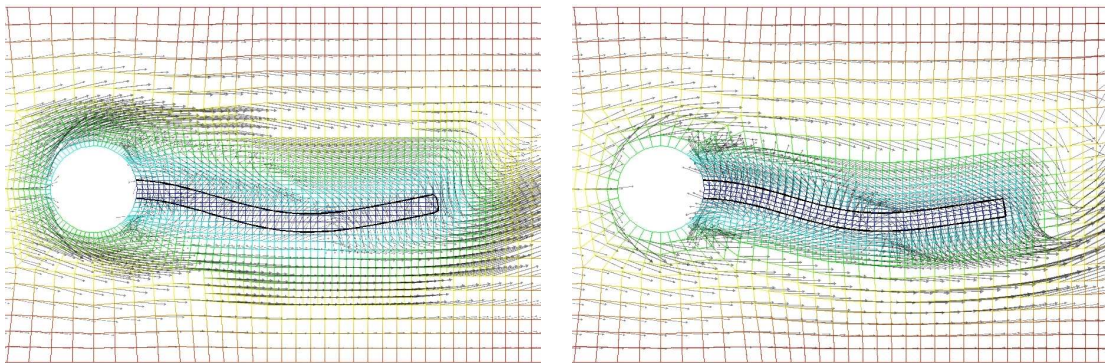
Figure 10.9: FSI-2: Snapshots of Eulerian (left, t=8.1800s) and ALE (ALE, t=8.3000s) results.
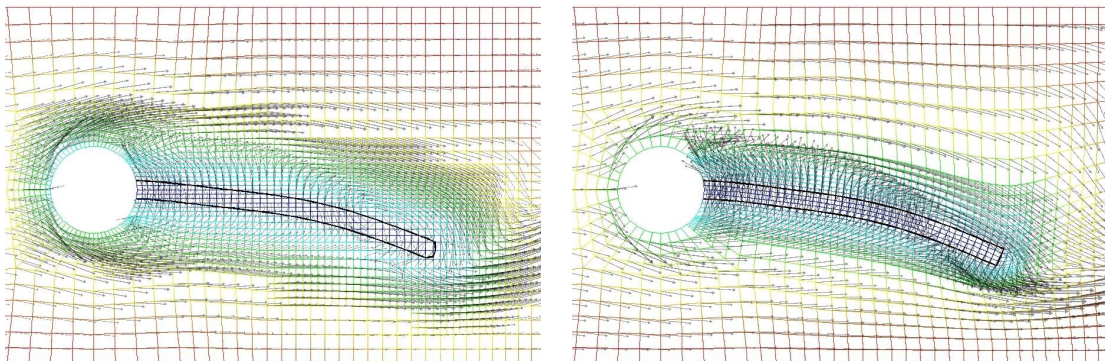
Figure 10.10: FSI-2: Snapshots of Eulerian (left, t=8.2400s) and ALE (ALE, t=8.3600s) results.
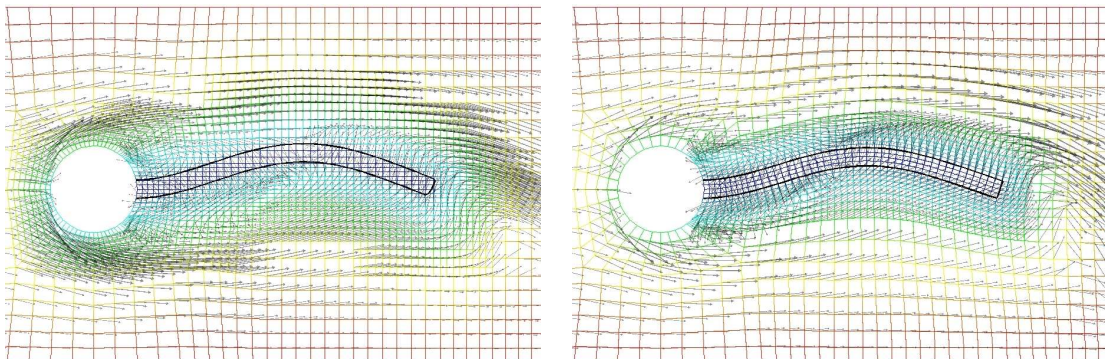
Figure 10.11: FSI-2: Snapshots of Eulerian (left, t=8.4200s) and ALE (ALE, t=8.5400s) results.
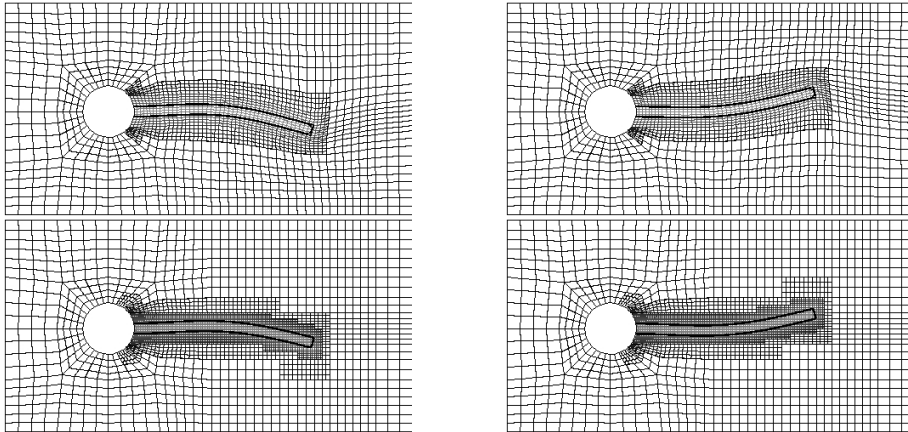
Figure 10.12: FSI-3 Test: Some snapshots of results obtained by the ALE (top two) and the Eulerian (bottom two) approaches.
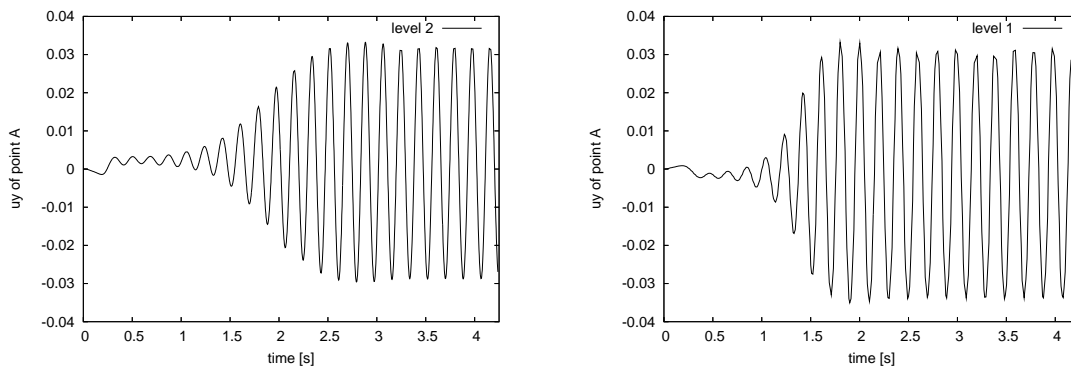
Figure 10.13: FSI-3 Test: Vertical Displacement of the control point A, obtained by the Eulerian approach (left, $N = 3876$ cells) with maximum amplitude $6.01 \cdot 10^{-2}$ and frequency $5.48\,s^{-1}$, and by the ALE approach (right, $N = 2082$ cells) with maximum amplitude $6.37 \cdot 10^{-2}$ and frequency $5.04\,s^{-1}$.

The FSI-3* test case is used to illustrate some special features of the Eulerian solution approach. Figure 10.14 illustrates the treatment of corners in the structure by the IP set approach compared to the LS approach. In the LS method the interface is identified by all points for which $\phi = 0$, while in the IP set method the interface is identified by all points which are on one of the respective isoline segments belonging to the edges of the bar. The differences are visible in the cells that contain the corners.
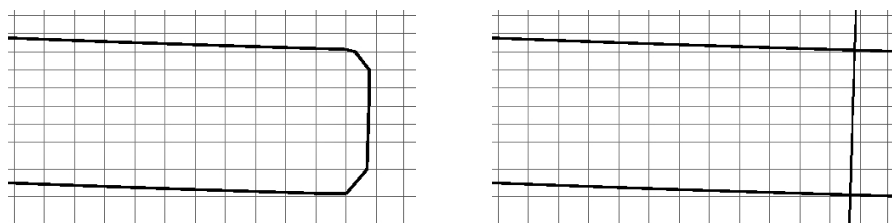
Figure 10.14: FSI-3*: Treatment of corners by the LS method (left) and by the IP set method (right).

Since in the Eulerian approach the structure deformations are not in a Lagrangian framework, it is not immediately clear, due to the coupling with the fluid, how well the mass of the structure is conserved in an Eulerian approach, especially in the course of an instationary simulation comprising hundreds of time steps. In Figure 10.15, we display the bar's relative mass error as a function of time. Except for certain initial jitters, the relative error is less than 1%.
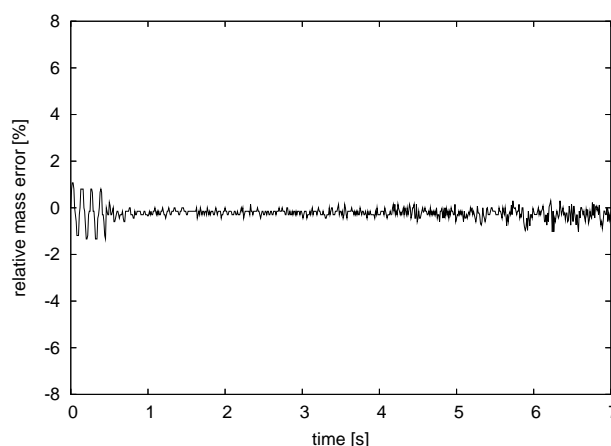
Figure 10.15: FSI-3*: Relative mass error of the bar.

Finally, Figure 10.16 illustrates the time dynamics of the structure and the adapted meshes over the time interval $[0, T]$. More detailed properties of this dynamics is shown in Figure 10.16. For both approaches, we obtain a periodic oscillation. For the Eulerian approach we obtain an amplitude of 1.6e-2 with an oscillation frequency of $6.86s^{-1}$. In comparison to that, based on the ALE approach, we obtain an amplitude of 1.51e-2 with an oscillation frequency of $6.70s^{-1}$.
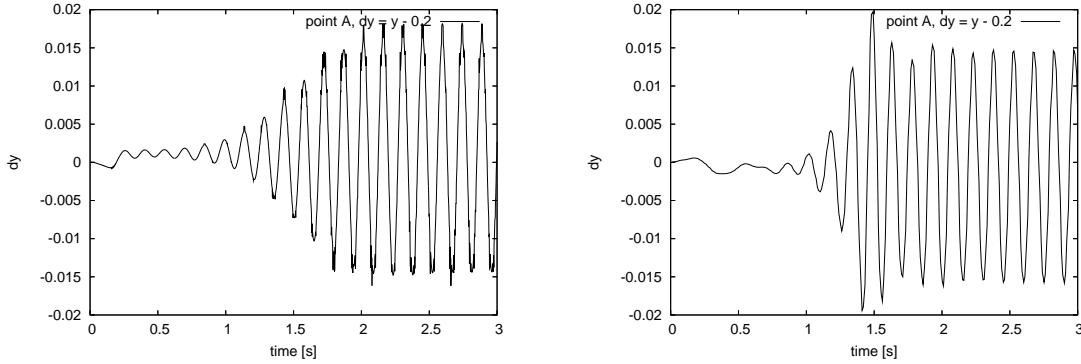
Figure 10.16: FSI-3*: Vertical displacement of the control point A, obtained by the Eulerian approach (left) with maximum amplitude $1.6 \cdot 10^{-2}$ and frequency $6.86\,s^{-1}$, and by the ALE approach (right) with maximum amplitude $1.51 \cdot 10^{-2}$ and frequency $6.70\,s^{-1}$.

10.4 FSI test with large deformations

In the test case FSI-2* (see Table 10.6) the fluid is initially in rest and the bar is subjected to a vertical force. This causes the bar to bend downward until it touches the bottom wall. A sequence of snapshots of the transition to steady state obtained by the Eulerian approach for this problem is shown in the Figures 10.18 and 10.19.

The simulation was done for three refinement strategies. For two simulations the heuristic zonal refinement strategy was used, for the first simulation only refining zonally twice around the interface and in the second simulation refining four times, Figure 10.18.

In the third simulation we used the DWR method to adaptively refine (and coarsen) the mesh at periodic intervals of the quasi-steady states within the time stepping process, Figure 10.19. The goal-functional in this case is as in the CSM cases:

$$J(u) = |K_A|^{-1} \int_{K_A} (e_1 + e_2)^T u(x)\, dx \ .$$

The position of the trailing-tip control point A for all three cases is show in Figure 10.17. The resulting vertical position of the trailing-tip control point A is in all three cases in good agreement. The advantage of adaptive refinement becomes very clear in this example, since the first two zonal refinement strategies need respectively 8 and 30 CPU-hours, whereas the adaptive strategy only requires 4 CPU-hours.
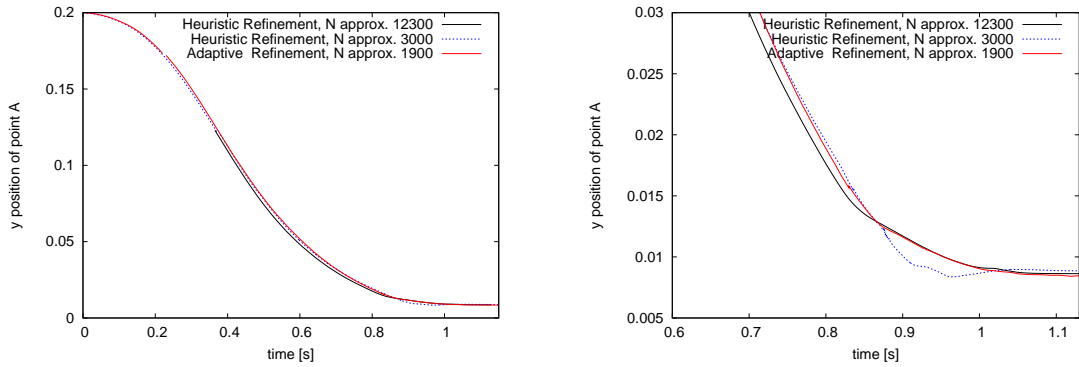
Figure 10.17: FSI-2*: y-Position of the trailing-tip control point A during the deformation of the bar.
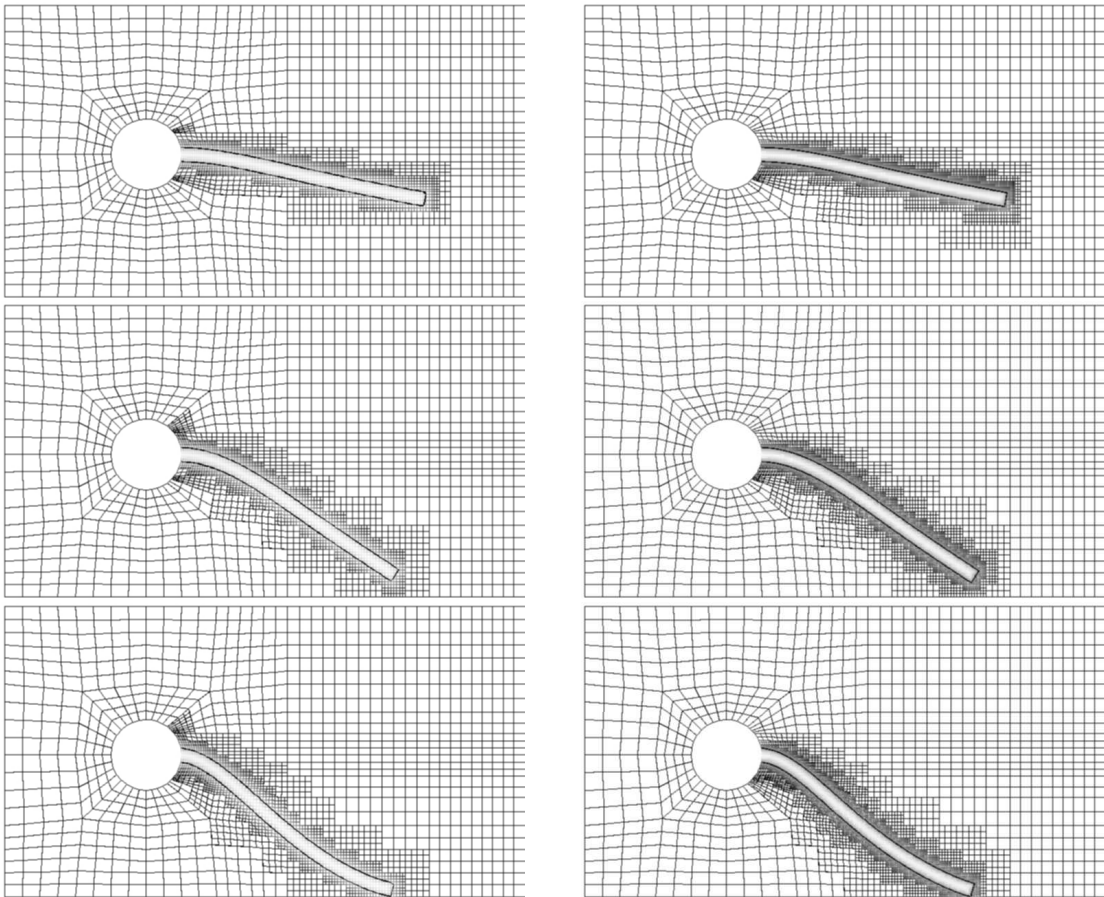

Figure 10.18: A sequence of snap-shots of the bar's large deformation under gravitational loading obtained by the Eulerian approach. Simulation with two heuristic refinements ($N \approx 3{,}000$, 8 CPU-hours) around the interface is shown in the left column. In the right column some snapshots can be seen in a simulation done based on four heuristic refinements ($N \approx 12{,}300$, 30 CPU-hours) .
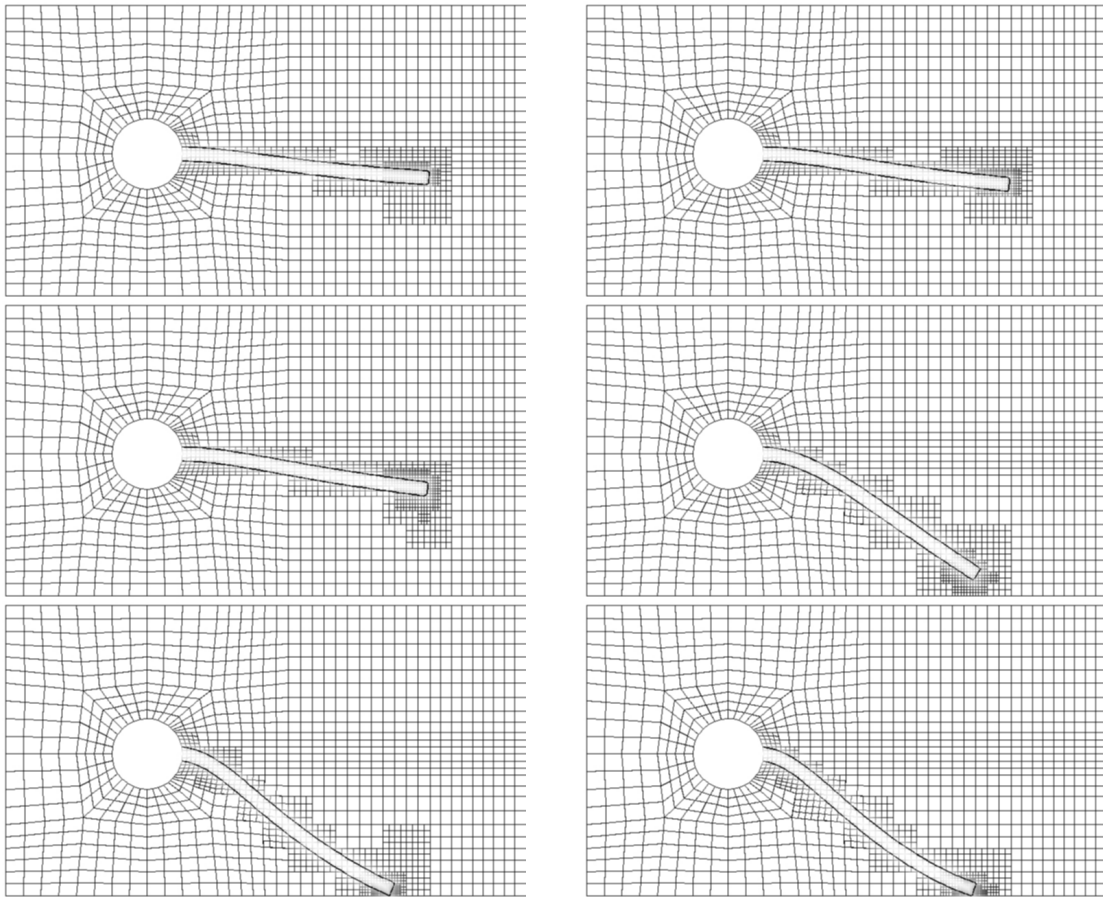
Figure 10.19: A sequence of snap-shots of the bar's large deformation under gravitational loading obtained by the Eulerian approach. Simulation with adaptive refinement ($N \approx 1{,}900$, 4 CPU-hours) around the interface is shown, left to right, top to bottom.

Chapter 11

Summary and future development

In this thesis we presented a fully Eulerian variational formulation for 'fluid-structure in-teraction' (FSI) problems. This approach uses the 'Initial Position' set (IP set) method for interface capturing, which is similar to the 'Level Set' (LS) method, but preserves sharp corners of the structure. The harmonic continuation of the structure velocity avoids the need of reinitialization of the IP set. This approach allows us to treat FSI problems with free bodies and large deformations. This is the main advantage of this method compared to interface tracking methods such as the 'arbitrary Lagrangian-Eulerian' (ALE) method. At several examples the Eulerian approach turns out to yield results, which are in good agree-ment with those we obtained by the ALE approach. In order to have a 'fair' comparison both methods have been implemented using the same numerical components and software library Gascoigne [Ga]. The method based on the Eulerian approach is inherently more expensive than the ALE method, by about a factor of two, but it allows to treat also large deformations and topology changes.

The full variational formulation of the FSI problem provides the basis for the application of the 'dual weighted residual' (DWR) method for 'goal-oriented' a posteriori error estimation and mesh adaptation. In this method inherent sensitivities of the FSI problem are utilized by solving linear 'dual' problems, similar as in the Euler-Lagrange approach to solving optimal control problems. The feasibility of the DWR method for FSI problems for both the Eulerian as well as the ALE framework has, in a first step, been demonstrated for the computation of steady state solutions. For nonstationary problems it was used in a heuristical manner for goal-oriented mesh adaption of the quasi-steady states within the time stepping process.

Based on the thusfar reached goals we consider the following next steps as promising future developments:

(1) *Application of the DWR method for nonstationary FSI problems:*
    Here the DWR method can be used for the simultaneous adaptation of spatial mesh and time step size. A promising additional development in this field is the 'check-pointing' method, which alleviates the necessity of saving all primal solutions for the whole time interval. This is achieved by only saving the primal solutions at designated 'check-points', and using these as starting points for later recalculations. This approach in combination with the DWR method has been implemented successfully in [BeMe+05].

(2) *Application of the developed methods for 3d cases:*
Specifically for a simple stationary model, e.g. the lid-driven cavity, as a way of demonstrating the applicability of the fully Eulerian approach for 3d FSI problems. The developed methods (the fully Eulerian framework, the IP-set method, the DWR method for a posteriori error estimation and goal-oriented mesh adaptation) are principally also applicable in 3d.

(3) *Application to FSI problems with large deformations and topology changes:*
When using an ALE framework, large deformations are known to lead to a breakdown of the solver. A well-known approach to circumventing this is either a 'remeshing' of the problem or a 'fixed grid' approach. In the 'fixed grid' approach a combination of overlapping domain decomposition and chimera-like formulations are used, [WaGe+06]. These approaches though entail an additional amount of data management, that would otherwise not occur. For the Eulerian framework this is not the case, since the deformation data is stored in the spatial Eulerian reference frame and thus no deformation of the fluid domain onto an arbitrary reference domain is needed.

(4) *Application to optimal control problems:*
In a first step one could consider stationary configurations. The goal of the optimization would be the minimization or stabilization of certain values, e.g. the drag or the suppression of vibrations of elastic structures. For the case of minimization this is achieved by solving the appropriate Karush-Kuhn-Tucker (KKT) system, thus the necessary effort is essentially identical to that of the DWR method. This has been demonstrated in [BeKa+00, BeRa03, BeBr+05].

11.1 Acknowledgements

Bibliography

[AGJT04] G. Allaire, F. de Gournay, F. Jouve, A. Toader, *Structural optimization using topological and shape sensitivity via a level set method*, Control and Cyb.,34 (2004), 59-80.

[BaOsPi80] Babushška, I. , Osborn, J., Pitkä ranta, J., *Analysis of mixed methods using mesh dependent norms.*, Math. Comp. 35, 1039-1062, 1980.

[BaRa03] W. Bangerth and R. Rannacher, *Adaptive Finite Element Methods for Differential Equations*, Birkhäuser, 2003.

[BeBr00] R. Becker and M. Braack, Multigrid techniques for finite elements om locally refined meshes. *Numerical Linear Algebra with Applications (Special Issue)*, 7:363-379, 2000.

[BeBr01] R. Becker and M. Braack, A finite element pressure gradient stabilization for the Stokes equations based on local projections, *Calcolo* 38, 173-199 (2001).

[BeBr03] R. Becker and M. Braack, A two-level stabilization scheme for the Navier-Stokes equations, *Proc. ENUMATH-03*, pp. 123-130, Springer, 2003.

[BeBr+05] R. Becker, M. Braack, D. Meidner, R. Rannacher und B. Vexler, *Adaptive finite element methods for PDE-constrained optimal control problems*, Abschlußbad SFB 359 "Reactive Flows, Diffusion and Transport" (R. Rannacher et al., eds), erscheint beim Springer-Verlag, Berlin-Heidelberg, 2006.

[BeKa+00] R. Becker, H. Kapp, and R. Rannacher *Adaptive finite element methods for optimal control of partial differential equations: basic concepts*, SIAM J. Optimization Control 39, 113-132 (2000).

[BeDu06] R. Becker, Th. Dunne, *VisuSimple: An interactive open source visualization utility for scientific computing*, in "Reactive Flows, Diffusion and Transport: From Experiments via Mathematical Modeling to Numerical Simulation and Optimization, Final Report of SFB (Collaborative Research Center) 359" Jäger, Willi; Rannacher, Rolf; Warnatz, Jürgen (Eds.) Springer; (October 31, 2006) 676 p., ISBN-10: 3-540-28379-X ISBN-13: 978-3-540-28379-9 . See [Vi].

[BeMe+05] R. Becker, D. Meidner, and B. Vexler: *Efficient numerical solution of parabolic optimization problems by finite element methods*, submitted to Optim. Meth. Software, 2005.

[BeRa95] R. Becker and R. Rannacher, Weighted a-posteriori error estimates in FE methods, Lecture ENUMATH-95, Paris, Sept. 18-22, 1995, in: *Proc. ENUMATH-97*, (H.G. Bock, et al., eds), pp. 621-637, World Scientific Publ., Singapore, 1998.

[BeRa01] R. Becker and R. Rannacher, An optimal control approach to error estimation and mesh adaption in finite element methods, *Acta Numerica 2000* (A. Iserles, ed.), pp. 1-101, Cambridge University Press, 2001.

[BeRa96] R. Becker and R. Rannacher, A feed-back approach to error control in finite element methods: basic analysis and examples, *East-West J. Numer. Math.* 4, 237-264 (1996).

[BeRa03] R. Becker and R. Rannacher, *Error control for model reduction by discretization in optimal control of flows*, in Topics in Mathematical Fluid Mechanics (G.P. Galdi, R. Rannacher, eds), pp. 34-39, Quaderni di Matematica 10, 2003.

[BiCa+92] C. Bischof, A. Carle, G. Corliss, A. Griewank, and P. Hovland, *ADIFOR: Generating derivative codes from Fortran programs*, Scientific Programming, 1, pp. 1-29, 1992

[BrRi05] M. Braack and T. Richter, Solutions of 3d Navier-Stokes benchmark problems with adaptive finite elements. *Computers & Fluids (submitted)*, 2005.

[Br97] D. Braess, *Finite elements*, Cambridge University Press, Cambridge, United Kingdom, 1997.

[BrBu+06] M. Brenk, H.-J. Bungartz, M. Mehl, T. Neckel, *Fluid-Structure Interaction on Cartesian Grids: Flow Simulation and Coupling Environment* p. 233-269, in H.-J. Bungartz, M. Schäfer (Eds.) *Fluid-Structure Interaction Modelling, Simulation, Optimization*, Springer Verlag, (2006). [BuSc+06]

[BrSc94] S.C. Brenner and L.R. Scott, *The mathematical theory of finite element methods*, Springer, New York, 1994.

[BrGl+87] M. O. Bristeau, R. Glowinski, and J. Periaux, Numerical methods for the Navier-Stokes equations, *Comput. Phys. Rep.* 6, 73-187 (1987).

[BuSc+06] H.-J. Bungartz, M. Schäfer (Eds.), *Fluid-Structure Interaction Modelling, Simulation, Optimization*, Springer Series: Lecture Notes in Computational Science and Engineering, Vol. 53 2006, VIII, 394 p., 251 illus., Softcover ISBN-10: 3-540-34595-7, ISBN-13: 978-3-540-34595-4

[CaOd84] G. Carey and J. Oden, *Finite Elements, Computational Aspects*, volume III. Prentice-Hall, 1984.

[Ci78] Ciarlet, *The Finite Element Method for Elliptic Problems.*, 530 pp., North-Holland, Amsterdam , 1978.

[ChHoMeOs] Y. C. Chang, T. Y. Hou, B. Merriman, and S. Osher, A level set formulation of Eulerian interface capturing methods for incompressible fluid flows, *J. Comp. Phys.* 123, 449-464 (1996).

[De99] B. Desjardins, *On weak solutions of the compressible isentropic Navier-Stokes equations.* Applied Math. Letters, Vol 12, (7), (1999), p. 107-111.

[DeEs99] B. Desjardins, M.J. Esteban, *Existence of weak solutions for the motion of rigid bodies in a viscous fluid,* Arch. in Rat. Mech. Anal., 146 (1999) p. 59-71.

[DeEs00] B. Desjardins, M.J. Esteban, *On weak solutions for fluid-rigid structure interaction: compressible and incompressible models,* Comm. P.D.E. 25(7-8) (2000), p. 1399-1413.

[DeEs+01] B. Desjardins, M.J. Esteban, C. Grandmont, and P. Le Tallec, Weak solutions for a fluid-elastic structure interaction model., Rev. Mat. Complut., 14 (2001), pp. 523 538.

[DuRa06] Th. Dunne., R. Rannacher, *Adaptive finite element simulation of fluid structure interaction based on an Eulerian variational formulation*, p. 371-386, in H.-J. Bungartz, M. Schäfer (Eds.) *Fluid-Structure Interaction Modelling, Simulation, Optimization*, Springer Verlag, (2006). [BuSc+06]

[Du06a] Th. Dunne *An Eulerian approach to fluid-structure interaction and goal-oriented mesh refinement*, Proc. "Finite Elements for Flow Problems (FEF05)", IACM Special Interest Conference supported by ECCOMAS, April 4-6, 2005, Swansea, Wales, UK, appeared in Int. J. Numer. Meth. Fluids 2006; 51: 1017-1039.

[Du06b] Th. Dunne *Adaptive Finite Element Approximation of Fluid-Structure Interaction Based on an Eulerian Variational Formulation*, Proc. "European Conference on Computational Fluid Dynamics (ECCOMAS CFD 2006)", September 5-8, 2006, Egmond aan Zee, The Netherlands.

[GiRa86] V. Girault and P.A. Raviart, *Finite element for Navier-Stokes equations*, Springer, Berlin, 1986.

[Gl03] R. Glowinski, Finite element methods for incompressible viscous flow, in *Handbook of Numerical Analysis Volume IX: Numerical Methods for Fluids (Part 3)* (P.G. Ciarlet and J.L. Lions, eds), North-Holland, Amsterdam, 2003.

[Gr89] A. Griewank, On Automatic Differentiation in *Mathematical Programming: Recent Developments and Applications* (M. Iri, K. Tanabe, eds), Kluwer Academic Publishers, pp. 83-108, 1989.

[ErEs+95] K. Eriksson, D. Estep, P. Hansbo, and C. Johnson, Introduction to adaptive methods for differential equations. *Acta Numerica 1995* (A. Iserles, ed.), pp. 105–158, Cambridge University Press, 1995.

[HeRaTu92] J. Heywood, R. Rannacher, and S. Turek, *Artificial boundaries and flux and pressure conditions for the incompressible Navier-Stokes equations*, Int. J. Numer. Math. Fluids 22, 325–352 (1992).

[Hi85] K.E. Hillstrom, *Users Guide for JAKEF*, Technical Memorandum ANL/MCSTM-16, Mathematical and Computer Science Division, Argonne NAtional Laboratory, Argonne IL 60439, 1985.

[HiNi81] C. W. Hirt and B. D. Nichols, Volume of Fluid (VOF) method for the dynamics of free boundaries. *Journal of Computational Physics* 39, 201-225 (1981).

[HoWo+88] J.E. Horwedel, B.A. Worley, E.M. Oblow, and F.G. Pin, *GRESS Version 0.0 Users Manual*, ORNL/TM 10835, Oak Ridge National Laboratory, Oak Ridge, Tennessee 47840, 1988.

[HronTurek206] J. Hron, S. Turek, *A Monolithic FEM/Multigrid Solver for an ALE Formulation of Fluid-Structure Interaction with Applications in Biomechanics*, p. 146-170, in H.-J. Bungartz, M. Schäfer (Eds.) *Fluid-Structure Interaction Modelling, Simulation, Optimization*, Springer Verlag, (2006). [BuSc+06]

[HuertaLiu] A. Huerta and W. K. Liu, Viscous flow with large free-surface motion, *Computer Methods in Applied Mechanics and Engineering*, 1988.

[HuLi+81] T.J.R. Hughes, W.K. Liu, and T.K. Zimmermann, *Lagrangian-Eulerian finite element formulations for incompressible viscous flows*, Computer Methods in Applied Mechanics and Engineering, 29 (1981) 329-349.

[Ga] GASCOIGNE, A C++ numerics library for scientific computing, `http://gascoigne.uni-hd.de/` .

[GeTo+06] S. Geller, J. Tölke, M. Krafczyk, *Lattice-Boltzmann Method on Quadtree-Type Grids for Fluid-Structure Interaction* p. 270-293, in H.-J. Bungartz, M. Schäfer (Eds.) *Fluid-Structure Interaction Modelling, Simulation, Optimization*, Springer Verlag, (2006). [BuSc+06]

[Iri84] M. Iri, *Simultaneous Computations of Functions, Partial Derivatives and Estimates of Rounding Errors - Complexity and Practicality*, Japan Journal of Applied Mathematics, Vol. 1, No. 2 pp. 223-252, 1984.

[IrKu87] M. Iri and K. Kubota, *Methods of Fast Automatic Differentiation and Applications*, Research memorandum RMI 87-0, Department of Mathematical Engineering and Instrumentation Physics, Faculty of Engineering, University of Tokyo, 1987.

[JoRe93a] D. D. Joseph and Y. Y. Renardy, *Fundamentals of two-fluid dynamics. Part I*, Springer, New York, 1993. Math. Theory and Applications.

[JoRe93b] D. D. Joseph and Y. Y. Renardy, *Fundamentals of two-fluid dynamics. Part II*, Springer, New York, 1993.

[LeChBe04] A. Legay, J. Chessa, and T. Belytschko, An Eulerian-Lagrangian method for fluid-structure interaction based on level sets, *Comp. Meth. in Applied Mech. and Engrg.*, accepted, 2004.

[LeMa00] P. Le Tallec, S. Mani, *Numerical Analysis of a Linearised Fluid Structure Interaction Problem.*, Numerische Mathematik, 87, pp 317-354, 2000.

[LoCe+06] R. Löhner, J.R. Cebral, C. Yang, J.D. Baum, E.L. Mestreau and O. Soto, *Extending the Range and Applicability of the Loose Coupling Approach for FSI Simulations*, p. 82-100, in H.-J. Bungartz, M. Schäfer (Eds.) *Fluid-Structure Interaction Modelling, Simulation, Optimization*, Springer Verlag, (2006). [BuSc+06]

[LuWa01] C. Liu and N. J. Walkington, An Eulerian description of fluids containing visco-elastic particles, *Arch. Rat. Mech. Anal.* 159, 229–252 (2001).

[MoKh+06] M. Moatamedi, M. Uzair Khan, T. Zeguer, M hamed Souli, *A New Fluid Structure Coupling Method for Airbag OOP*, p. 101-109, in H.-J. Bungartz, M. Schäfer (Eds.) *Fluid-Structure Interaction Modelling, Simulation, Optimization*, Springer Verlag, (2006). [BuSc+06]

[MU94] S. Müller-Urbaniak, *Eine Analyse des Zweischritt-θ-Verfahrens zur Lösung der instationären Navier-Stokes-Gleichungen*, Preprint 94-01, University of Heidelberg, IWR, SFB 359, Januar 1994.

[OsherSethian] S. Osher and J. A. Sethian, Propagation of fronts with curvature based speed: algorithms based on Hamilton-Jacobi formulations, *Journal of Computational Physics* 79, 12 (1988).

[Pironneau84] O. Pironneau, *Optimal shape design for elliptic systems*, Springre-Verlag, New York, 1984.

[Rall81] L.B. Rall, *Automatic Differentiation - Techniques and Applications*, Springer Lecture Notes in Computer Science, Vol. 120, 1981.

[Rannacher00] R. Rannacher, Finite element methods for the incompressible Navier-Stokes equations, in *Fundamental Directions in Mathematical Fluid Mechanics* (G. P. Galdi, J. Heywood, R. Rannacher, eds), pp. 191–293, Birkhäuser, Basel-Boston-Berlin, 2000.

[Rannacher04] R. Rannacher, Incompressible Viscous Flow, in *Encyclopedia of Computational Mechanics* (E. Stein, et al., eds), John Wiley, Chichester, 2004.

[RaSu02] R. Rannacher and F.-T. Suttmeier Error estimation and adaptive mesh design for FE models in elasto-plasticity, in *Error-Controlled Adaptive FEMs in Solid Mechanics* (E. Stein, ed.), pp. 5–52, John Wiley, Chichster, 2002.

[Saad] Y. Saad, *Iterative Methods for Sparse Linear Systems*, PWS Publishing Company, 1996.

[ScHeYi06] M. Schäfer, M. Heck, S. Yigit, *An Implicit Partitioned Method for the Numerical Simulation of Fluid-Structure Interaction* p. 171-194, in H.-J. Bungartz, M. Schäfer (Eds.) *Fluid-Structure Interaction Modelling, Simulation, Optimization*, Springer Verlag, (2006). [BuSc+06]

[ScKo+06] D. Scholz, S. Kollmannsberger, A. Düster, Ernst Rank, *Thin Solids for Fluid-Structure Interaction*, p. 294-335, in H.-J. Bungartz, M. Schäfer (Eds.) *Fluid-Structure Interaction Modelling, Simulation, Optimization*, Springer Verlag, (2006). [BuSc+06]

[Sethian99] J.A. Sethian, *Level set methods and fast marching methods.* Cambridge University Press, 1999.

[SoZo92] J. Sokolowski, J.P. Zolésio, *Introduction to shape optimization: shape sensitivity analysis*, Springer Series in Computational Mathematics, Vol. 10, Springer, Berlin, 1992.

[TezBehLiouI] T.E. Tezduyar, M. Behr, and J. Liou, A new strategy for finite element floow computations involving moving boundaries and interfaces-the deforming-spatial-domain/space-time procedures: I. The concept and preliminary tests, *Computer Methods in Applied Mechanics and Engineering*, 1992.

[TezBehLiouII] T. E. Tezduyar, M. Behr, and J. Liou, A new strategy for finite element floow computations involving moving boundaries and interfaces-the deforming-spatial-domain/space-time procedures: II. Computation of free-surface ows, two-liquid ows and ows with drifting cylinders, *Computer Methods in Applied Mechanics and Engineering*, 1992.

[HeHa+06] M. Heil, A.L. Hazel *oomph-lib An Ob ject-Oriented Multi-Physics Finite-Element Library*, p. 19-49, in H.-J. Bungartz, M. Schäfer (Eds.) *Fluid-Structure Interaction Modelling, Simulation, Optimization*, Springer Verlag, (2006). [BuSc+06]

[TeSa+06] T.E. Tezduyar, S. Sathe, K. Stein, L. Aureli, *Modeling of Fluid-Structure Interactions with the Space-Time Techniques*, p. 50-81, in H.-J. Bungartz, M. Schäfer (Eds.) *Fluid-Structure Interaction Modelling, Simulation, Optimization*, Springer Verlag, (2006). [BuSc+06]

[Turek99] S. Turek, *Efficient solvers for incompressible flow problems: an algorithmic and computational approach*, Springer, Heidelberg-Berlin-New York, 1999.

[TuHr06] S. Turek, J. Hron, *Proposal for Numerical Benchmarking of Fluid-Structure Interaction between an Elastic Object and Laminar Incompressible Flow* p. 371-386, in H.-J. Bungartz, M. Schäfer (Eds.) *Fluid-Structure Interaction Modelling, Simulation, Optimization*, Springer Verlag, (2006). [BuSc+06]

[TurSchae96] S. Turek and M. Schäfer, Benchmark computations of laminar flow around a cylinder. In E.H. Hirschel, editor, 'Flow Simulation with High-Performance Computers II', volume 52 of *Notes on Numerical Fluid Mechanics*. Vieweg, 1996.

[Wa99] W.A. Wall, *Fluid-Structure Interaction with Stabilized Finite Elements*, doctoral dissertation, Report No. 31 (1999), Institute of Structural Mechanics, University of Stuttgart.

[WaGe+06] W.A. Wall, A. Gerstenberger, P. Gamnitzer, C. Forster, E. Ramm, *Large Deformation Fluid-Structure Interaction Advances in ALE Methods and New Fixed Grid Approaches*, p. 195-232, in H.-J. Bungartz, M. Schäfer (Eds.) *Fluid-Structure Interaction Modelling, Simulation, Optimization*, Springer Verlag, (2006). [BuSc+06]

[Vi06] J. Vierendeels, *Implicit Coupling of Partitioned Fluid-Structure Interaction Solvers using Reduced-Order Models* p. 1-18, in H.-J. Bungartz, M. Schäfer (Eds.) *Fluid-Structure Interaction Modelling, Simulation, Optimization*, Springer Verlag, (2006). [BuSc+06]

[Vi] VISUSIMPLE, An open source interactive visualization utility for scientific computing, `http://visusimple.uni-hd.de/` . See [BeDu06].

[Zol79] J.P. Zolésio, *Identification de domaines par deformations*, Thèse d'état, Univ. Nice, 1979.